The Establishment and Maintenance of Centrosome Asymmetry in Neural Stem Cells

Roberto Carlos Segura

A dissertation

submitted in partial fulfillment of the

requirements for the degree of

Doctor of Philosophy

University of Washington

2025

Reading Committee:

Clemens Cabernard, Chair
Young Kwon
Jeff Rasmussen

Program Authorized to Offer Degree:

Molecular and Cellular Biology

University of Washington

Abstract

The Establishment and Maintenance of Centrosome Asymmetry in Neural Stem Cells

Roberto Carlos Segura

Chair of the Supervisory Committee: Clemens Cabernard
Department of Biology

Asymmetric cell division (ACD) is used by stem cells to create diverse cell types while self-renewing the stem cell population. Nested within ACD is the biased segregation of organelles, which carries functional consequences on the functionality of sister cells from ACD. Centrosomes, which are the microtubule organizing centers of cells, are comprised of a pair of centrioles that differ by age and molecular composition. Biased segregation of molecularly distinct centrosomes could provide a mechanism to maintain stem cell fate, induce cell differentiation or both. However, the molecular mechanisms generating molecular and functional asymmetric centrosomes remain incompletely understood. The neural stem cell lineage in the developing *Drosophila* larval brain (neuroblasts) provide a robust model to address our mechanistic understanding of centrosome asymmetry within the context of ACD. Neuroblasts divide asymmetrically to form one neuroblast, which retains its stemness, and one ganglion mother cell (GMC), which will differentiate and divide once more to form neuronal and glial cells. Here, we show how to utilize *Drosophila* neuroblasts to study basic cell biology and ACD, and using *Drosophila* neuroblasts, we show that protein phosphatase 4 (Pp4) is functionally required for centrosome asymmetry.

TABLE OF CONTENTS

ACKNOWLEDGEMENTS

This work would not have been possible without the outstanding support from my lab mates, PI, and collaborators who aided in the completion of this work. I would also like to acknowledge the non-scientific support of my friends and family, who helped me believe in the value of this work when the experimental process seemed insurmountable.

DEDICATION

This work represents the culmination of a promise made to my parents as a child. I promised to achieve the highest degree of education possible, and over the course of a decade, I committed myself to academic excellence. Therefore, this work is dedicated to my mother, Maribel Segura Paredes, and my father, Roberto Segura. My mother immigrated from Maracaibo, Venezuela, and my father immigrated from Jalisco, Mexico. As they transitioned from their native countries to the US, each of their families endured countless hardships in pursuit of the American dream, ranging from economic inequalities to interpersonal hardships. In the course of one generation, my family has transitioned from agricultural workers and street vendors to educators, financial accountants, and now Ph.D. graduates. The hardships I endured and overcame in pursuit of this degree pale in comparison to the hardships my family encountered to give me the opportunity to pursue this work. I can only hope that the work done here represents the collective effort and successes of those that came before me.

Este trabajo representa la culminación de una promesa que les hice a mis padres de niño. Prometí alcanzar la más alta educación posible y, a lo largo de una década, me comprometí con la excelencia académica. Por lo tanto, este trabajo está dedicado a mi madre, Maribel Segura Paredes, y a mi padre, Roberto Segura. Mi madre emigró de Maracaibo, Venezuela, y mi padre de Jalisco, México. Al mudarse de sus países natales a los Estados Unidos, cada una de sus familias soportó innumerables dificultades en la búsqueda del sueño americano, desde desigualdades económicas hasta dificultades interpersonales. En el transcurso de una generación, mi familia ha pasado de ser trabajadores agrícolas y vendedores ambulantes a educadores, contadores financieros y, ahora,

graduados de doctorado. Las dificultades que soporté y superé para obtener este título son insignificantes en comparación con las dificultades que mi familia enfrentó para darme la oportunidad de dedicarme a este trabajo. Solo puedo esperar que el trabajo realizado aquí representa el esfuerzo colectivo y los éxitos de quienes me precedieron.

CHAPTER 1. INTRODUCTION

1.1 ASYMMETRIC CELL DIVISION (ACD)

Asymmetric Cell Division (ACD) is the process by which an original mother cell gives rise to two daughter cells with different properties. This contrasts with symmetric division, which gives rise to two daughter cells with identical properties. Stem cells routinely utilize ACD to maintain a population of cells that retain their stem-ness while also forming a population of cells that can undergo differentiation. Indeed, during development of the human forebrain, neural progenitor cells (NPCs) undergo asymmetric divisions to form self-renewed progenitor cells and differentiating cells that migrate into the ventricular zone (VZ) (Royall *et al.*, 2023). These asymmetries between daughter cells are orchestrated either by external or internal cues. Extrinsic cues arise from external signals from the local cell niche, and intrinsic cues can include factors such as cortical cell fate determinants, biased localization of RNAs, biased segregation of organelles, and biased segregation of protein aggregates (Sunchu and Cabernard, 2020).

ACD can manifest via (1) physical differences between daughter cells, and (2) differential inheritance of sub-cellular components. ACD has been observed in multiple diverse species and cell types. One example of size asymmetries can be observed in the budding yeast *Saccharomyces cerevisiae*, where the original mother cell will divide and form a smaller bud cell that is roughly half the size of its mother, exemplifying the physical size difference of ACD (Chan and Marshall, 2014; Higuchi-Sanabria *et al.*, 2014; Chan *et al.*, 2016). Among other asymmetries, molecular asymmetries can be observed in the first zygotic division in the nematode *C. elegans*, where sperm entry breaks the original symmetry of the unfertilized egg and establishes the anterior-posterior axis. The anterior and posterior regions of the cell will cluster different sets of partitioning (PAR)

proteins, such that upon the first division, the posterior region of the cell gives rise to the germline and some somatic lineages, while the anterior region of the cell will only generate somatic cells (Munro and Bowerman, 2009; Gallo *et al.*, 2010) .

Both physical and molecular asymmetries can be observed in the neural stem cell lineage in *Drosophila melanogaster*. Extrinsic cues from the neuroectoderm establish an apical-basal polarity axis, where the activity of the PAR proteins PAR-3, PAR-6, and aPKC exclude cell fate determinants from the apical region of the cell and enrich them in the basal region. After cell division occurs, the apical cell retains its stemness while the basal cell forms a ganglion mother cell (GMC), which will give rise to differentiated neuronal cells (Doe, 2008; Prehoda, 2009; Loyer and Januschke, 2020).

Finally, ACD can also be observed in higher order mammals, such as mice and humans; in the developing vertebrate nervous system, neuronal precursor cells undergo a period of symmetric cell division to establish a "founder population" of stem cells before switching to ACD to produce differentiating cells that migrate into the developing tissue (Noctor *et al.*, 2004; Huttner and Kosodo, 2005).

1.2 Nucleic Acid Asymmetry

Asymmetric RNA segregation provides both spatial and temporal control of protein synthesis (Sallés *et al.*, 1994; Dahanukar *et al.*, 1999; Forrest *et al.*, 2004; Nelson *et al.*, 2004; Shlyakhtina *et al.*, 2019). This asymmetric RNA segregation is one method through which cells can become polarized. RNA segregation also plays a role in development, where 71% of mRNAs expressed during fly embryogenesis have preferential subcellular localization, implying that asymmetric RNA segregation plays a role in early development (Lécuyer *et al.*, 2007). Indeed, the

anterior-posterior axis in *Drosophila melanogaster* development is controlled by the localization of *gurken*, *bicoid*, *oscar*, and *nanos* mRNA. These RNA are sorted either by microtubule-dependent transport (*gurken*, *bicoid*, *oscar*) or via diffusion combined with trapping (*nanos*) (Pokrywka and Stephenson, 1991; Clark *et al.*, 1994; González-Reyes *et al.*, 1995; Johnston, 2005; Jaramillo *et al.*, 2008; Zimyanin *et al.*, 2008; Pilaz and Silver, 2017).

RNA patterns can also persist in asymmetric divisions, where there is preferential inheritance of RNA transcripts into specific daughter cells. In Drosophila neuroblasts, *Prospero* mRNA interacts with and is bound by the RNA-binding protein Staufen, leading to Prospero accumulation on the basal cortex (Broadus *et al.*, 1998). Similarly, while the protein product of the gene Miranda localizes basally towards the differentiating ganglion mother cell, the mRNA of *Miranda* localizes apically towards the renewing neuroblast (Schuldt *et al.*, 1998). The correlation between Staufen and biased RNA inheritance is not exclusively restricted to fly development; Staufen is asymmetrically segregated during neural stem cell division in the developing mouse cortex and contributes to normal cortical development (Kusek *et al.*, 2012). Indeed, many of the mRNAs that bind with Staufen in the mouse cortex control mitotic exit and metabolism of non-coding RNAs, suggesting that asymmetric inheritance of Staufen (and thus, Staufen-bound RNAs) could contribute to stem cell differentiation (Kusek *et al.*, 2012).

S. cerevisiae has been used as a model for ACD due to the preferential segregation of organelles between a mother and its bud (expanded on in chapter 1.3, “Organelle Asymmetry”), the size asymmetry between mother and bud cells, and the regenerative properties of the bud cell compared to its mother. A prime example of RNA segregation in yeast comes from the mRNA transcript of the gene *ASH1*, which is asymmetrically concentrated at the bud neck to be inherited by the bud cell after division during asexual reproduction (Heym and Niessing, 2012). This causes

the product of *ASH1* to be exclusively expressed in the daughter cell, where it prevents mating type switching. In other words, this preferential segregation of the mRNA of *ASH1* has a direct impact on cellular identity in progeny cells. Another example in *S. cerevisiae* comes from the RNA for the gene ENO2 (which catalyzes the conversion of substrates during glycolysis and glucogenesis), which again is preferentially distributed to the bud cell. This preferential segregation of *ENO2* RNA into bud cells decreases as the mother cell increases in age but does not impact cell size asymmetry between mother and bud cells (Kukhtevich *et al.*, 2022).

Chimeric Antigen Receptor T cells (CAR-Ts) divide asymmetrically to distribute their proteome and transcriptome to result in daughter cells with divergent fates. Both pre-existing RNA transcripts and changes in gene expression ("RNA velocity," the estimation of gene expression by distinguishing between spliced and un-spliced RNA as an approximation in gene expression (Manno *et al.*, 2018)) contribute to changes in fate. This results in different transcriptional priorities in daughter cells, where one daughter will inherit transcripts/transcription factors to support proliferation and effector function, while the other daughter cell will inherit transcripts/transcription factors that restrain differentiation and promote longevity (Lee *et al.*, 2024).

In developing mollusk embryos, differential RNA segregation is achieved via centrosome localization. First, RNAs are transported to the centrosome via microtubule-dependent transport, where they are then shunted to the cell cortex via actin-dependent transport. Importantly, these mRNA transcripts only arrive to the cell cortex if they first move to the centrosome, implying that centrosomes/organelles transport may act as a mediator of specific RNA delivery (Lambert and Nagy, 2002) . Similar dynamics can be seen in 24 different mRNA transcripts that preferentially

segregate to centrosomes in Drosophila, implying that this centrosome-specific form of RNA delivery may occur in other organisms (Lécuyer *et al.*, 2007).

1.3 Organelle Asymmetry

Like RNA, organelles can also be asymmetrically segregated between daughter cells following ACD. Among other examples expanded on below, several examples of asymmetric organelle inheritance include: mitochondria with higher potential for energy synthesis are preferentially inherited by the younger bud cell in *S. cerevisiae* (McFaline-Figueroa *et al.*, 2011; Yang *et al.*, 2022; 2024; Chelius *et al.*, 2023; 2025); Lysosomes carrying Notch signaling proteins are preferentially inherited by neural progenitor cells in the mouse neocortex (Coumailleau *et al.*, 2009; Kressmann *et al.*, 2015); and younger daughter centrosomes are preferentially inherited by the neuroblast in the developing *Drosophila* brain (Conduit and Raff, 2010; Januschke *et al.*, 2011; Chen and Yamashita, 2021). This presents an interesting quandary: in symmetrically dividing cells, it is logical to equally partition the organelles of the mother cell equally between its progenies. How does this change in ACD? Organelles are synthesized to replace damaged or degraded older organelles, and these changes can conceivably confer differential organelle function (Lerit *et al.*, 2013) . So, do asymmetrically dividing stem cells preferentially segregate their organelles into specific progeny cells to confer unto them specific capabilities? Below I detail examples of organelle asymmetry with respect to notable organelles, such as the mitochondria, the endoplasmic reticulum, the lysosome, and lastly, the centrosome.

1.3.1 *Mitochondria*

Mitochondria are responsible for generating ATP from the glycolysis pathway in eukaryotic cells. The mitochondria is comprised of an inner and outer membrane which give rise to the ion concentration gradient that is used to generate ATP.

Mitochondria have been observed to segregate asymmetrically within the context of stem cell ACD: In mouse oocyte meiosis, mitochondria aggregate around the division spindle via dynein mediated mechanisms and move with the spindle towards the oocyte cortex. This asymmetric distribution of mitochondria is dependent on the actin cytoskeleton, spindle formation, and cell cycle progression (Dalton and Carroll, 2013). Later in division, mitochondria are excluded from the polar body, because the polar body is destined to degenerate, resulting in mitochondria preferentially segregating into the oocyte (Dalton and Carroll, 2013). This exemplifies the importance of asymmetric organelle inheritance, where improper segregation would result in a cell with a vastly depleted reserve of mitochondria.

Similar dynamics can be observed in the budding yeast *Saccharomyces cerevisiae*, where the mother cell will retain lower-functioning, lower redox-potential mitochondria while the bud cells will inherit the higher-functioning, newly-synthesized mitochondria (McFaline-Figueroa *et al.*, 2011; Yang *et al.*, 2022; 2024; Chelius *et al.*, 2023; 2025). Biased mitochondrial fission facilitates the clustering of protein aggregates in the mitochondrial matrix and keeps older mitochondria in mother cells, underlying the asymmetric inheritance of mitochondria in yeast (Sun *et al.*, 2023).

This characteristic inheritance of preferential mitochondria also extends to humans. In human mammary stem-like cells, daughter cells that received fewer older mitochondria maintained their stem-ness, while inheriting older mitochondria was associated with losing stem-ness,

implicating oxidative capacity with cell fate decisions (Katajisto *et al.*, 2015). Indeed, in epithelial stem-like cells, mitochondria are segregated asymmetrically - cells that inherit newer mitochondria promotes stemness after division (Spinelli and Zaganjor, 2022). Indeed, similar dynamics extend to *Drosophila* neuroblasts, where mitochondria preferentially segregate into the renewed neuroblast (Sen *et al.*, 2013). This segregation is dependent on the positioning of the bipolar spindle and distribution of the cytoplasm, further implicating other ACD regulators in the biased segregation of organelles (Sen *et al.*, 2013). Morphological changes are observable in GMCs after neuroblast division, where mitochondria change from forming discrete puncta in neuroblasts to forming elongated, branched filaments in GMCs, implying differences in the capacities of mitochondria inherited (Sen *et al.*, 2013). However, the quality of mitochondria distributed to neuroblasts and GMCs remains unknown.

1.3.2 *Endoplasmic Reticulum*

If mitochondria show a biased inheritance pattern of segregating older or less favorable cellular components away from the stem cell, then there must be a mechanism regulating this biased partitioning. The Endoplasmic Reticulum (ER) is one such organelle that can mediate the transport of subcellular components into progeny cells. In budding yeast, specialized ER structures are formed at the bud neck, implying asymmetric distribution of ER between mother and bud cells (Luedeke *et al.*, 2005) . Indeed, a diffusion barrier in the ER is a mediator determining the segregation of aging factors in yeast (Shcheprova *et al.*, 2008; Clay *et al.*, 2014). Similar patterns are observable in the single-celled embryo of *C. elegans*, where the ER is compartmentalized into an anterior and posterior domain during the first division, indicating a difference in diffusion barriers at the two domains (Lee *et al.*, 2016).

The pattern of ER-partitioning of damaged cellular components to the non-stem cell persists in mammalian systems. In mouse neural stem cells, the ER forms a diffusion barrier to promote the asymmetric segregation of cellular components; damaged cellular components are inherited by the non-stem cell in embryonic and young neural stem cell divisions, but are symmetrically inherited in the adult brain (Moore *et al.*, 2015). Similarly, in human embryonic stem cells and induced pluripotent stem cells, the ER segregates asymmetrically (Imtiaz *et al.*, 2022).

In *Drosophila* neuroblasts, the ER is asymmetrically partitioned to centrosomes in early mitosis. This partitioning of the ER to centrosomes is dependent on interactions with astral microtubules (Smyth *et al.*, 2015); Because ER localization overlaps with the asymmetric MTOC activity in neuroblasts, it is suggested that MTOCs are required for asymmetric partitioning of the ER in ACD of *Drosophila* neuroblasts (Smyth *et al.*, 2015). The specific pattern by which the ER segregates (i.e., preferential differences in the capacity of the ER membrane components inherited by the neuroblast versus those inherited by the GMC) in *Drosophila* neuroblasts remains to be seen.

1.3.3 *Lysosomes*

Lysosomes work to break down cellular components that are no longer required or are marked for degradation. They also serve as intermediary transport vesicles in signaling pathways and have been observed to segregate asymmetrically. In yeast, vacuoles (lysosome homologs) are asymmetrically inherited; mother cells will partition off newly synthesized portions of their vacuoles for transport to the developing bud cell via myosin motors, which is in line with the preferential inheritance observed in mitochondria and ER inheritance patterns (Legesse-Miller *et al.*, 2006; Peng and Weisman, 2008; Ekal *et al.*, 2024) . Similarly, lysosomes, autophagosomes,

and mitophagosomes are asymmetrically inherited in mouse hematopoietic stem cell (HSC) daughters. Autophagy and mitochondrial clearance are lysosome-dependent processes and are required for hematopoietic stem cell function. HSC's that inherit a low number of lysosomes go on to differentiate, while those that inherit a high number of lysosomes retain their stemness (Loeffler *et al.*, 2019). This knowledge has functional consequences for human hematopoietic stem and progenitor cells (HSPCs), where polarization occurs in interphase with the centrosome, Golgi, and lysosomes positioning near the point of contact with the cell micro-environment. During mitosis, cells orient their spindle perpendicular to the point of contact, giving rise to sibling cells with unequal amounts of lysosomes and the differentiation marker CD34, which indicates that preferential inheritance of lysosomes is tied to cell fate (Candelas *et al.*, 2024).

In neuron progenitor cells (both mouse embryonic neocortex and human embryonic stem cell derived brain organoid), lysosomes are asymmetrically inherited during radial glial cell (RGC) division, and there are increased numbers of endolysosomes (also known as phagolysosomes, which clear debris) in intermediate progenitor cells and autolysosomes (specific lysosomes tuned for autophagy) instead in newborn differentiated neurons, implying that inheriting endolysosomes promotes stemness, while inheriting autolysosomes leads to differentiation (Zou *et al.*, 2024) .

As mentioned previously, lysosomes can act as transportation intermediaries in cell signaling cascades. In both Drosophila sensory organ precursor (SOP) cells and in the zebrafish spinal cord, subsets of endosomes are preferentially inherited due to their concentrations of Notch receptors and ligands, with renewing stem cell progeny preferentially receiving endosomes rich in Notch components (Coumailleau *et al.*, 2009; Kressmann *et al.*, 2015). Further, lysosomes carrying Notch signaling proteins are segregated asymmetrically in human neural stem cells, which in turn impacts Notch activity in daughter cells. Cells that receive more Notch-containing

lysosomes retain their stem-ness, while those which receive fewer Notch-containing lysosomes go on to differentiate (Bohl *et al.*, 2022).

1.3.4 *Centrosomes*

The centrosome is the main microtubule organizing center (MTOC) of the cell and is responsible for orienting the bipolar spindle during mitosis. The centrosome is comprised of a pair of centrioles that duplicate once per cell cycle. At the onset of this duplication, Polo Like Kinase 4 (PLK4, Sak in Humans) is recruited to the side of the pre-existing mother centriole (Habedanck *et al.*, 2005). This enrichment of PLK4 on the mother centriole is mediated by Asterless in flies, and by CEP152 and CEP192 in humans (Dzhindzhev *et al.*, 2010; Sonnen *et al.*, 2013). Following this, the structural proteins SAS-5 and SAS-6 form a central cartwheel structure that establishes the ninefold symmetry of the centriole (Breugel *et al.*, 2011). Once these two proteins are present, they then promote the recruiting of SAS-4 (CENP-J in humans), which then integrates into the outer region of the cartwheel and helps assemble the surrounding centriolar microtubules (Tang *et al.*, 2011).

With this duplication event comes age asymmetries, where in mammalian cells, only the mother centriole contains distal appendages that have accumulated on the mother due to its older age, while the daughter does not have these appendages due to being recently formed (Chen and Yamashita, 2021; Kumar and Reiter, 2021) . With this difference in age come other differences in centriole composition between mother and daughter centrioles; The mother centriole is more enriched for Asterless, a centriolar protein (Gallaud *et al.*, 2020) while Centrobin localizes only to the daughter centriole (Januschke *et al.*, 2013; Gallaud *et al.*, 2020) Additionally, the outer dense fiber protein 2 (ODF2), Ninein, and Cep164 preferentially enriches the mother centriole due to the aforementioned distal appendages on the mother centriole (Lange and Gull, 1995; Nakagawa *et*

al., 2001; Zou *et al.*, 2005; Graser *et al.*, 2007; Chen and Yamashita, 2021; Jaiswal and Singh, 2021).

These differences between mother and daughter centrioles confer different functional capacities in the centrosomes that are formed from mother and daughter centriole in interphase upon separation. One example of functional differences between centrioles is their capacity to recruit and form a pericentriolar matrix (PCM). The process of establishing a PCM is started by pericentrin, which forms fibrils that extend away from the centriole (Lawo *et al.*, 2012) . At this point, both Asterless and Polo are present in the PCM. Upon activation of Polo, Polo phosphorylates Centrosomin (Cnn), which promotes the formation of an interconnected scaffold (Lee and Rhee, 2011). The Cnn scaffold then interacts with the protein Spindle defective 2 (Spd2), which allows Spd2 to be kept in the PCM and spread out and away from the centrioles, such that Spd2 moves away from the center of the PCM and centriole(Conduit *et al.*, 2015) . New Spd2 will be incorporated near the centriole where it will then be pushed outwards. This then forms a positive feedback loop, where the expansion of Cnn allows for the further recruitment of Polo and Spd2, which in turn makes more space for more Cnn. To form active MTOCs, the PCM components of gamma tubulin (γTubulin) and gamma tubulin ring complexes (γTuRCs) are recruited to the Cnn-Spd2 scaffold via phosphorylation of NEDD1 by NEK9, where they connect with other PCM components to strengthen the PCM (Sdelci *et al.*, 2012). In most systems, the older mother centrosome, due to having a more mature centriolar structure, retains the capacity to interact with and recruit PCM factors to form an active MTOC, while the daughter centrosome, which lacks a mature structural centriole, remains inactive until it matures (Chen and Yamashita, 2021).

These differences in molecular composition and functional capacity is accompanied by preferential segregation during stem cell divisions. Indeed, many different cell types and

organisms display preferential centrosome inheritance, and impairing this inheritance is associated with developmental defects; In *Drosophila* male germ line cells, mouse neural progenitors and mouse embryonic stem cells, the stem cell retains the older mother centrosome, while in *Drosophila* female germline cells and neuroblasts, the stem cells inherits the daughter centrosome (Chen and Yamashita, 2021; Burkhalter *et al.*, 2024; Kiermaier *et al.*, 2024; Pei *et al.*, 2025; Xu *et al.*, 2025).

These inheritance patterns have developmental impact, where missegregation of centrosomes in the developing mouse cortex results in a decrease in number of progenitor stem cells and differentiated neuronal cells (Wang *et al.*, 2009) . Given that the mother centrosome is generally more functionally capable than it's daughter, an exciting hypothesis to consider is the "immortal centrosome" hypothesis, where in stem cell divisions, the renewing stem cell preferentially keeps the mother centrosome to ensure the stem cell always has access to a fully capable, mature centrosome (Chen and Yamashita, 2021). Indeed, this is observable in *Drosophila* male germline cells, where the renewed stem cell retains the mother centrosome while the differentiating cell inherits the daughter centrosome (Yamashita *et al.*, 2007; Chen and Yamashita, 2021). The same is seen mouse radial glial progenitor cells, neural progenitor cells, and embryonic stem cells (Wang *et al.*, 2009; Habib *et al.*, 2013; Chen and Yamashita, 2021).

However, there are also cell types where the inverse occurs, and the cell that retains its stem-ness inherits the younger centrosome, contrasting the immortal centrosome hypothesis. This is readily seen in *Saccharomyces cerevisiae*, where the bud cell (the equivalent of a younger stem cell) inherits the older spindle pole body (SPB = centrosome equivalent) (Pereira *et al.*, 2001; Chen and Yamashita, 2021). Indeed, while the stem cell retains the mother centrosome in the *Drosophila* male germline cell lineage, the opposite occurs in the *Drosophila* female germ line cells, where

the stem cell inherits the daughter centrosome and the differentiating cell receives the mother centrosome (Salzmann *et al.*, 2014; Chen and Yamashita, 2021). Finally, in Drosophila neuroblasts, the stem cells retain the daughter centrosome, while differentiating cells retain the mother centrosome (Conduit and Raff, 2010; Januschke *et al.*, 2011; Chen and Yamashita, 2021).

1.4 *DROSOPHILA* AS A SYSTEM TO STUDY ACD

Drosophila melanogaster provide a robust model organism to study ACD, centrosome asymmetry, and brain development (Homem and Knoblich, 2012) . *Drosophila* neural stem cells (neuroblasts) display similar asymmetrically divisions as comparable stem cells in higher organisms and have relatively fast generation time compared to mammalian systems (Figure 1A). Because of this faster generation time, the waiting period between experiment conceptualization and experiment execution is drastically reduced compared to similar experiments in organoid culture or *in vivo* murine models. In addition to this, the *Drosophila* genome is thoroughly understood, making the fly genome readily accessible genetic perturbations, such as recombinant chromosomes and manipulation via CRISPR-Cas9. This is additionally supported by the relatively short generation time of *Drosophila*, meaning that genetic manipulations are generally faster to implement than similar processes in murine models.

The central nervous system (CNS) of *Drosophila* larvae is easily accessible via microdissection, allowing researchers to study cellular processes in intact *ex vivo* tissue ((Segura and Cabernard, 2023) Figure 1B). The CNS of *Drosophila* larval brains is relatively transparent and readily imaged with conventional confocal microscopy, and due to their smaller size, introducing fluorescent labels via immunohistochemistry (IHC) is straightforward and does not require the laborious permeation and tissue clearing required in the CNS of other model systems (Segura and Cabernard, 2023). Finally, extensive work has revealed identity markers allowing for

the distinction between neuroblasts, GMCs, intermediate neuronal progenitor (INP) cells, mature neurons and glial cells (Homem and Knoblich, 2012) Figure 1C).

In *Drosophila*, there are two types of neuroblasts: Type I neuroblasts undergo ACD during the larval stage of development every 60-90 minutes to produce one renewed neuroblast and one ganglion mother cell (GMCs), which will divide once more over the next six to eight hours to produce neuronal and glial cells (Homem and Knoblich, 2012; (Fichelson *et al.*, 2005), Figure 2A). Type II neuroblasts also undergo ACD every 60-90 minutes, but instead of producing a GMC, they instead form an INP cell. These INPs will then undergo transcriptional changes and mature into a mature INP over the next 6-8 hours, after which it will divide asymmetrically three to six times to produce a renewed INP and one GMC (Chaya *et al.*, 2025). This GMC will then go on to divide into neuronal and glial cells as they do with Type I neuroblasts (Homem and Knoblich, 2012, Figure 2B).

Therefore, *Drosophila* neuroblasts provide an exceptionally robust system to functionally test centrosome asymmetry within the context of asymmetric cell division due to their ease of genetic manipulation and observation with high-temporal confocal imaging (Sunchu *et al.*, 2022; Segura and Cabernard, 2023; Segura *et al.*, 2025). Below, I outline our current understanding of centrosome asymmetry in *Drosophila* neuroblasts.

1.5 Centrosome Asymmetry in Neural Stem Cells

Drosophila neuroblasts display functional and molecular centrosome asymmetry in addition to other manifestations of ACD. In neuroblasts, the daughter centrosome is destined to segregate into the renewed neuroblast, while the mother centrosome will segregate into the differentiating ganglion mother cell (GMC). The GMC will divide once more to give rise to

differentiated neuronal cells (Cabernard and Doe, 2009; Januschke *et al.*, 2011; Homem and Knoblich, 2012). During mitosis, centrioles in the mother and daughter centrosomes are duplicated (Gallaud *et al.*, 2020). In the following interphase, these centrioles will separate and form two new centrosomes (Figure 3A). How does a daughter centrosome distinguish itself from its mother, and how do these differences contribute to asymmetric cell division?

1.5.1 *Daughter centrosome regulation in neuroblasts*

Centrosomes functionally differ from one another in neuroblasts via their different capacities to recruit and retain MTOCs. In early interphase following cytokinesis, centrioles separate from one another to form two distinct centrosomes. One of these centrosomes will remain near the apical region of the cell, while the other moves through the cytoplasm as kinesin cargo (Rebollo *et al.*, 2007; Rusan and Peifer, 2007; Singh *et al.*, 2014; Hannaford *et al.*, 2022; Hannaford and Rusan, 2024). This difference in localization is thought to be ascribed to MTOC activity, with the apical centrosome remaining in the apical region of the cell via microtubule-mediated interactions with Pins and the apical cortex (Rebollo *et al.*, 2007). This then primes the question: at the molecular level, what grants the apical centrosome the ability to retain an MTOC, and what removes MTOC capacity from the basal centrosome?

The most prominent molecular regulation of centrosomes arises from an asymmetric distribution of the centriolar protein Centrobin (Cnb, CENTROB in humans) that localizes exclusively to the daughter centrosome (Januschke *et al.*, 2013). Centrobin then interacts with other PCM proteins such as γTubulin, Plp, Sas-4, Sas-6, and Cnn which is hypothesized to promote the formation of an interphase MTOC at the daughter centrosome (Januschke *et al.*, 2013). Microtubules at the apical centrosome are stabilized by Wdr62, which allows for the recruitment of Polo Kinase (Plk1 in mammals) to the centrosome along microtubules as cargo (Ramdas Nair

et al., 2016). Once at the daughter centrosome, Polo phosphorylates Centrobin, forming a positive feedback loop to promote the localization of Centrobin, Polo, and MTOC activity at the daughter centrosome (Januschke *et al.*, 2013, Figure 3C). This MTOC activity is believed to anchor the daughter centrosome in the apical region of the cell, thereby establishing the apical-basal division axis that arises in mitosis (Rebollo *et al.*, 2007; Rusan and Peifer, 2007) . This further ensures that the active daughter centrosome, and not the inactive mother centrosome, segregates into the neuroblast after division.

1.5.2 *Centriole duplication and establishing asymmetry*

Upon entry into mitosis, centrioles will duplicate, reconstituting the age asymmetry between mother and daughter centrioles (Figure 3D, 3I). To re-establish molecular asymmetry in the following interphase after division, Centrobin and Polo are dynamically transferred from the mother centriole to the daughter, such that upon centriole separation in the next interphase, the daughter centriole (which will form the daughter centrosome) contains Centrobin and Polo, while the mother centriole (which will form the mother centrosome) does not (Figure 3E). This "passing of the torch" of molecular asymmetry is mediated by the phosphorylative activity of Polo on Centrobin, which is hypothesized to remove Centrobin and Polo from the mother centriole (Gallaud *et al.*, 2020). Thus, at the end of mitosis, all of the Centrobin originating from the mother centriole has been removed from the mother and has been enriched on the daughter, and the apical pair of centrioles segregate into the renewed neuroblast (Figure 3F). While this illustrated the importance of phosphorylative control of molecular centrosome identity, it remained unclear if phosphatase activity is equally important for orchestrating this process.

1.5.3 *Mother centrosome regulation in neuroblasts*

The daughter centrosome is therefore characterized by containing components (Cnb, Polo, PCM) that are absent from the mother centrosome. Thus, there must be regulatory pathways that remove these factors from the mother centrosome. Indeed, the centriolar protein Bld10 (Cep135 in mammals) is responsible for the removal of Polo from the mother centrosome in early interphase, thereby contributing to the inactivation of MTOC activity at the mother centrosome (Singh *et al.*, 2014). This PCM shedding is further promoted by the activity of Plp and Plk4 (Polo Kinase 4), which preferentially phosphorylates PCM components on the mother centrosome to facilitate PCM shedding (Gambarotto *et al.*, 2019). Because of this PCM shedding, the mother centrosome loses PCM components like Cnn and γTubulin, while the daughter centrosome actively retains these components (Conduit and Raff, 2010). Without a PCM to recruit MTOC activity with, the mother centrosome instead moves through the cytoplasm on the interphase microtubule network as Kinesin-1 cargo. Later in mitosis, the basal centrosome will mature, recruit a PCM and MTOC, and position on the basal cortex to segregate into the GMC (Hannaford *et al.*, 2022; Hannaford and Rusan, 2024). In tandem with Centrobin transfer at the apical centrosome, Centrobin incorporates onto the daughter centriole at the basal centrosome during mitosis before segregation into the GMC (Gallaud *et al.*, 2020).

1.6 Consequences of Centrosome Regulation and Centrosome Asymmetry

Centrosomal genes have been implicated in multiple developmental disorders, including primary microcephaly, retinal development, and craniofacial development (Yu *et al.*, 2020; Kiermaier *et al.*, 2024; Pei *et al.*, 2025). Clearly, centrosome function is a critical contributor to

normal development; While centrosomes are dispensible for normal development in flies, mutant flies without centrosomes die shortly after birth (Basto *et al.*, 2006). Does this mean that miss-regulation of centrosome asymmetry carries equal impact on development? Here, I outline several examples of centrosomal regulation in relation to developmental disorders.

1.6.1 *Microtubule activity and neurodevelopmental disorders*

Sas-4 (CENP-J) is a centriolar protein that is required for proper centrosome assembly. By getting recruited to the centrosome via the activity of Ana2, Sas-4 contributes to the recruitment of microtubules at active centrosomal MTOCs (Gallaud *et al.*, 2014). Sas-4 is further required for proper asymmetric division orientation in neuroblasts, And mutant loss-of-function *sas-4* flies lack detectable centrosomes and die shortly after birth due a lack of cilia in their sensory neurons (Basto *et al.*, 2006; Januschke and Gonzalez, 2010). Similarly, CEP135 (Bld10) is another centrosomal protein that promotes microtubule binding, centrosome asymmetry, and spindle orientation in neuroblasts. It is chiefly responsible for inhibiting MTOC activity at the mother centrosome in neuroblasts, where it works to shed PCM factors to prevent abnormal MTOC development (Singh *et al.*, 2014). These studies highlight how Sas-4 and CEP135 are critical for microtubule regulation at centrosomes; mutations to CENP-J and CEP135 have been implicated in neurodevelopmental disorders, mild to severe intellectual disability, and global developmental delay in other systems. While the direct connection between MTOC/MT regulation and neurodevelopmental defects remains elusive, these studies implicate that centrosomal MTOC regulation may be functionally critical during development. Further, mutations to these genes suggest substantial changes to protein structure, suggesting a role on centrosomal function (Saima *et al.*, 2024).

The Ubiquitin-fold mediator 1 (UFM1) degradation pathway has been implicated in microcephaly, and UFM1 mutant neuroblasts exhibit defects in mitotic progression and defective

centrosomal MTOC, implicating that centrosomal function and regulation is developmentally important in the developing brain (Yu *et al.*, 2020). Similarly, WDR62, which stabilizes microtubules at the apical daughter centrosome in interphase neuroblasts, is also implicated in primary microcephaly, further solidifying this link between centrosome regulation and neurodevelopment (Ramdas Nair *et al.*, 2016). Indeed, integral PCM components such as gamma tubulin associate with other microcephaly-related proteins, such as CDK5RAP2, which is required to promote gamma tubulin ring complex activation and therefore microtubule activity (Gao *et al.*, 2025). Similarly, the protein MLL/WDR5 is required for microtubule nucleation and growth at centrosomes, and loss of MLL/WDR5 in U2OS cells resulted in chromosomes failing to align to the metaphase plate during mitosis, implying that centrosome function, via interaction with chromosome alignment, is a possible functional link between centrosome regulation and developmental disorders (Chodisetty *et al.*, 2024). Thus, errors in centrosome alignment to the metaphase plate during mitosis can result in miss-segregation of chromosomes. Depletion of the centriolar protein SPOUT1 (ptch in flies) regulates centrosome attachment to spindle poles and is required for proper chromosome alignment. In its absence, Zebrafish mutants show reduction in larval head size. Additionally, these mutants displayed apoptosis that is likely related to alterations of cell cycle progression (Dharmadhikari *et al.*, 2024). The position of the cleavage furrow is one mechanism that gives rise to physical asymmetries between sibling cells. Extensive work has been performed in *Drosophila* neural stem cells to identify the effectors of cleavage furrow positioning. During anaphase onset, the early and late furrow proteins Pavarotti, Anillin, and Myosin localize to the basal cortex in a microtubule-independent manner (Cabernard *et al.*, 2010) . Specifically, the spatiotemporal regulation of Myosin is orchestrated by Rho kinase, which enriches myosin on the apical cortex before nuclear envelope breakdown, after which Partner of Inscuteable (Pins) and

Protein Kinase N (Pkn) contribute to the down-regulation and removal of Myosin from the apical cortex (Tsankova *et al.*, 2017) . This clearing of Myosin from the apical cortex results in expansion from the apical cortex before the basal cortex, and occurs in tandem with spindle positioning, spindle asymmetry, and centrosome MTOC asymmetry (Roubinet *et al.*, 2017). Finally, in addition to the clearing of non-muscle myosin (Pham *et al.*, 2019), centrosome-associated asters during mitosis are one of the required components for cell cleavage furrow positioning, where the positioning of the centralspindlin complex is dependent on peripheral astral microtubules. When these astral microtubules are removed, the cleavage furrow is repositioned such that the size asymmetry between daughter cells is reduced (Thomas *et al.*, 2021). Therefore, astral microtubules originating from the centrosomes play a key role in regulating ACD (Thomas *et al.*, 2021).

1.6.2 *Centriole duplication and neurodevelopmental disorders*

Errors in centriole duplication are associated with microcephaly. Furter, amplified numbers of centrioles are associated with chromosomal instability, metastasis, and cyst formation (Kiermaier *et al.*, 2024). Centrioles duplicate once during mitosis, and this duplication is initiated by Plk4 in mammals (Kiermaier *et al.*, 2024). This initiation via Plk4 gives one model to restrict abnormal centriolar duplication, as Plk4 only localizes to the pre-existing centriole to initiate duplication, after which it will self-degrade to prevent extra centriole formation (Ohta *et al.*, 2014; Klebba *et al.*, 2015; Kiermaier *et al.*, 2024). Alstrom syndrome is a rare autosomal recessive genetic disorder characterized by developmental delay, childhood obesity, and multiple organ dysfunction (Marshall *et al.*, 2015). Alstrom syndrome is caused by mutations to the gene ALMS1, which regulates the formation of cellular cilia. Alstrom syndrome protein (Alms1a and Alms1b in flies) regulates centriolar cartwheel assembly via Plk4 activity, further linking centrosomal regulation to developmental disorders (Brunet *et al.*, 2025). Plk4 has an established role in

regulating centrosome asymmetry in fly neuroblasts, implying a connection between Plk4 regulation of CS asymmetry and neurodevelopmental disorders via Plk4 regulation of centriolar duplication (Singh *et al.*, 2014; Gambarotto *et al.*, 2019) . Similarly, NUBP2 has been implicated in primary microcephaly, and transgenic mice deficient in NUBP2 revealed changes in neuronal progenitor cell proliferation and supernumerary centrosomes and cilia, further implicating supernumerary centrioles/centrosomes in developmental disorders (Rushforth *et al.*, 2025). lastly, In zebrafish, the kinase ZYG-1 phosphorylates the centriolar proteins Sas-5 and Sas-6 to regulate centriole duplication during mitosis, and in phospho-mimetic Sas-5 mutants, supernumerary centrioles are formed, which likely carries developmental consequences (Sankaralingam *et al.*, 2024). Centriole duplication occurs in tandem with the centriolar transfer of Centrobin and Polo which give rise to molecular asymmetry (Gallaud *et al.*, 2020; Segura *et al.*, 2025). Because these two processes happen in the same temporal window, it is likely that errors in centriole duplication would be accompanied by transfer defects, which would disrupt centrosome asymmetry.

1.6.3 *Primary cilia*

In non-dividing cells, centrosomes contribute towards the formation of primary cilia, which can be used as mechanoreceptors to interact with the extracellular environment. They can also regulate signaling pathways (such as the Sonic hedgehog pathway) and are vital for the sense of olfaction, vision, and mechanosensation (Brown and Zhang, 2020). Unsurprisingly, WDR4, another microcephaly implicated gene, is required for head growth and neurogenesis via cilia formation, and loss of WDR4 results in aberrant cilia formation (Burkhalter *et al.*, 2024). Centrosomes also function to form primary cilia, which is critical for photoreceptor cells in eye development. Kinesin-5 (KIF11, Klp61F in flies) is essential for MTOC organization, centrosome separation, and spindle assembly. In KIF11's absence, mutant mouse models develop defects in

retinal development and vision loss. Further, KIF11 inhibition induces monopoloar spindles and mitotic arrest, leading to tetraploidy and cell death, implying that centrosomal regulation impacts developmental pathways in other tissue types (Xu *et al.*, 2025). Indeed, centrioles also play a role in tooth development; mutant mice with Sas-4 (CPAP) mutations showed disrupted centriole organization in molar odontoblast cells, while increased centriole presence in control mice correlated with enhanced enamel development. It is unsurprising that these molar defects are also observed in patients with primary microcephaly, further linking developmental defects to centrosome activity (Pei *et al.*, 2025). In cultured mouse fibroblast cells, the cell that inherits the mother centrosome has the capacity to develop a primary cilia (and is therefore more sensitive to Sonic hedgehog signaling) sooner than the cell that inherits the daughter centrosome, implying that centrosome asymmetry has a consequence on cilia formation (Chen and Yamashita, 2021).

1.6.4 *Centrosomal transport of RNAs*

In snails, centrosomes act as a mediator vessel to move cell fate determinants into their assigned progeny cell (Lambert and Nagy, 2002). This suggests that centrosomes may act as transitionary mediums to deliver specific cell fate determinants to the proper progeny cell, providing a mechanical consequence to centrosome asymmetry in neural stem cells. In snails, mRNA move into specific progeny cells via microtubule and actin-dependent delivery mechanisms to and from the centrosome, respectively (Lambert and Nagy, 2002; Suter, 2018). Indeed, similar dynamics can be observed in flies; the cell fate determinant Miranda (Mira), which segregates into the differentiating GMC, has both Mira RNA and Mira protein localized to the basal cortex, while a population of Mira RNA localizes to the apical centrosome (Ramat *et al.*, 2017) . Mechanistically, it is likely that Miranda dephosphorylated by Pp4 at the centrosome to ensure its proper basal localization, which may work similarly to the exclusionary actions of the

PAR complex at the apical cortex (Connell *et al.*, 2024). Future work will focus on determining if a loss of centrosome asymmetry results in a loss of biased mRNA delivery, if such systems exist in *Drosophila*.

1.7 FIGURES

1.7.1 *Figure 1: Drosophila as a Model for ACD*

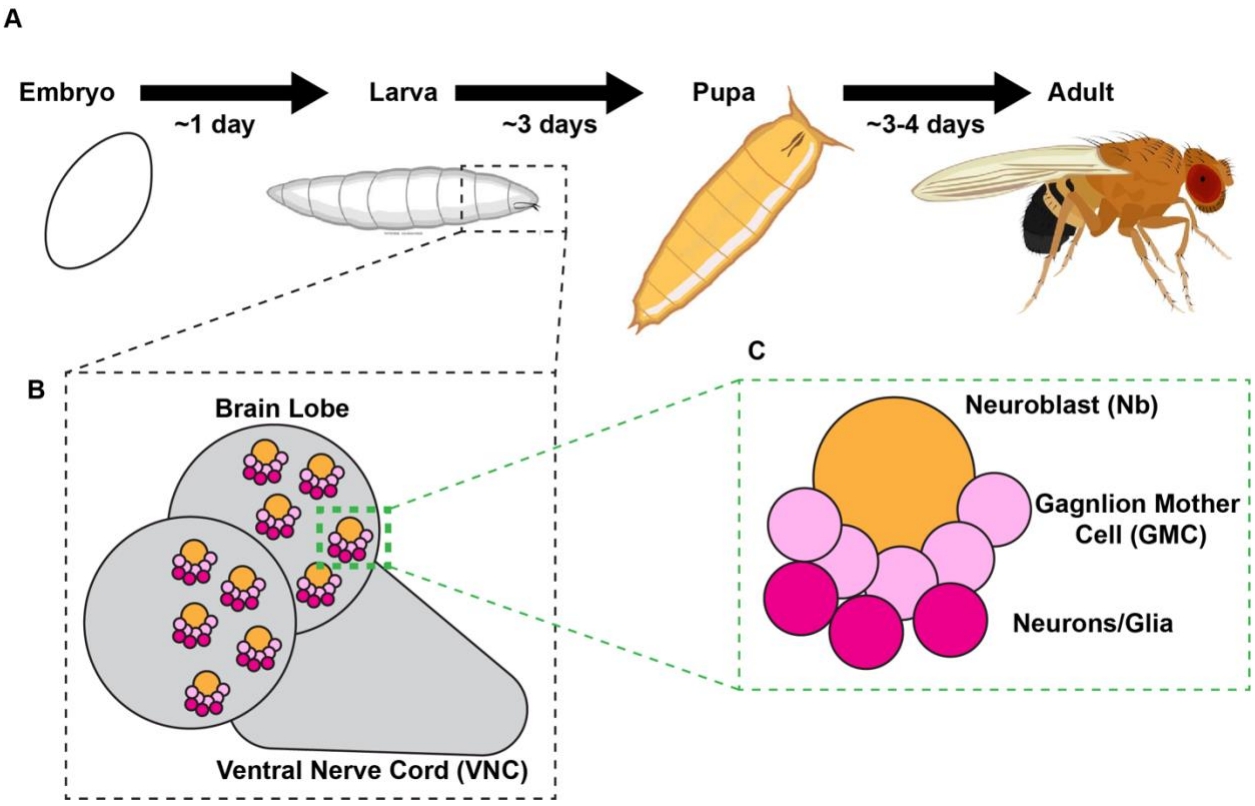

(A) Drosophila lifecycle. (B) Schematic of the *Drosophila* larval brain. (C) Schematic of neuroblasts (orange), ganglion mother cells (GMCs, light pink) and neurons/glia (magenta).

1.7.2

1.7.3 *Figure 2: Overview of Neuroblast Biology in Drosophila*

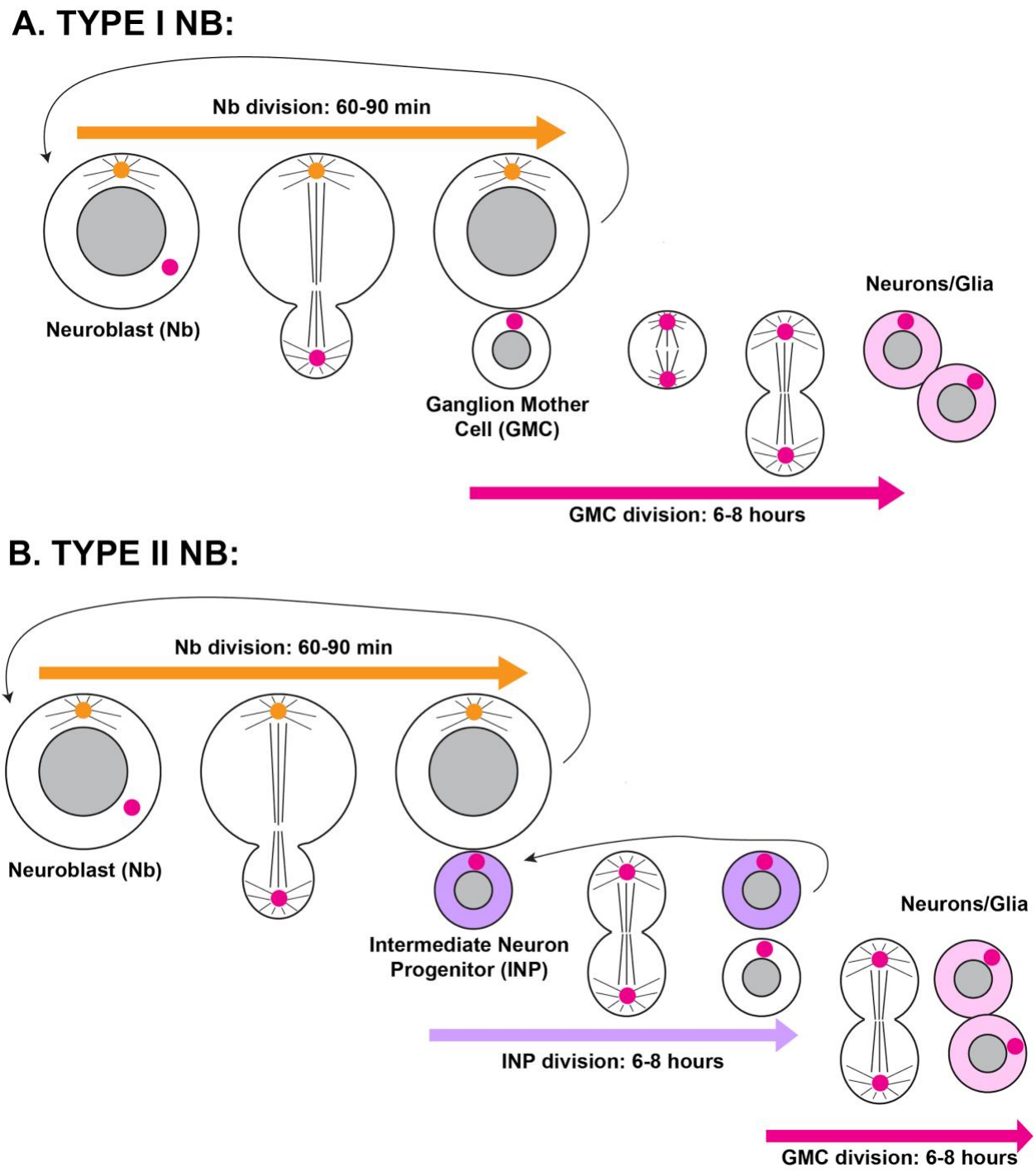

(A) Type I Neuroblasts form neuroblasts and GMCs, which then divide once more to form mature neuron and glial cells. (B) Type II neuroblasts form neuroblasts and intermediate neuronal

progenitor (INP) cells, which divide asymmetrically three to six more times to self-renew one INP and one GMC, which then divides once to form mature neuron and glial cells.

1.7.4 *Figure 3: The Centrosome Cycle in Drosophila Neuroblasts*

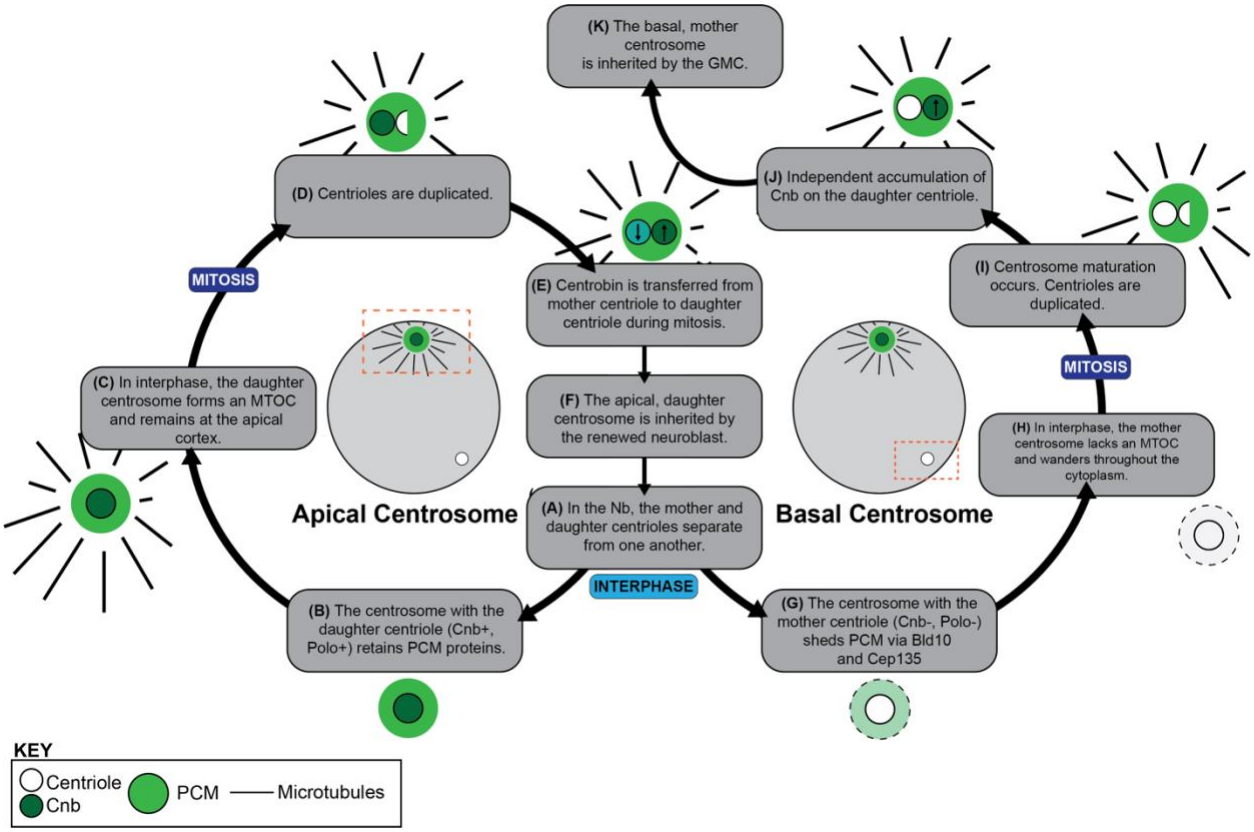

(A) early in mitosis, centrioles will separate from one another to form two new centrosomes. (B) The centrosome containing the daughter centriole will retain PCM components such as gamma tubulin and SPD2. (C) Via the microtubule supporting action of Wdr62, microtubules are incorporated into the centrosome, which allows for the recruitment of more Polo kinase to the centrosome to phosphorylate Centrobin, which retains Cnb on the centrosome. This then forms a positive feedback loop supporting an active MTOC. (D) in mitosis, centrioles will undergo duplication. (E) in tandem with centriole duplication, Centrobin is downregulated from the mother centriole and is enriched onto the nascent daughter centriole. (F) this culminates with the apical

centrosome segregating into the renewed neuroblast to begin the cycle anew. (G) in contrast to the daughter centriole in interphase, the mother centriole, lacking Centrobin, cannot retain its PCM, and instead sheds it via Bld10, Cep135 and Plk4, resulting in (H) a mother centrosome with no discernable MTOC activity. (I) After centrosome maturation, the mother centrosome acquires MTOC activity and begins to duplicate its centriole. (J) there is an independent accumulation of Centrobin on the daughter centriole at the mother centrosome, ending with (K) the basal centrosome segregating into the differentiating GMC.

CHAPTER 2. LIVE CELL IMAGING OF *DROSOPHILA* THIRD INSTAR LARVAL BRAINS

jove

Live-Cell Imaging of *Drosophila melanogaster* Third Instar Larval Brains

Roberto Carlos Segura[1], **Clemens Cabernard**[1]

[1] Department of Biology, University of Washington

Corresponding Author

Clemens Cabernard
ccabern@uw.edu

Citation

Segura, R.C., Cabernard, C. Live-Cell Imaging of *Drosophila melanogaster* Third Instar Larval Brains. *J. Vis. Exp.* (196), e65538, doi:10.3791/65538 (2023).

Date Published

June 23, 2023

DOI

10.3791/65538

URL

jove.com/video/65538

Abstract

Drosophila neural stem cells (neuroblasts, NBs hereafter) undergo asymmetric divisions, regenerating the self-renewing neuroblast, while also forming a differentiating ganglion mother cell (GMC), which will undergo one additional division to give rise to two neurons or glia. Studies in NBs have uncovered the molecular mechanisms underlying cell polarity, spindle orientation, neural stem cell self-renewal, and differentiation. These asymmetric cell divisions are readily observable *via* live-cell imaging, making larval NBs ideally suited for investigating the spatiotemporal dynamics of asymmetric cell division in living tissue. When properly dissected and imaged in nutrient-supplemented medium, NBs in explant brains robustly divide for 12-20 h. Previously described methods are technically difficult and may be challenging to those new to the field. Here, a protocol is described for the preparation, dissection, mounting, and imaging of live third-instar larval brain explants using fat body supplements. Potential problems are also discussed, and examples are provided for how this technique can be used.

Introduction

Asymmetric cell division (ACD) is the process by which subcellular components such as RNA, proteins, and organelles are partitioned unequally between daughter cells[1,2]. This process is commonly seen in stem cells, which undergo ACD to give rise to daughter cells with different developmental fates. *Drosophila* NBs divide asymmetrically to produce one NB, which retains its stemness, and one ganglion mother cell (GMC). The GMC undergoes further divisions to produce differentiating neurons or glia[3]. Asymmetrically dividing NBs are abundant in the developing brains of third-instar larvae, which are readily observed via microscopy. At the third instar larval stage, there are roughly 100 NBs present in each central brain lobe[3,4,5,6].

Asymmetric cell division is a highly dynamic process. Live-cell imaging protocols have been used to measure and quantify the dynamics of cell polarity[7,8,9,10], spindle orientation[11,12,13], the dynamics of the actomyosin cortex[14,15,16,17,18], microtubule and centrosome biology[19,20,21,22,23,24,25,26,27], and membrane[10,28] and chromatin dynamics[29]. Qualitative and

quantitative descriptions of ACD rely on robust methods and protocols to image dividing NBs in intact living brains. The following protocol outlines methods to prepare, dissect, and image third instar larval brains for live-cell imaging *in vivo* using two different mounting approaches. These methods are best suited for researchers interested in the spatiotemporal dynamics of stem cell divisions, as well as divisions in other brain cells, as they allow for short- and long-term observations of cellular events. Additionally, these techniques are readily accessible to newcomers to the field. We demonstrate the effectiveness and adaptability of this approach with larval brains expressing fluorescently tagged microtubule and cortical fusion proteins. We additionally discuss methods of analysis and considerations for application in other studies.

Protocol

NOTE: **Figure 1** shows the materials required to perform this study.

1. Considerations and preparations for the experiment

1. Prevent the larvae from overcrowding.
   NOTE: The quality of explant larval brains is directly related to the health and quality of the larvae prior to dissection. Larvae that are malnourished from overcrowding will generally yield lower-quality brains[30].
   1. Ensure that no more than 20-30 larvae are present per meal cap dish to avoid malnutrition. Examples of these can be seen in **Figure 2**.
2. Filter and aliquot Schneider's medium before use.
   1. For each dissection, prepare fresh imaging and dissection medium by supplementing aliquoted Schneider's insect medium with 1% bovine growth serum (BGS). A volume of 5 mL of dissection and imaging medium is usually sufficient for an imaging experiment.
   2. Warm the supplemented medium to room temperature (RT) before use.
3. Consider the length of the movie to be collected, and use that to factor the supplementation of the imaging medium, the mounting approach, and the acquisition settings of the microscope.
   NOTE: Under optimal conditions, NBs in brains supplemented with only BGS will robustly divide for upward of 3 h.
   1. Supplement the imaging medium by adding larval fat body tissues to the imaging medium to support divisions past 4 h when conducting experiments that require longer movies.
      NOTE: Fat bodies secrete mitogens that support NB proliferation[31], and whole fat bodies from 10 larvae are sufficient to support four to five brains. Further, samples imaged with a membrane-bound slide have been shown to divide for over 10 h[13,32], while samples imaged with a multi-well slide usually divide less often (unpublished observations).
   2. Alternatively, implement a more complex imaging medium for longer movies, as described previously[33]. Minimize photodamage by adjusting the exposure time, laser power, and sampling frequency for best results.

2. Larvae staging and collection (Figure 2)

1. Cross 1-5 day old female virgin flies with 1-7 day old adult male flies to produce progeny with the desired genotype. For optimal yield, cross 10-15 female virgins with 5-10

males. Deposit these flies into a fly cage with a meal cap (**Figure 2A-C**), and incubate at 25 °C.

2. Swap the meal cap daily. This prevents the meal caps from becoming overcrowded with larvae, which reduces the quality of the dissected brains.

3. If the meal cap is significantly covered in larvae (i.e., >30), split this meal cap in half, and replace one half with a fresh meal cap that has also been cut in half. Alternatively, swap the meal caps on a more frequent basis (i.e., every 12 h instead of every 24 h). Examples of overpopulated meal caps can be seen in **Figure 2E, F**.

4. Incubate the meal cap with larvae at 25 °C until the larvae reach the desired age.

3. Larval fat body dissection (Figure 3)

NOTE: This protocol describes dissections using a 3-well dissection dish.

1. Pipette ~400 µL of dissection and imaging medium into each well of a 3-well dissection dish.

2. Wash ten 72-96-h old well-fed wild-type larvae by gently holding them with dissection forceps and dipping them in and out of dissection solution in the bottom-most well until all food particulates have been washed off. After rinsing, move the clean larvae to the middle well.

3. Using one set of tweezers, hold the larva by the mouth hooks. With the other set of tweezers, rupture one side of the larva's cuticle.

4. This rupture will cause the fat bodies to spill out of the larva. The fat bodies are off-white and semi-translucent and will have a lattice-like structure (**Figure 3I**). The fat bodies will also tend to stick to themselves and the dissection tweezers. Once identified, collect as much fat body from each larva as possible, and transfer it with the forceps to the top-most well with 400 µL of RT dissection medium.

4. Larval brain dissection (Figure 3)

1. Wash the experimental larvae in dissection and imaging medium as above to free them of food residues. For best results, avoid storing undissected larvae in the dissection solution. This will cause the larvae to "drown" and will negatively impact the quality of the dissected brains.

2. Using one set of tweezers, hold the larva by the mouth hooks. Using another set of tweezers, gently cut/rip off approximately 1/3 of the larva from the posterior side (**Figure 3A**). This will cause elements of the digestive tract, fat bodies, connective tissue, and nervous system to "burst" out of the ruptured side of the larva (**Figure 3B**).

3. Using one set of tweezers, hold the larva by the mouth hooks. With the other set of tweezers, gently brush the cuticle toward the mouth hooks while "pushing" inward with the tweezers holding the mouth hooks until the entire larva is turned inside out. This motion is similar to turning a sock "inside out" (**Figure 3C, D**).

4. Invert the larva so that the central nervous system and other tissues face outward while still being connected to the cuticle. At this step, locate the central nervous system (CNS) to avoid accidental removal. Using tweezers, gently remove all the non-CNS tissue, leaving only the CNS and brain attached to the cuticle (**Figure 3E**).

5. The brain will be attached to the cuticle *via* axonal connections. Using microdissection scissors, cut these axonal connections to release the brain from the cuticle. To do this, first gently cut underneath the brain lobes

(**Figure 3F**). Repeat with the connections under the ventral nerve cord.

NOTE: This step may be done with tweezers if microdissection scissors are not available. Take special care when using tweezers to ensure that the brain tissue is not over-stretched during removal from the cuticle because mechanical stress will negatively affect the brain health.

6. Transfer the dissected brain into a well with dissection and imaging medium. For imaging experiments longer than 3 h, use dissection and imaging medium supplemented with fat bodies as described above. Dissect the larvae in batches to keep the dissection time under 20 min.

5. Mounting and imaging (Figure 4)

1. For imaging with a membrane-bound slide[34]:
    1. Collect both dissected brains and isolated fat bodies in the last well of the dissection dish.
    2. Assemble half of the slide by placing a gas-permeable membrane over the back of the slide, and press the split ring into the center, holding it in place (**Figure 4A-C**).
    3. Using a 200 µL micropipette, transfer up to 10 dissected brains and as much fat body as possible (see above) in ~130-140 µL of dissection and imaging medium to the membrane. Make sure to deposit the medium with the samples in the center of the gas-permeable membrane (**Figure 4D, E**).
    4. Orient the brains for the population of NBs to be imaged and for the type of microscope being used (**Figure 4E**). Position the sample as close to the microscope's objective as possible. For example, to image NBs in the central brain lobes, orient the brains such that the brain lobes are closest to the objective (**Figure 4H**).
    5. Once the brains are oriented, gently place a glass coverslip on top of the solution on the membrane. This will cause the solution containing the brains and fat bodies to spread over the entirety of the membrane (**Figure 4F**).
    6. Blot excessive solution by holding a laboratory tissue close to the coverslip edge. The optimal amount of solution is achieved when the brains touch the coverslip without being squashed. If reorientation is required at this step, carefully move the coverslip to move the brains.
    7. Immobilize the coverslip by applying melted petroleum jelly along the edges of the coverslip with a paintbrush. Allow the jelly to solidify (**Figure 4G**).
2. For imaging with a multi-well imaging slide (**Figure 4**):
    1. Add 400 µL of imaging medium to a well of a multi-well slide (in the experiment performed here, a chambered 8-well micro[µ]-slide was used; **Figure 4I**). Transfer the previously dissected fat bodies to this well (see step 3.4).
    2. Deposit up to 10 brains in a cluster near the center of the well (**Figure 4J**).
    3. Orient the brains for the population of NBs to be imaged and for the type of microscope being used, as described in step 5.1.4 (**Figure 4K**). Arrange the samples so they are close to each other. This will minimize the distance the stage must move between samples, which reduces sample drift during acquisition.

4. Once the brains have been oriented in the well, allow the brains to settle for 2-5 min. This increases their stability during transport/imaging. Prepare the microscope for acquisition during this time.
5. Cover the µ-slide with the slide cover, and transfer it to the microscope. Begin acquisition with the lowest laser power and exposure time possible to minimize photobleaching.

6. Data processing and management best practices

1. Process the data as needed according to the available analysis software.
    1. For the example shown here, save the acquired data with SlideBook software as a SlideBook Image File (.sld).
    2. To convert into Imaris' proprietary file type (.ims) using the Imaris File Converter, open the Imaris File Converter in a separate window. Click on and drag the .sld files into the " input" section of the Imaris File Converter.
    3. Determine the desired output location for the converted files, and click on "**Start all.**"
    4. After conversion, view and annotate the data in the Imaris software.

        NOTE: Alternatives for image analysis can be used in place of Imaris, such as Fiji (https://hpc.nih.gov/apps/Fiji.html), Aivia (https://www.aivia-software.com/), Volocity (https://www.volocity4d.com/), or others.
2. Retain as much of the original data as possible for proper record-keeping. For example, if the acquisition software is saved in one file format but is converted to a different format for analysis, retain the acquired version of the data.
3. For data analysis, maintain a record of as many details as possible about the sample and acquisition settings. Key information to retain includes the genotype of the dissected larvae, the age of the larvae prior to dissection, the state of the meal cap they were reared in, the laser power used during imaging, the exposure time, the length of acquisition, and the temporal resolution.

7. Example quantification of cell cycle length (Figure 5)

NOTE: in this example, larvae expressing the polarity marker Pins (Pins::EGFP[16]) and the microtubule-binding protein Jupiter[25] (cherry::Jupiter[13]) were imaged. The subsequent analysis was performed using Imaris software.

1. Open the movie using the image analysis software of choice. Scroll through the length of the movie to identify dividing NBs, and label them for future reference. Identify the dividing NBs by their distinct mitotic spindles (**Figure 5C-E**).
2. Identify a reference cell cycle stage to determine the cell cycle length. In this example, metaphase is used as a reference.
3. Manually determine the number of frames between successive metaphases, and convert it to minutes or hours to determine the time taken to complete one cell cycle.
    1. Do this by taking the temporal resolution of the movie and multiplying it by the number of frames between metaphases. For example, if the temporal resolution of the movie is one frame every 5 min, and metaphases are observed in frame 13 and frame 35,

the time between these metaphases would be 110 min ([35 − 13] × 5).

4. Plot the data with any appropriate software. The data shown here were plotted using PRISM software.

8. Example quantification of cell spindle alignment (Figure 5)

NOTE: In this example, the analysis is performed using Imaris software.

1. Open the movie file in Imaris or another software of choice. Scroll through the length of the movie to identify dividing NBs, and label them for future reference.

2. Determine the vector formed by the spindle poles using the apical and basal centrosomes (represented by *m*), as follows:

$$m(x_1, y_1, z_1) = (A_x - B_x, A_y - B_y, A_z - B_z)$$

where *Ax*, *Ay*, and *Az* are the coordinates of the apical centrosome, and *Bx*, *By*, and *Bz* are the coordinates of the basal centrosome. Similarly, the axis of the division vector (represented by *n*) is formed by the midpoint of the apical Pins::EGFP crescent and the basal cortex:

$$n(x_2, y_2, z_2) = (A_x - B_x, A_y - B_y, A_z - B_z)$$

where *Ax*, *Ay*, and *Az* are the coordinates of the midpoint of the Pins::EGFP crescent, and *Bx*, *By*, and *Bz* are the coordinates of the midpoint of the basal cortex.

3. Determine the magnitude of the vectors *m* and *n*:

Magnitude of *m*: $|m| = \sqrt{x_1^2 + y_1^2 + z_1^2}$

Magnitude of *n*: $|n| = \sqrt{x_2^2 + y_2^2 + z_2^2}$

4. Determine the dot product (represented by *k*) of *m* and *n*:

$$k = m \cdot n = (x_1 * x_2) + (y_1 * y_2) + (z_1 * z_2)$$

5. Using the dot product *k* and vector magnitudes *m* and *n*, determine the angle between the vectors:

$$Angle\ between\ Spindles\ and\ Division\ Axis: \theta = cos^{-1}\frac{k}{|m||n|}$$

6. Plot the data in the software of choice. The data shown here were prepared in Microsoft Excel and visualized in PRISM.

Representative Results

Dissection and imaging of central brain lobe NBs expressing Pins::EGFP and Cherry::Jupiter

To showcase this protocol, larvae expressing UAS-driven Cherry::Jupiter[13] and endogenously tagged Pins::EGFP[16] (w; worGal4, UAS-cherry::jupiter/CyO; Pins::EGFP/TM6B, Tb) were imaged for 4 h using the described protocol using multi-well imaging slides (**Figure 5C**,**D**). Additional data were taken from larvae expressing UAS-driven Cherry::Jupiter[13] and endogenously tagged Miranda::EGFP (w; worGal4, UAS-cherry::Zeus/CyO; UAS-Miranda::GFP/TM6B), which were imaged for 10 h using a membrane-bound slide (**Figure 5E**,**F**). Larvae were reared in cages as described in section 1 of this protocol. Upon reaching 72-96 h old, the larvae were dissected (**Figure 3**), mounted (**Figure 4**), and imaged. For the experiments performed here, a 561 nm laser was used at 10% laser power with 100 ms of exposure time, and a 488 nm laser was used at 15% laser power with 100 ms of exposure time. Z-stacks (41 µm) were acquired with a 1 µm step size. Images were acquired every 5 min at RT on an Intelligent Imaging Innovations (3i) spinning disc confocal system, consisting of a Yokogawa CSU-W1 spinning disc unit and two Prime 95B Scientific CMOS cameras. A 60x/1.4NA oil immersion objective mounted on a Nikon Eclipse Ti microscope was used for imaging. The live imaging voxels were 0.22 µm x 0.22 µm x 0.75 µm (60x/1.4NA spinning disc).

Consistent with previous reports[16], the Pins formed a pronounced apical crescent in dividing NBs during mitosis, and the mitotic spindles consistently aligned to this apical crescent (**Figure 5C**). The cell cycle length was determined by measuring the time between successive metaphases of the individual NBs (**Figure 5D**,**F**).

In samples that were imaged on a multi-well imaging slide for 4 h without fat body supplementation, the cell cycle length increased with increasing imaging time (**Figure 5C**,**D**). Samples that were imaged in fat body-supplemented medium on a membrane-bound slide did not show an increase in cell cycle length (**Figure 5E**, **F**). Furthermore, NBs with four divisions were observed on the 10 h membrane-bound slide (**Figure 5D** vs. **Figure5F**).

Lastly, the angle between the division axis and the mitotic spindle was determined using GFP-tagged Pins as a reference (schematic shown in **Figure 5G**). The division axis was determined by identifying the midpoint of the apical crescent formed by the Pins in mitosis and bisecting the cell in half (**Figure 5G**, red dashed line). As previously described, the wild-type NBs displayed mitotic spindles that were oriented no more than 30° from the division axis (Loyer and Januschke[36] and **Figure 5H**).

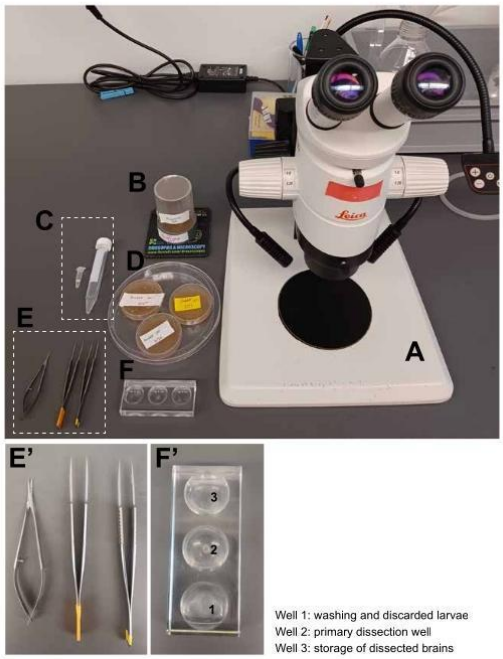

Figure 1: Materials. (**A**) Dissection microscope. (**B**) Collection cage containing flies of the desired genotype and a meal cap with growing larvae. (**C**) Dissection and imaging medium, 5 mL. (**D**) Meal caps with larvae from three different collections.

(**E**,**E'**) Microdissection tools, from left to right: microdissection scissors, forceps. (**F**,**F'**) Dissection dish. (**G**) An 8-welled µ-slide for imaging the samples. Please click here to view a larger version of this figure.

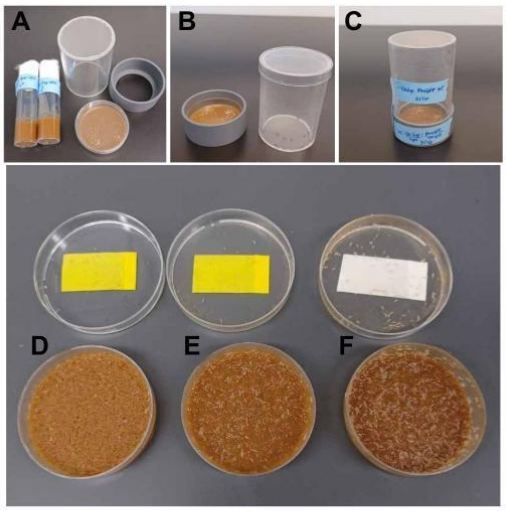

Figure 2: Example meal caps. (**A**) Two vials with male and female flies to be crossed, an empty embryo collection cage, and a fresh meal cap. (**B**) The bottom of the embryo collection cage with the new meal cap (left) and the top of the cage with flies (right). (**C**) The fully assembled fly cage. (**D**) An example of a well-staged meal cap with larvae for dissection. Note that the food is disturbed by the larvae, but not over-disturbed. (**E**,**F**) Two examples of 4 day old, overcrowded meal caps. Note that that food now has a soup-like consistency to it. Please click here to view a larger version of this figure.

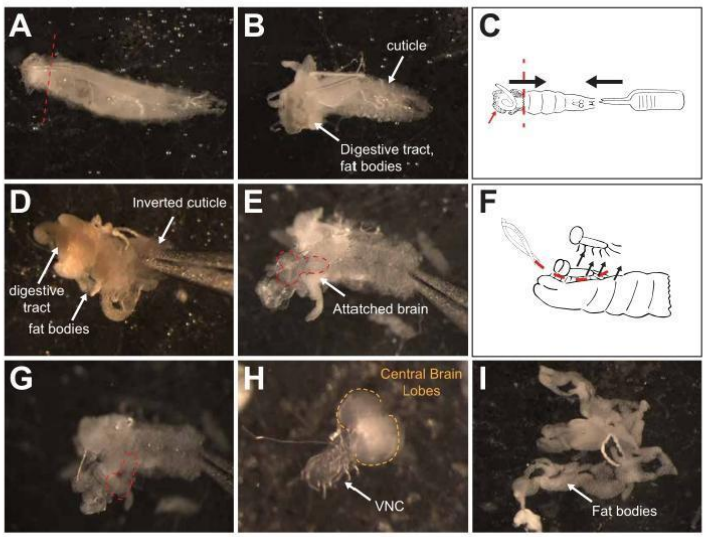

Figure 3: Dissection. (**A**) Dorsal view of a third instar larva. The red line on the posterior end of the larva denotes where the first cut should be made. (**B**) Dorsal view of the larva after removing the posterior end. (**C**) Diagram showing how to invert the larva. Using one set of forceps, hold the larva by the cuticle near where the first cut was made. Using the other forceps, press into the anterior end of the larva to invert. The black arrows denote the direction of the forceps, with one "pushing into" the larvae from the anterior side and the other moving the cut posterior end towards the anterior end. The smaller red arrow denotes a cartoon of fat bodies. (**D**) View of an inverted larva with the fat bodies and digestive tract still attached. (**E**) View of an inverted larva with the non-CNS tissue removed. The red dashed line outlines the still-attached brain. (**F**) Schematic showing how to remove the brain from the cuticle. The red dashed line indicates the path to cut with microdissection scissors to release the brain from the inverted cuticle, and the black arrows denote the removal of the brain from the cuticle. (**G**) A view of the inverted brain that is still attached to the cuticle by a small number of axonal connections under the ventral nerve cord (VNC). (**H**) An isolated larval brain. The brain lobes are outlined with dashed orange lines. (**I**) Isolated fat bodies. Please click here to view a larger version of this figure.

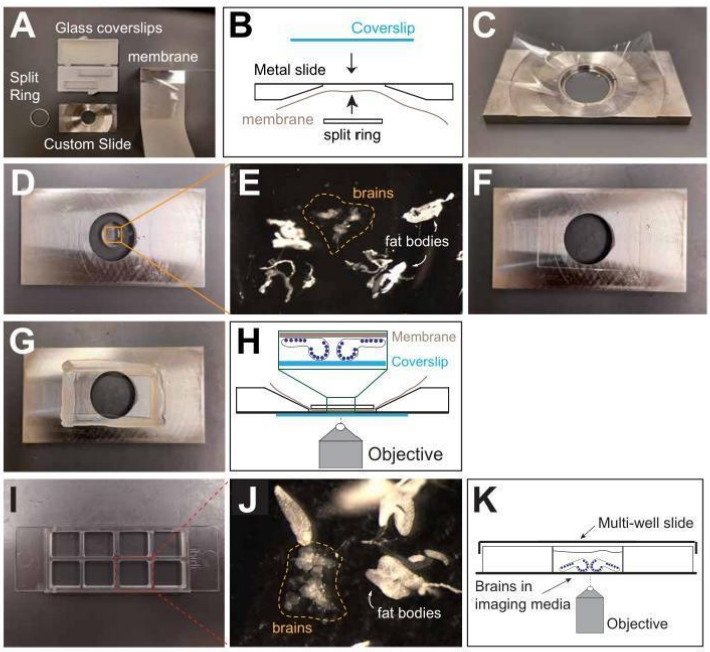

Figure 4: Mounting and imaging. (**A**) View of the components for assembling a membrane-bound metal slide. (**B**) Schematic of the components of the membrane-bound slide and their assembly. (**C**) Side view of the membrane inserted into the metal slide, held in place by the split metal ring. (**D**) Top view of the assembled imaging slide without a coverslip. The dissection and imaging medium containing fat bodies and dissected brains has been placed onto the membrane. (**E**) Zoomed-in view of the fat bodies and brains in the drop of medium. (**F**) Top view of the metal slide after adding the glass coverslip. (**G**) Top view of the assembled slide with the glass coverslip fixed to the slide with melted petroleum jelly. Covering the edges of the coverslip with petroleum jelly also prevents evaporation of the medium. (**H**) Schematic of the assembled membrane slide with brains oriented for observation on an inverted microscope. The blue circles denote NBs in the central brain lobes and VNC. (**I**) View of an empty multi-well slide. (**J**) Zoomed-in view of one well of the multi-well imaging slide. (**K**) Schematic showing the brain orientation for imaging the central brain lobes on an inverted microscope with a multi-well slide. The blue circles denote NBs in the central brain lobes and VNC. Please click here to view a larger version of this figure.

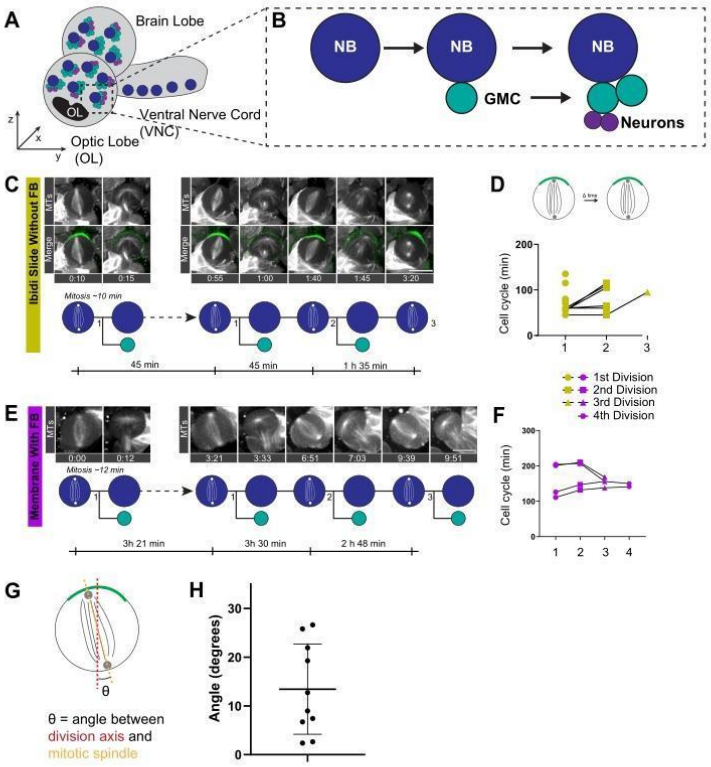

Figure 5: Quantification of the cell cycle length. (**A**) Diagram of a third instar larval brain, highlighting the brain lobes, the optic lobe (OL, dark gray), the ventral nerve cord (VNC), NBs (dark blue), GMCs (light blue), and neurons (purple) within the central brain lobes and VNC. (**B**) Schematic of NB and GMC divisions. (**C**) Image series of a wild-type NB with microtubules labeled in white (MTs, UAS-Cherry::Jupiter) and apical Pins (Pins::EGFP in green) imaged in a multi-well slide without fat body supplementation for 4 h. Merged images and the corresponding lineage tree with cell cycle timing are shown below. Scale bar = 10 µm. (**D**) Quantification of the cell cycle length (metaphase - metaphase) for the first, second, and third divisions in samples imaged on a multi-well slide without fat bodies.(**E**) Image series of a wild-type NB with microtubules labeled in white (MTs, UAS-Cherry::Jupiter) imaged with a membrane-bound slide with fat body supplementation for 10 h with the corresponding lineage tree and cell cycle timing shown below. Scale bar = 10 µm. (**F**) Quantification of cell cycle length (metaphase - metaphase) for the first, second, third, and fourth divisions in samples imaged on a membrane-bound slide with fat bodies. (**G**) Schematic of how the angle between the spindle axis (orange dashed line) and division axis (θ, red

dashed line) was determined. (**H**) Quantification of θ from 10 cells imaged using a multi-well slide without fat bodies. Please click here to view a larger version of this figure.

Discussion

This protocol outlines one approach for the imaging of live explant brains from *Drosophila melanogaster* larvae. The protocol described here allows for explant brains to be observed for 12-20 h under the right experimental conditions. Special consideration must be given to the preparation of samples and the design of the desired experiments. As mentioned above, one of the most critical factors that determines the quality of the dissected tissue is the health of the larvae. To achieve the highest quality possible, one must ensure that larvae are well-fed before collection. Unhealthy larvae most commonly originate from overcrowding. To address this, one must ensure that overcrowding is minimized, either by increasing the frequency of harvest or by splitting dishes with freshly laid eggs with an empty dish.

Another critical element of this protocol is the method of dissection to isolate the brain tissue. The brain and the NBs within them are extremely sensitive to outside factors, such as the temperature of the dissection medium and the invasiveness of the dissection itself. Medium that is too cold will tend to depolymerize the microtubules. Similarly, a dissection that stretches or ruptures the brain will have detrimental effects on the quality of the NBs. To prevent this, one should avoid pulling on the brain tissue directly and instead anchor the dissection tools on the cuticle or other tissue. Microdissection scissors greatly assist in this regard, as they minimally pull on the brain tissue. If scissors are not available, tweezers can be used to carefully remove the connecting tissue between the ventral nerve cord and the cuticle.

This protocol presents two methods to mount larval brains for confocal microscopy. From a technical standpoint, mounting samples in a multi-well slide is simpler than mounting on a membrane-bound slide. However, each method is best suited for different types of experiments. The data shown here demonstrate that for shorter movies (i.e., less than 4 h) or movies with high temporal resolution (i.e., acquiring a z-stack every 10 s), imaging in a multi-well slide is sufficient to observe multiple divisions in the larval central brain. For longer acquisition windows, mounting on a membrane-bound slide is ideal, as samples prepared this way divide more frequently throughout the movie. Normally, wild-type larval NBs divide once every 40-90 min[13]. Although multi-well slides can be used for long (> 4 h) movies, an increase in the cell cycle length and a decrease in proliferating NBs has been observed in this condition (**Figure 5D**). Therefore, the method used to mount samples and the type of data to be measured must be considered when designing experiments.

This protocol recommends imaging multiple brains in one well or slide, as this increases the efficiency of data collection for any given experiment. However, the orientation and placement of the brains within the well will affect how much shifting occurs throughout the movie due to the stage moving between brain positions. Clustering the brains together in one centralized spot in a well minimizes this issue. However, some shifting may occur over the course of longer movies in experiments using multi-well slides. In many cases, the shifting observed in these longer movies is minimal and can be corrected during analysis. Brain movement is also preventable by using a metal slide setup because the capillary forces prevent the dissected brains from shifting.

With a multi-well slide, it is technically possible to perform multi-well imaging experiments. However, this requires adjustments in the stack size and temporal resolution to account for the extra time spent by the microscope moving between positions. This may be beneficial for large-scale genetic screening experiments, where one may image multiple genotypes in different wells.

There are instances where brains will display little or no dividing NBs over the course of an experiment. This is likely due to several factors that depend on the nature of the sample being imaged, the quality of the food used to rear the larvae, the quality of the dissection, and the acquisition settings used to generate the data. Although it is advisable to remove as much tissue as possible when preparing larval brains for imaging, it is ill-advised to over-prune the brain to minimize mechanical stress, as this may negatively impact the quality of the data. Additionally, frequent exposure to powerful imaging lasers will negatively impact the neuroblast health. Thus, one should consider adjusting the laser power, exposure time, and imaging frequency when collecting the imaging data.

For mounting samples, alternative methods may be used. For instance, explant brains can be mounted in a solid matrix[37]. The availability of different mounting protocols provides an opportunity to image larval brain explants on a wide variety of microscopes.

Disclosures

The authors have no financial disclosures to declare.

Acknowledgments

This research is supported by R35GM148160 (C. C.) and a National Institutes of Health (NIH) Training Grant T32 GM007270 (R. C. S)

References

1. Delgado, M. K., Cabernard, C. Mechanical regulation of cell size, fate, and behavior during asymmetric cell division. *Current Opinion in Cell Biology*. **67**, 9-16 (2020).
2. Sunchu, B., Cabernard, C. Principles and mechanisms of asymmetric cell division. *Development*. **147** (13), dev167650 (2020).
3. Homem, C. C. F., Knoblich, J.A. Drosophila neuroblasts: A model for stem cell biology. *Development*. **139** (23), 4297-4310 (2012).
4. Gallaud, E., Pham, T., Cabernard, C. *Drosophila melanogaster* neuroblasts: A model for asymmetric stem cell divisions. *Results and Problems in Cell Differentiation*. **61** (1489), 183-210 (2017).
5. Loyer, N., Januschke, J. Where does asymmetry come from? Illustrating principles of polarity and asymmetry establishment in *Drosophila* neuroblasts. *Current Opinion in Cell Biology*. **62**, 70-77 (2020).
6. Pollington, H. Q., Seroka, A. Q., Doe, C. Q. From temporal patterning to neuronal connectivity in *Drosophila* type I neuroblast lineages. *Seminars in Cell & Developmental Biology*. **142**, 4-12 (2023).
7. Oon, C. H., Prehoda, K. Asymmetric recruitment and actin dependent cortical flows drive the neuroblast polarity cycle. *eLife*. **8**, e45815 (2019).
8. Ramat, A., Hannaford, M., Januschke, J. Maintenance of miranda localization in *Drosophila* neuroblasts involves interaction with the cognate mRNA. *Current Biology*. **27** (14), 2101-2111.e5 (2017).

9. Oon, C. H., Prehoda, K. E. Phases of cortical actomyosin dynamics coupled to the neuroblast polarity cycle. *eLife.* **10**, e66574 (2021).
10. LaFoya, B., Prehoda, K. E. Actin-dependent membrane polarization reveals the mechanical nature of the neuroblast polarity cycle. *Cell Reports.* **35** (7), 109146 (2021).
11. Siller, K. H., Doe, C. Q. Lis1/dynactin regulates metaphase spindle orientation in *Drosophila* neuroblasts. *Developmental Biology.* **319** (1), 1-9 (2008).
12. Siller, K. H., Cabernard, C., Doe, C. Q. The NuMA-related Mud protein binds Pins and regulates spindle orientation in *Drosophila* neuroblasts. *Nature Cell Biology.* **8** (6), 594-600 (2006).
13. Cabernard, C., Doe, C. Q. Apical/basal spindle orientation is required for neuroblast homeostasis and neuronal differentiation in *Drosophila*. *Developmental Cell.* **17** (1), 134-141 (2009).
14. Cabernard, C., Prehoda, K. E., Doe, C. Q. A spindle-independent cleavage furrow positioning pathway. *Nature.* **467** (7311), 91-94 (2010).
15. Connell, M., Cabernard, C., Ricketson, D., Doe, C. Q., Prehoda, K. E. Asymmetric cortical extension shifts cleavage furrow position in *Drosophila* neuroblasts. *Molecular Biology of the Cell.* **22** (22), 4220-4226 (2011).
16. Tsankova, A., Pham, T. T., Garcia, D. S., Otte, F., Cabernard, C. Cell polarity regulates biased myosin activity and dynamics during asymmetric cell division via *Drosophila* rho kinase and protein kinase N. *Developmental Cell.* **42** (2), 143-155.e5 (2017).
17. Montembault, E. et al. Myosin efflux promotes cell elongation to coordinate chromosome segregation with cell cleavage. *Nature Communications.* **8** (1), 326 (2017).
18. Roubinet, C. et al. Spatio-temporally separated cortical flows and spindle geometry establish physical asymmetry in fly neural stem cells. *Nature Communications.* **8** (1), 1383 (2017).
19. Januschke, J. et al. Centrobin controls mother-daughter centriole asymmetry in *Drosophila* neuroblasts. *Nature Cell Biology.* **15** (3), 241-248 (2013).
20. Januschke, J., Llamazares, S., Reina, J., Gonzalez, C. *Drosophila* neuroblasts retain the daughter centrosome. *Nature Communications.* **2** (1), 243 (2011).
21. Rebollo, E. et al. Functionally unequal centrosomes drive spindle orientation in asymmetrically dividing *Drosophila* neural stem cells. *Developmental Cell.* **12** (3), 467-474 (2007).
22. Januschke, J., Gonzalez, C. The interphase microtubule aster is a determinant of asymmetric division orientation in *Drosophila* neuroblasts. *The Journal of Cell Biology.* **188** (5), 693-706 (2010).
23. Rusan, N. M., Peifer, M. A role for a novel centrosome cycle in asymmetric cell division. *The Journal of Cell Biology.* **177** (1), 13-20 (2007).
24. Lerit, D.A. et al. Interphase centrosome organization by the PLP-Cnn scaffold is required for centrosome function. *Journal of Cell Biology.* **210** (1), 79-97 (2015).
25. Gallaud, E. et al. Dynamic centriolar localization of Polo and Centrobin in early mitosis primes centrosome asymmetry. *PLoS Biology.* **18** (8), e3000762 (2020).
26. Ramdas Nair, A. et al. The microcephaly-associated protein Wdr62/CG7337 is required to maintain

centrosome asymmetry in *Drosophila* neuroblasts. *Cell Reports*. **14** (5), 1100-1113 (2016).

27. Singh, P., Nair, A. R., Cabernard, C. The centriolar protein Bld10/Cep135 is required to establish centrosome asymmetry in *Drosophila* neuroblasts. *Current Biology*. **24** (13), 1548-1555 (2014).
28. LaFoya, B., Prehoda, K. E. Consumption of a polarized membrane reservoir drives asymmetric membrane expansion during the unequal divisions of neural stem cells. *Developmental Cell*. S1534-5807 (23), 00159-4 (2023).
29. Sunchu, B. et al. Asymmetric chromatin retention and nuclear envelopes separate chromosomes in fused cells in vivo. *Communications Biology*. **5** (1), 953 (2022).
30. Oliveira, A. C., Rebelo, A. R., Homem, C. C. F. Integrating animal development: How hormones and metabolism regulate developmental transitions and brain formation. *Developmental Biology*. **475**, 256-264 (2021).
31. Britton, J. S., Edgar, B. A. Environmental control of the cell cycle in Drosophila: nutrition activates mitotic and endoreplicative cells by distinct mechanisms. *Development*. **125** (11), 2149-2158 (1998).
32. Lee, C. -Y. et al. *Drosophila* Aurora-A kinase inhibits neuroblast self-renewal by regulating aPKC/Numb cortical polarity and spindle orientation. *Genes & Development*. **20** (24), 3464-3474 (2006).
33. Homem, C. C. F., Reichardt, I., Berger, C., Lendl, T., Knoblich, J. A. Long-term live cell imaging and automated 4D analysis of *Drosophila* neuroblast lineages. *PLoS ONE*. **8** (11), e79588 (2013).
34. Cabernard, C., Doe, C.Q. Live imaging of neuroblast lineages within intact larval brains in Drosophila. *Cold Spring Harbor Protocols*. **2013** (10), 970-977 (2013).
35. Karpova, N., Bobinnec, Y., Fouix, S., Huitorel, P., Debec, A. Jupiter, a new *Drosophila* protein associated with microtubules. *Cell Motility and the Cytoskeleton*. **63** (5), 301-312 (2006).
36. Loyer, N., Januschke, J. The last-born daughter cell contributes to division orientation of Drosophila larval neuroblasts. *Nature Communications*. **9** (1), 3745 (2018).
37. Bostock, M.P. et al. An immobilization technique for long-term time-lapse imaging of explanted *Drosophila* tissues. *Frontiers in Cell and Developmental Biology*. **8**, 590094 (2020).

CHAPTER 3. ASYMMETRY OF CENTROSOMES IN *DROSOPHILA* NEURAL STEM CELLS REQUIRES PROTEIN PHOSPHATASE 4

MBoC | ARTICLE

Asymmetry of centrosomes in *Drosophila* neural stem cells requires protein phosphatase 4

Roberto Carlos Segura[a], Emmanuel Gallaud[a,†], Adam von Barnau Sythoff[a,‡], Kumar Aavula[§,‖], Jennifer A. Taylor[a], Danielle Vahdat[a], Fabian Otte[a,‖], Jan Pielage[b], and Clemens Cabernard[a,*]

[1]Department of Biology, University of Washington, Life Sciences Building, Seattle, WA 98105; [2]Department of Neurobiology, RPTU University of Kaiserslautern, 67663 Kaiserslautern, Germany

ABSTRACT **Asymmetric cell division is used by stem cells to create diverse cell types while self-renewing the stem cell population. Biased segregation of molecularly distinct centrosomes could provide a mechanism to maintain stem cell fate, induce cell differentiation or both. However, the molecular mechanisms generating molecular and functional asymmetric centrosomes remain incompletely understood. Here, we show that in asymmetrically dividing fly neural stem cells, protein phosphatase 4 (Pp4) is necessary for correct centrosome asymmetry establishment during mitosis, and microtubule organizing center (MTOC) maintenance in interphase. Using in vivo live-cell imaging, we show that while wild-type neural stem cells always maintain one active MTOC, *Pp4* mutant neuroblasts contain two inactive centrioles in interphase. Furthermore, centrosomes of *Pp4* mutant neural stem cells mature in mitosis but fail to correctly transfer the centriolar protein Centrobin (Cnb) from the mother to the daughter centriole. Using superresolution imaging, we find that phosphomimetic Centrobin fails to accurately relocalize in mitosis. We propose that Pp4 regulates the timely relocalization of Cnb in mitosis to establish two molecularly distinct centrosomes. In addition, Pp4 is also necessary to maintain MTOC activity in interphase, ensuring biased centrosome segregation. Mechanistically, Pp4 could regulate centrosome asymmetry by dephosphorylating both Cnb and gamma-Tubulin.**

SIGNIFICANCE STATEMENT

- Asymmetric centrosome segregation occurs in stem cells and has been linked with cell fate decisions.
- Protein phosphatase 4 (Pp4), a conserved serine/threonine phosphatase, regulates centrosome asymmetry in *Drosophila* neural stem cells by acting upon gamma tubulin and Centrobin.
- Pp4 regulates centrosome asymmetry establishment in mitosis and interphase, necessary for biased centrosome segregation.

Monitoring Editor
Dennis Discher
University of Pennsylvania

Received: Jan 17, 2025
Revised: Mar 6, 2025
Accepted: Mar 7, 2025

This article was published online ahead of print in MBoC in Press (http://www.molbiolcell.org/cgi/doi/10.1091/mbc.E25-01-0021) on March 12, 2025.

†Present addresses: Institut National de Recherche pour l'Agriculture, l'Alimentation et l'Environnement, Laboratoire de Physiologie et Génomique des Poissons, 35000, Rennes, France;

INTRODUCTION

Asymmetric cell division (ACD) is an evolutionarily conserved process that produces two cells with different fates. Stem cells routinely employ ACD to produce differentiating cells while maintaining a pool of stem cells at the same time. ACD can induce binary cell fate decisions through biased segregation of proteins, RNAs or organelles such as centrosomes (Rebollo *et al.*, 2007a; Yamashita *et al.*, 2007; Lerit *et al.*, 2013; Collins *et al.*, 2017; Shlyakhtina *et al.*, 2019; Delgado and Cabernard, 2020; Sunchu and Cabernard, 2020a; Gonzalez, 2021).

Centrosomes are the microtubule organization centers (MTOCs) of the cell and are composed of a pair of centrioles surrounded by a layer of pericentriolar matrix proteins (PCM). Centrioles duplicate once every cell cycle, whereby a single centriole provides a template for the formation of a younger daughter centriole. Based on this cycle, centrioles are intrinsically asymmetric by age (Conduit *et al.*, 2015; Blanco-Ameijeiras *et al.*, 2022). Mother and daughter centrioles will later separate and form two new centrosomes (Conduit *et al.*, 2015). Centrioles are also molecularly distinct. For instance, proteins such as Ninein, Cep194, and outer dense fiber protein 2 (ODF2) localize to the mother centriole, while Centrobin only localizes to the daughter centriole (Chen and Yamashita, 2021; Jaiswal and Singh, 2021).

Asymmetric or biased centrosome segregation has been observed in different organisms and various stem cell lineages, and the biased inheritance of centrosomes may provide a mechanistic explanation for the delivery of determinants important for cell fate decisions and development (Lambert and Nagy, 2002; Yamashita *et al.*, 2007; Collins *et al.*, 2017; Chen and Yamashita, 2021; Royall and Jessberger, 2021). For instance, in the developing mouse cortex, the self-renewing neuron progenitor cell (NPC) inherits the older mother centrosome, while the differentiating neuron receives the younger daughter centrosome (Wang *et al.*, 2009). This is further observed in human embryonic stem cell–derived forebrain organoids, where the mother centrosome is preferentially inherited by the renewing NPC. Disrupting this asymmetric centrosome segregation alters NPCs' fate decisions and their maintenance in the Ventral Zone (VZ) of human cortical organoids (Royall *et al.*, 2023). Many genes that regulate centrosome function and asymmetry have also been implicated in developmental disabilities, such as primary microcephaly (Nigg and Raff, 2009; Gilmore and Walsh, 2013; Conduit *et al.*, 2015; Ramdas Nair *et al.*, 2016a; Link *et al.*, 2019; Marthiens and Basto, 2020; Robinson *et al.*, 2020; Jaiswal and Singh, 2021). However, there are fundamental gaps in our understanding of the underlying regulation of centrosome asymmetry, its function in ACD, and its impact on development.

Drosophila neural stem cells, called neuroblasts, provide an ideal model to study centrosome asymmetry. *Drosophila* neural stem cells divide asymmetrically, giving rise to a self-renewed neuroblast and a differentiating ganglion mother cell (GMC) (Gallaud *et al.*, 2020a). Neuroblasts invariably retain the daughter centriole-containing centrosome (hereafter daughter centrosome), whereas differentiating GMCs inherit the older mother centriole-containing centrosome (hereafter mother centrosome) (Rusan and Peifer, 2007a; Homem and Knoblich, 2012; Januschke *et al.*, 2013a; Lerit *et al.*, 2013). These centrosomes further differ in MTOC activity, where the daughter centrosome maintains MTOC activity throughout interphase while the mother centrosome sheds PCM proteins in early interphase and remains inactive until centrosome maturation in prophase. Whereas microtubule-nucleating daughter centrosomes remain anchored to the apical cell cortex, the inactive mother centrosome moves through the cytoplasm on the interphase microtubule network as Kinesin-1 cargo until prophase before being positioned on the basal cell cortex (Rebollo *et al.*, 2007a; Rusan and Peifer, 2007a; Singh *et al.*, 2014b; Hannaford *et al.*, 2022a).

This difference in MTOC activity is determined by the centrosome's molecular identity. In interphase neuroblasts, the apical centrosome retains the daughter-centriole protein Centrobin (Cnb) and the mitotic kinase Polo (Plk1). Polo and PCM proteins are shed from the basal centrosome via the actions of Pericentrin-like protein (Plp), Polo kinase 4 (Plk4), and Bld10 (Januschke *et al.*, 2013a; Singh *et al.*, 2014b; Lerit *et al.*, 2015; Ramdas Nair *et al.*, 2016a; Gambarotto *et al.*, 2019; Gallaud *et al.*, 2020a). Centrobin interacts with γTubulin and other PCM members such as Plp, Sas-4, Sas-6, and Centrosomin (Cnn), and is required for the maintenance of MTOC activity in interphase (Januschke *et al.*, 2013a; Ramdas Nair *et al.*, 2016a). Centrobin's localization is dependent on phosphorylation by Polo, and proper microtubule nucleation is required for active recruitment of Polo to the apical centrosome (Januschke *et al.*, 2013a; Gallaud *et al.*, 2020a). Recently, we showed that neuroblast centrioles replicate in mitosis, isochronous with a dynamic relocalization of Centrobin from the original mother centriole to the nascent daughter centriole. This transfer is facilitated by Polo-mediated phosphorylation of Cnb, such that by the end of mitosis, only the daughter centriole contains Cnb. Upon centriole separation, the younger Cnb^{+} centriole retains microtubule-nucleating activity, tethering it to the apical neuroblast cortex, whereas the older Cnb^{-} centriole sheds Polo and PCM, thereby down-regulating MTOC activity (Singh *et al.*, 2014b; Gallaud *et al.*, 2020a). Thus, dynamic Cnb relocalization in mitosis is necessary to establish centrosome asymmetry, manifested in biased MTOC activity in the following interphase (Gallaud *et al.*, 2020a).

The molecular mechanisms of centrosome asymmetry in general and Cnb relocalization in particular are largely unknown. Because Polo regulates Cnb's dynamic relocalization in mitosis, we reasoned that yet-to-be identified phosphatases could also regulate centrosome asymmetry in fly neural stem cells. Here, we characterize protein phosphatase 4 (Pp4), a conserved serine/threonine phosphatase belonging to the phosphoprotein phosphatase superfamily as a new regulator of neuroblast centrosome asymmetry in vivo. Pp4 regulates centrosome maturation, and spindle orientation in the developing neocortex and in stem cell development (Helps *et al.*, 1998; Kloeker and Wadzinski, 1999; Sumiyoshi *et al.*, 2002; Martin-Granados *et al.*, 2008; Toyo-oka *et al.*, 2008; Sousa-Nunes *et al.*, 2009; Lyu *et al.*, 2013; Voss *et al.*, 2013; Xie *et al.*, 2013; Karman *et al.*, 2020a; Park and Lee, 2020). Pp4 localizes to

‡Present addresses: Department of Veterans Affairs, Puget Sound Health Care System, Seattle, WA 98108;

§Present addresses: Department of Cell Biology, Blavatnik institute, Harvard Medical School, Boston, 02115, MA;

‖Present addresses: Department of Biomedicine, University of Basel, Basel, Switzerland

Author contributions: R.C.S., E.G., K.A., J.P., and C.C. conceived and designed the experiments; R.C.S., E.G., A.v.B.S., J.A.T., and F.O. performed the experiments; R.C.S. and D.V. analyzed the data; R.C.S. and C.C. drafted the article; R.C.S. prepared the digital images.

Conflicts of interest: The authors declare no competing financial interests.

[AQ2] *Address correspondence to: Clemens Cabernard (ccabern@uw.edu).

centrosomes in both human neuronal progenitor cells and in developing fly embryos, where it is required for microtubule nucleation, growth, and stabilization (Helps *et al.*, 1998). Pp4 forms a complex with two regulatory subunits Pp4R2 and Pp4R3 (Falafel, Flfl), the latter of which has been shown to be a key mediator of cell fate determinants in neuroblast divisions (Sousa-Nunes *et al.*, 2009; Connell *et al.*, 2021). We show that the removal of Pp4 results in a loss of MTOC activity in interphase neuroblasts without compromising centrosome maturation in mitosis. *Pp4* mutants also show altered Centrobin and Polo localization in interphase and mitosis. We propose that Pp4 plays dual roles in the regulation of centrosome asymmetry in neural stem cells: in interphase, Pp4 dephosphorylates γTubulin to promote microtubule nucleation, and in mitosis, Pp4 dephosphorylates Centrobin to facilitate its transfer from mother to daughter centriole.

RESULTS

Pp4 is required for centrosome MTOC asymmetry in neural stem cells

We identified Pp4-19C, the catalytic subunit of the Pp4 complex (Pp4, hereafter. PPP4C in humans) as a possible regulator of centrosome asymmetry in a phosphatase RNAi screen (Supplemental Figure S1A). To characterize Pp4's role in centrosome asymmetry, we generated a CRISPR-Cas9 deletion allele (see *Materials and Methods*), that removed *Pp4*'s entire coding sequence ($Pp4^{\Delta}$ hereafter) and performed live-cell imaging experiments in intact larval brains (see *Materials and Methods* for details). To that end, we crossed the MTOC marker mCherry::Jupiter (Cabernard and Doe, 2009a) (Jupiter encodes a microtubule [MT]-binding protein [Karpova *et al.*, 2006]) and the centriolar marker Asl::GFP (Blachon *et al.*, 2008a) to $Pp4^{\Delta}$ flies. As reported previously (Rebollo *et al.*, 2007a; Lerit *et al.*, 2013; Singh *et al.*, 2014b; Ramdas Nair *et al.*, 2016a; Gallaud *et al.*, 2020a), the apical centrosome maintained robust MTOC activity in wild-type interphase neuroblasts, whereas the basal centriole contained little to no mCherry::Jupiter signal (Figure 1A; timepoints −00:32 and −00:29; orange and magenta dashed boxes, respectively; Supplemental Movie 01). Upon entering prophase, the basal centrosome began to mature, forming an active MTOC (Figure 1A, timepoint −00:14; magenta dashed box). From prometaphase through metaphase, apical and basal centrosomes contained comparable levels of MTOC activity (timepoints −00:04 and 00:00, Figure 1, A, C, and D). In contrast to wild type, 100% of $Pp4^{\Delta}$ mutant neuroblasts failed to maintain an active apical MTOC in interphase (0xMTOC, hereafter; Figure 1B, timepoints −1:03 and −0:36; Supplemental Movie 02; Supplemental Figure S1B). However, both centrosomes matured normally and displayed robust mCherry::Jupiter signal from prometaphase onward (Figure 1, B–D, timepoints −00:09 and −00:06).

$Pp4^{\Delta}$'s loss of MTOC activity phenotype could be rescued by expressing full-length wild-type *Pp4* (5X-UAS-Pp4::GFP) in $Pp4^{\Delta}$ mutants, using the neuroblast specific worniuGal4 (worGal4 [Albertson *et al.*, 2004]) driver (Figure 1, E and F). To test whether interphase MTOC activity depends on Pp4's catalytic activity, we expressed a phosphatase-dead (10X-UAS-Pp4[D85N, H115N]) construct in $Pp4^{\Delta}$ mutants. Pp4[D85N, H115N] carries mutations to the predicted active (D85) and binding (H115) sites of Pp4 (Umezawa *et al.*, 2010; Park and Lee, 2020; Sandal *et al.*, 2021). $Pp4^{\Delta}$ mutant neuroblasts expressing 10X-UAS-Pp4[D85N, H115N] still lacked MTOC asymmetry, matching the phenotype seen in *Pp4* mutants (Figure 1, G and H).

Sustaining an active MTOC in interphase allows the apical centrosome to maintain its position in the apical region, presumably via interactions with the cell cortex (Lerit *et al.*, 2013; Singh *et al.*, 2014b; Ramdas Nair *et al.*, 2016a; Varadarajan and Rusan, 2018; Hannaford and Rusan, 2024). Because in $Pp4^{\Delta}$ mutant neuroblasts the apical centrosome loses MTOC activity, we hypothesized that the lack of a robust interphase MTOC could compromise the centrosome's apical tethering. To compare the apical centrosome's position in wild type with $Pp4^{\Delta}$ mutants, we recorded the position of the centrosome in interphase and metaphase and calculated the deviation angle between the two timepoints. Apical wild-type centrosomes do not move much between interphase and mitosis, consistent with an observed average angle of displacement of 33.0° (± 18.8°). Basal wild-type centrosomes display more movement between interphase and metaphase, with an observed average displacement angle of 101° (± 36.0; Figure 1, I and K). In $Pp4^{\Delta}$ mutants, the average displacement angle of the apical centrosome—defined as the centrosome that segregates into the renewed neuroblast—increased to 55.7° (± 39.5), and the average displacement angle of the basal centrosome was 90.6° (± 38.2; Figure 1, J and K). Comparing wild type with $Pp4^{\Delta}$ mutant neuroblasts show that apical, but not basal centrosome positioning is more varied in $Pp4^{\Delta}$ mutants (Figure 1K). Together, these data suggest that Pp4 maintains interphase MTOC activity in fly neural stem cells via its catalytic activity, which is necessary for tethering the active centrosome to the apical neuroblast cortex.

Pp4's regulatory subunits Pp4r2 and Pp4r3 are required for interphase MTOC activity

Pp4 is part of a heterotrimeric complex, consisting of the catalytic subunit Pp4c and two regulatory subunits, Pp4r2 and Pp4r3 (Pp4r3 is called Falafel (Flfl) in *Drosophila*) (Lipinszki *et al.*, 2015a; Karman *et al.*, 2020a; Park and Lee, 2020). Flfl is responsible for directing Pp4 to the centromere to regulate kinetochore integrity during mitosis and facilitates the basal localization of the basal cell fate determinant Miranda (Mira) (Sousa-Nunes *et al.*, 2009; Lipinszki *et al.*, 2015a). Additionally, Flfl physically interacts with the daughter-centriole protein Centrobin (Karman *et al.*, 2020b). To test whether Falafel is also required for interphase centrosome MTOC asymmetry, we imaged *flfl* mutant neuroblasts (*flfl[795]* (Sousa-Nunes *et al.*, 2009) crossed to a deficiency, removing the entire *flfl* locus), expressing mCherry::Jupiter and Asl::GFP. Similar to $Pp4^{\Delta}$ mutants, we observed that *flfl[795]/def* mutant neuroblasts lacked interphase MTOC activity (Supplemental Figure S2, A–D).

Previous work identified Pp4r2 as a regulatory subunit responsible for binding to Pp4 substrates (Park and Lee, 2020). We sought to determine whether Pp4r2 was also required for regulating neuroblast centrosome asymmetry. We knocked down Pp4r2 with inducible RNAi in fly neuroblasts, coexpressing the MTOC marker mCherry::Jupiter and the centriolar marker Asl::GFP. We observed that 25% of cells showed a phenotype identical to that seen in $Pp4^{\Delta}$ mutants (timepoints 0:10 and 0:16 in Supplemental Figure S2E). We also observed a subset of cells that showed two active MTOCs in interphase (2xMTOC, hereafter. Supplemental Figure S2, F–H). From these data, we conclude that both Pp4r2 and Pp4r3 are required for interphase MTOC asymmetry.

Pp4 is required for interphase γTubulin localization at the apical centrosome

Pp4 interacts with γTubulin in vitro (Helps *et al.*, 1998; Sumiyoshi *et al.*, 2002; Martin-Granados *et al.*, 2008; Alvarado-Kristensson *et al.*, 2009; Voss *et al.*, 2013; Karman *et al.*, 2020a) and is required

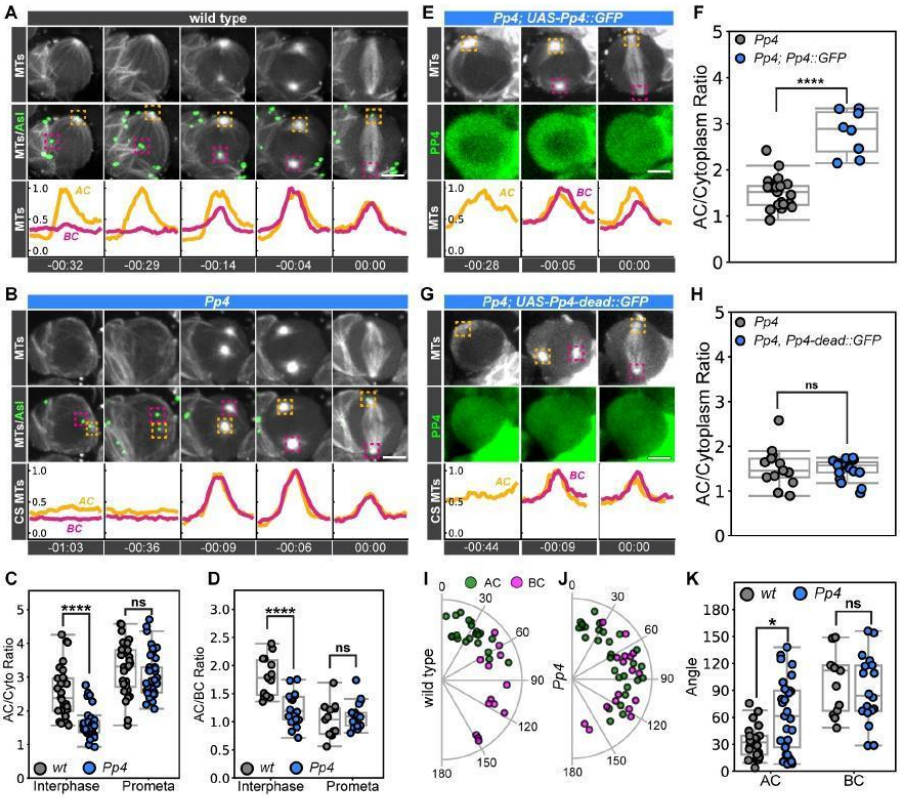

FIGURE 1: Pp4 is required for centrosome asymmetry in fly neural stem cells.Representative image sequences of a (A) wild-type and (B) $Pp4^{\Delta}$ mutant neuroblast, expressing *worGal4, UAS-mCherry::Jupiter* (gray, top row) and *Asterless::GFP* (green, merge on second row). Orange and magenta dashed boxes denote the apical (AC) and basal (BC) centrosome, respectively. Line scans of microtubule intensity at the apical (orange) and basal (magenta) centrosomes are shown below. (C) Normalized AC/Cytoplasm ratio of microtubule intensity in wild-type (gray) and $Pp4^{\Delta}$ mutant (blue) neuroblasts for interphase and prometaphase. (D) Normalized AC/BC ratio of microtubule intensity in wild-type (gray) and $Pp4^{\Delta}$ mutant (blue) neuroblasts for interphase and prometaphase. (E) Representative image sequence showing a $Pp4^{\Delta}$ mutant neuroblast-expressing *worGal4, UAS-mCherry::Jupiter* (gray, top row) and *UAS-Pp4::GFP* (green, second row). (F) Normalized AC/Cytoplasm ratio of microtubule intensity in interphase $Pp4^{\Delta}$ mutant neuroblasts (gray) and $Pp4^{\Delta}$ mutant neuroblasts, expressing *UAS-Pp4::GFP* (blue) under control of *worGal4*. (G) Representative image sequence showing a $Pp4^{\Delta}$ mutant neuroblast-expressing *worGal4, UAS-mCherry::Jupiter* (gray, top row) and *UAS-*$Pp4^{[D85N,\ H115N]}$*::GFP* (green, second row). (H) Normalized AC/Cytoplasm ratio of microtubule intensity in interphase $Pp4^{\Delta}$ (gray) and $Pp4^{\Delta}$ mutant neuroblasts, expressing *UAS-*$Pp4^{[D85N,\ H115N]}$*::GFP* (blue). Radial plots of apical (AC; green dots) and basal (BC; magenta dots) centrosome displacement between interphase and metaphase for (I) wild-type and (J) $Pp4^{\Delta}$ mutant neuroblasts. (K) Apical and basal centrosome displacement angles (between interphase and metaphase) are plotted for wild-type (gray) and $Pp4^{\Delta}$ mutant (blue) neuroblasts. Asl; Asterless. MTs; microtubules. Scale bar denotes 5 µm. Each point denotes one neuroblast. $p < 0.05$ were considered significant; * $p < 0.05$, ** $p < 0.01$, *** $p < 0.001$, **** $p < 0.0001$. Time in: h:mins. The following statistical tests were used: Mann–Whitney U (C, H, K (AC)); Unpaired Student's *t* test (D, F, K (BC)).

for centrosome maturation and microtubule regulation (Helps *et al.*, 1998; Sumiyoshi *et al.*, 2002; Martin-Granados *et al.*, 2008). Further, phosphorylation of γTubulin has been shown to impact microtubule nucleation (Alvarado-Kristensson *et al.*, 2009; Voss *et al.*, 2013). Based on Pp4's interactions with γTubulin, we hypothesized that Pp4 is required for proper γTubulin localization at centrosomes. There are two γTubulin genes in *Drosophila*: *γTubulin23C*, which has been shown to regulate centrosome activity in neuroblasts (Sunkel *et al.*, 1995), and *γTubulin37C*, which controls meiosis during gametogenesis and early development (Tavosanis *et al.*, 1997). We first sought to determine whether γTubulin37C and γTubulin23C are localized to centrosomes in both wild-type and $Pp4^{\Delta}$ mutant neuroblasts. In wild-type neuroblasts, expressing endogenously-tagged γTubulin23C::GFP (Mukherjee *et al.*, 2020), the apical centrosome contains robust levels of γTubulin23C throughout interphase, while the basal centrosome only recruits

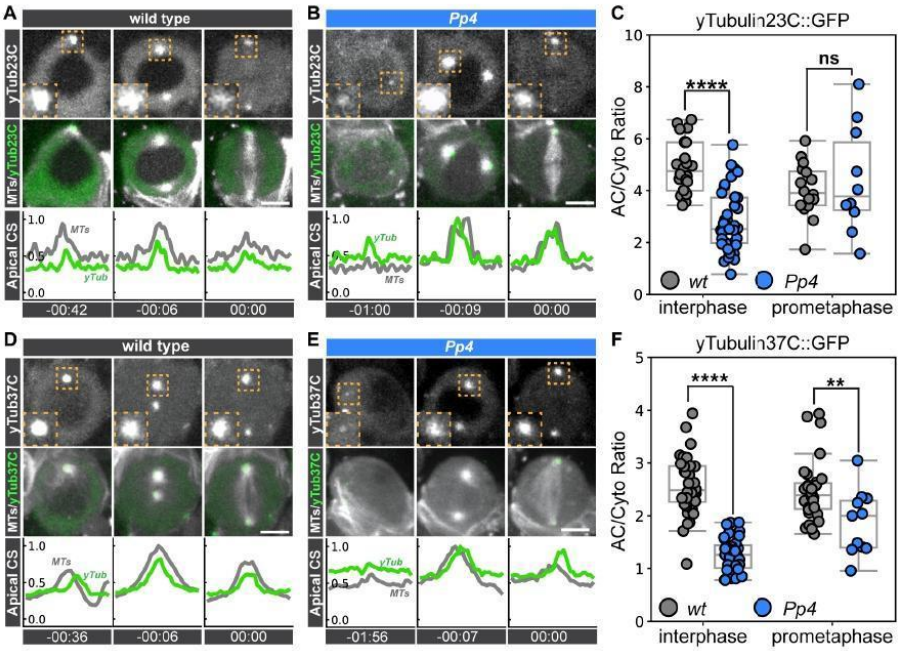

FIGURE 2: Pp4 is required for γTubulin localization at the apical centrosome in interphaseRepresentative image sequences of a (A) wild-type or (B) *Pp4*$^{\Delta}$ mutant neuroblast-expressing *worGal4, UAS-mCherry::Jupiter* and *γTubulin23C::GFP*. γTubulin23C::GFP (top row: white; middle row; green) and mCherry::Jupiter (middle row: white). Inserts in the top row show high magnification images of the apical centrosome (dashed orange box). Bottom row shows normalized microtubule (MTs; gray line) and γTubulin23C (γTub; green line) intensity line scans for the apical centrosome. (C) Quantification of γTubulin23C intensity at apical centrosomes, normalized to cytoplasmic signal, in interphase and prometaphase for wild-type (gray) and *Pp4*$^{\Delta}$ mutant (blue) neuroblasts. Representative image sequence of a (D) wild-type or (E) *Pp4*$^{\Delta}$ mutant neuroblast-expressing *worGal4, UAS-mCherry::Jupiter* and *ncd-γTubulin37C::GFP*. ncd-γTubulin37C::GFP (top row: white; middle row; green) and mCherry::Jupiter (middle row: white). Inserts in the top row show high magnification images of the apical centrosome (dashed orange box). Bottom row shows normalized microtubule (MTs; gray line) and γTubulin37C (γTub; green line) intensity line scans for the apical centrosome. (F) Quantification of γTubulin23C intensity at apical centrosomes, normalized to cytoplasmic signal, in interphase and prometaphase for wild-type (gray) and *Pp4* mutant (blue) neuroblasts. MTs; microtubules. CS; centrosome. Scale bar denotes 5 µm. Each point denotes one neuroblast $p < 0.05$ were considered significant; * $p < 0.05$, ** $p < 0.01$, *** $p < 0.001$, **** $p < 0.0001$. Time in: h:mins. The following statistical tests were used: Unpaired Student's *t* test (C); Mann–Whitney U (F).

γTubulin23C upon entry into mitosis. During mitosis, γTubulin23C localizes on both centrosomes (Figure 2, A and C; Supplemental Movie 03). In *Pp4*$^{\Delta}$ mutants, we observed that γTubulin23C levels are reduced by ~ 50% on the apical interphase centrosome compared with wild type but showed similar levels at prometaphase (Figure 2, B and C; Supplemental Movie 04).

In wild-type cells, γTubulin37C::GFP expressed under the oocyte and early-embryo promoter *ncd* (Hallen *et al.*, 2008a, 2008b), displayed robust localization at the apical centrosome in interphase as observed previously (Conduit and Raff, 2010; Singh *et al.*, 2014a; Ramdas Nair *et al.*, 2016b). The basal centrosome lacked γTubulin37C in interphase but later acquired γTubulin37C upon entry into mitosis (Figure 2, D and F). In contrast to this, *Pp4*$^{\Delta}$ mutants displayed low levels of γTubulin37C in interphase. Upon entry into mitosis, γTubulin37C localized to both centrosomes in *Pp4*$^{\Delta}$ mutants, albeit at significantly lower levels compared with wild type (Figure 2, E and F). These data suggest that Pp4 is required for the proper localization of γTubulin23C and γTubulin37C at centrosomes in interphase neuroblasts.

γTubulin37C and γTubulin23C mutants disrupt centrosome asymmetry

γTubulin contributes to the formation of γTubulin Ring Complexes (γTuRCs), which promotes microtubule nucleation. These γTuRCs are rapidly incorporated into the PCM of mature centrosomes, where they contribute to the formation of active MTOCs (Nigg and Stearns, 2011; Böhler *et al.*, 2021). Both γTubulin23C and γTubulin37C are required for γTuRC integrity in flies (Böhler *et al.*, 2021). To clarify the role of both γTubulin isoforms in interphase MTOC formation in fly neural stem cells, we live-imaged mutant alleles for *γTubulin23C* (*γTubulin23C*$^{[A14\text{-}9]}$, a hypomorph with an R217 to H replacement; *γTubulin23C*$^{[A9\text{-}2]}$, a hypomorph with a S233 to F mutation; *γTubulin23C*$^{[A15\text{-}2]}$, a potential null allele with W104 changed to a premature stop codon) and

γTubulin37C (γTubulin37C$^{[3]}$, a potential null allele replacing a W at 352 with a premature stop codon; γTubulin37C$^{[e00793]}$, containing a piggybac insertion) (Wilson and Borisy, 1998a; Vaźquez *et al.*, 2008; Hughes *et al.*, 2011) with mCherry::Jupiter and Sas4::GFP and assessed MTOC activity in interphase. Several γ*Tubulin* alleles showed altered MTOC asymmetry: 7% of γTubulin23C$^{[A6\text{-}2]}$, 74% of γTubulin23C$^{[A14\text{-}9]}$, and 54% of γTubulin23C$^{[A15\text{-}2]}$ mutant neuroblasts displayed two interphase MTOCs. Similarly, 70% of γTubulin37C$^{[e00793]}$ and 42% of γTubulin37C$^{[3]}$ mutants contained two interphase MTOCs (Supplemental Figure S3, A–E). However, 20% of γTubulin37C$^{[3]}$ mutants lacked discernable MTOC activity in interphase, the same phenotype as *Pp4*$^{\Delta}$ mutants, albeit less penetrant (Figure 3A–F; Supplemental Figure S3E). To determine remaining protein levels in γ*Tubulin23C* and γ*Tubulin37C* mutants, we stained γTubulin23C$^{[A14\text{-}9]}$ and γTubulin37C$^{[3]}$ mutant larval brains with an anti-γTubulin antibody that recognizes both isoforms of fly γTubulin (see *Materials and Methods* for details). Neither γTubulin37C$^{[3]}$ nor γTubulin23C$^{[A14\text{-}9]}$ mutants showed a loss of γTubulin at centrosomes in interphase or metaphase, respectively (Supplemental Figure S4, A–D). Additionally, both γTubulin37C$^{[3]}$ and γTubulin23C$^{[A14\text{-}9]}$ showed increased presence of γTubulin on the basal centrosome, which is consistent with the observation of two active MTOCs in our live-cell data (Supplemental Figure S4, A–D). For these experiments, γTubulin23C$^{[A14\text{-}9]}$ and γTubulin37C$^{[3]}$ were crossed over deficiency chromosomes, removing the entire γ*Tubulin23C* or γ*Tubulin37C* coding region, respectively. Because these crosses create strong loss-of-function conditions, it is unlikely that the presence of γTub is a consequence of low allele penetrance. Considering that γTubulin37C and γTubulin23C both contribute to the formation of a γTuRC (Tariq *et al.*, 2020), it is more likely that the two isoforms are redundant with each other. To test for genetic redundancy, we created a recombinant γTubulin37C$^{[3]}$, γTubulin23C$^{[A15\text{-}2]}$ chromosome. γTubulin37C$^{[3]}$, γTubulin23C$^{[A15\text{-}2]}$ double-mutant interphase neuroblasts centrosomes were devoid of γTubulin (Supplemental Figure S4E) and predominantly showed a 0xMTOC phenotype in interphase, similar to *Pp4*$^{\Delta}$ mutants (Supplemental Figures S4F and S5, A–E). γTubulin37C$^{[3]}$, γTubulin23C$^{[A15\text{-}2]}$ double mutants also developed slower compared with control larvae. Most double-mutant neuroblasts showed normal MTOC maturation in mitosis although a few displayed monopolar spindles (Supplemental Figures S4F and S5, B and D). These data suggest that both γTubulin37C and γTubulin23C are required for MTOC asymmetry in interphase neural stem cells.

γTubulin phosphomutants exhibit impaired centrosome asymmetry

In U2OS human cell culture, phosphorylation of γTubulin at Serine 131 prevents microtubule nucleation, implicating phosphorylation of Serine 131 as a regulator of MTOC formation (Alvarado-Kristensson *et al.*, 2009). Both *Drosophila* γTubulin isoforms are highly conserved with Human TUBG1 at and around Serine 131 (Figure 3G). We therefore hypothesized that Pp4-mediated dephosphorylation of γTubulin at Serine 131 could promote microtubule nucleation. Because γTubulin37C$^{[3]}$ mutants exhibited a loss-of-function phenotype similar to the *Pp4*$^{\Delta}$ phenotype, we chose to examine the requirement of Serine 131 phosphorylation of γTubulin37C. Because none of the characterized γTubulin mutants described above appear to directly mutate Serine 131, we mutated endogenous Serine 131 in γTubulin37C to Alanine (γTubulin$^{[S131A]}$) using CRISPR/Cas9 (see *Materials and Methods*) and crossed this allele to a deficiency stock that lacks the entire γTubulin37C coding region. We reasoned that the S131A mutant would mimic the unphosphorylated state of γTubulin37C and display an increase in MTOC activity in interphase neuroblasts. Indeed, 60% of γTubulin$^{[S131A]}$ neuroblasts displayed two active interphase MTOCs, albeit with lower mCherry::Jupiter levels compared with wild type (Figure 3, H–K; Supplemental Figure S3E). γTubulin$^{[S131A]}$ mutants also showed elevated levels of γTubulin at the basal centrosome in interphase, consistent with the observation of two interphase MTOCs in our in vivo movies (Supplemental Figure S4, A–D). These data suggest that the phosphorylation state of γTubulin at Serine 131 is involved in the maintenance of interphase MTOCs in *Drosophila* neuroblasts.

Cdk1 contributes to interphase centrosome asymmetry

In vitro, cyclin-dependent kinase 1 (Cdk1) phosphorylates the γTubulin residues Serine 80 and Threonine 196. Cdk1 also directly phosphorylates PP4r2 and PP4r3, which is predicted to decrease the catalytic activity of the Pp4 complex (Toyo-oka *et al.*, 2008; Voss *et al.*, 2013). Therefore, Cdk1 could regulate γTubulin via direct phosphorylation, or indirectly by inactivating Pp4 (Figure 4A). Phosphorylated γTubulin is predicted to result in reduced microtubule nucleation, as suggested previously (Alvarado-Kristensson *et al.*, 2009; Voss *et al.*, 2013). To further explore the role of γTubulin regulation via phosphorylation, we first knocked down Cdk1 in larval neuroblasts using the neuroblast-specific driver worGal4 and imaged MTOC activity with mCherry::Jupiter. In either model, the removal of Cdk1 would decrease γTubulin phosphorylation, potentially increasing microtubule nucleation in interphase. Indeed, in contrast to wild-type neuroblasts, we observed that 38% of Cdk1 RNAi-expressing neuroblasts display interphase MTOC activity on both centrosomes (Figure 4B, F–H; timepoints −1:18). However, in 24% of Cdk1 RNAi-expressing neuroblasts, neither centrosome displayed interphase MTOC activity, similar to *Pp4*$^{\Delta}$ mutants (Figure 4, C and F–H; timepoints −1:24). The former finding suggests that Cdk1 has an inactivating role in microtubule nucleation, whereas the latter phenotype is more in line with a model where Cdk1 has a microtubule nucleation–promoting function.

If Cdk1 down-regulates MTOC activity, an increase in Cdk1 levels on neuroblast centrosomes should cause a decrease in microtubule nucleation, manifested in a Pp4-like MTOC phenotype. To this end, we employed a previously used nanobody strategy, localizing the single-chain anti-GFP nanobody (vhhGFP4; [Saerens *et al.*, 2005; Caussinus *et al.*, 2012]) to centrosomes with the PACT domain (Gillingham and Munro, 2000; Gallaud *et al.*, 2020a). Crossing this PACT-vhhGFP4 construct to endogenously-tagged Cdk1::GFP should enrich Cdk1 at neuroblast centrosomes throughout the cell cycle. In wild-type neuroblasts, Cdk1::GFP localizes to the apical centrosome in interphase and appears on both centrosomes in early mitosis (Figure 4D). However, crossing Cdk1::GFP with the PACT-vhhGFP4 construct enriched Cdk1 on centrosomes in interphase and mitosis. Under these conditions, 60% of interphase neuroblasts displayed no MTOC activity, similar to *Pp4*$^{\Delta}$ mutants. However, mitotic spindle formation progressed normally (Figure 4, E–H). Although the exact mechanisms are unknown, these data suggest that Cdk1 is required for regulating centrosome asymmetry in interphase neuroblasts.

Pp4 is required for apical centrosome localization of Polo

We and others previously showed that centrosome asymmetry requires the mitotic kinase Polo (Plk1 in vertebrates) and the daughter-centriole protein Centrobin (Cnb; CNTROB in humans).

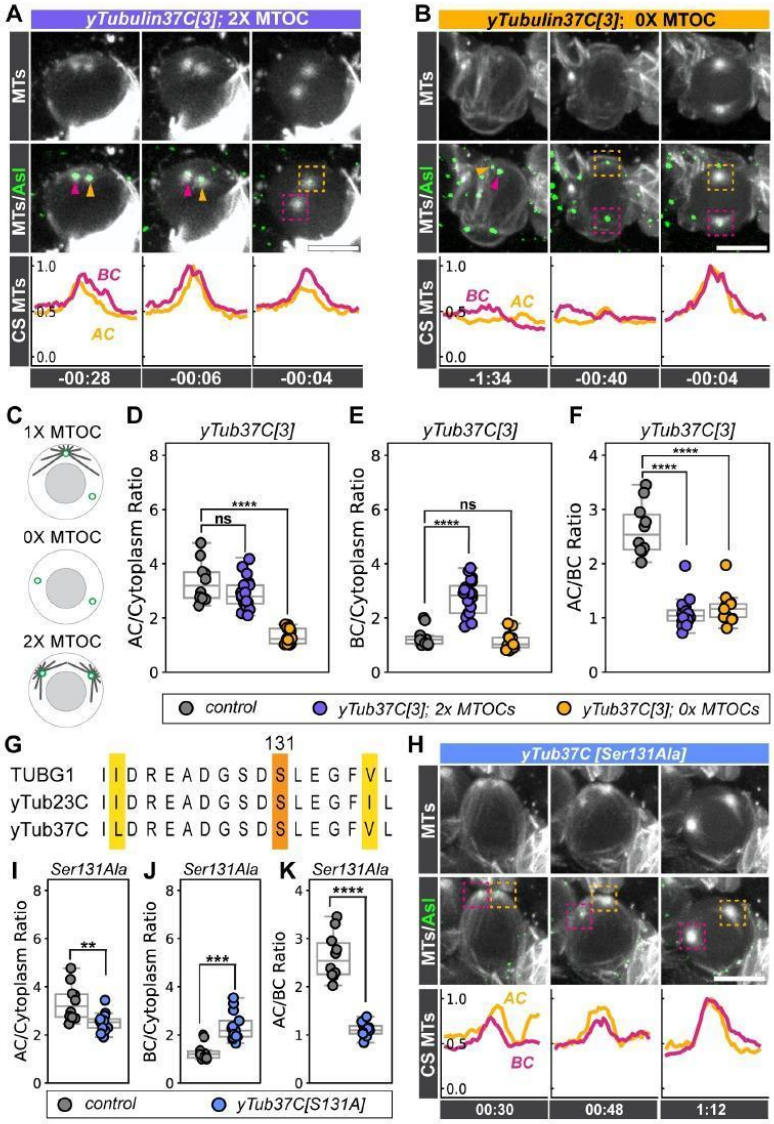

FIGURE 3: γTubulin mutants exhibit impaired interphase centrosome asymmetryRepresentative time series of a (A) *γTubulin37C[3]* mutant neuroblast-expressing *worGal4, UAS-mCherry::Jupiter* (white, top row) and Sas4::GFP (green, merge in second row). Apical (AC) and basal centrosomes (BC) are highlighted with orange and magenta arrowheads and dashed boxes, respectively. Microtubule (MT) intensity line scans of the apical (orange) and basal (magenta) centrosome (CS) is shown below. Note that the shown *γTubulin37C[3]* mutant neuroblast has two active MTOCs (2xMTOC). (B) Representative *γTubulin37C[3]* mutant neuroblast with no active MTOC (0x MTOC). (C) Schematic illustration of the different MTOC phenotypes. (D) Normalized AC/Cytoplasm, (E) BC/Cytoplasm, or (F) AC/BC ratios for wild-type (gray circles) and *γTubulin37C[3]* mutants (purple circles: 2xMTOC phenotype; yellow circles: 0xMTOC phenotype). (G) Protein sequence alignment of human TUBG1, γTubulin23C, and γTubulin37C. Variations in sequence are highlighted in yellow. The conserved Serine at position 131 is highlighted in orange. (H) Representative image sequence of a *γTubulin37C[S131A]* mutant neuroblast, expressing worGal4, UAS-mCherry::Jupiter (white, top row) and Sas4::GFP (green, merge in second row). Normalized (I) AC/Cytoplasm, (J) BC/Cytoplasm, or (K) AC/BC ratios in wild-type controls (gray) and *γTubulin37C[S131A]* mutants (blue). MTs; microtubules. CS; centrosome. Scale bar denotes 5 μm. Each point denotes one neuroblast. $p < 0.05$ were considered significant; * $p < 0.05$, ** $p < 0.01$, *** $p < 0.001$, **** $p < 0.0001$. Time in: h:mins. The following statistical tests were used: Kruskal–Wallis with uncorrected Dunn's test for multiple comparisons (D–F); Mann–Whitney U (I–K).

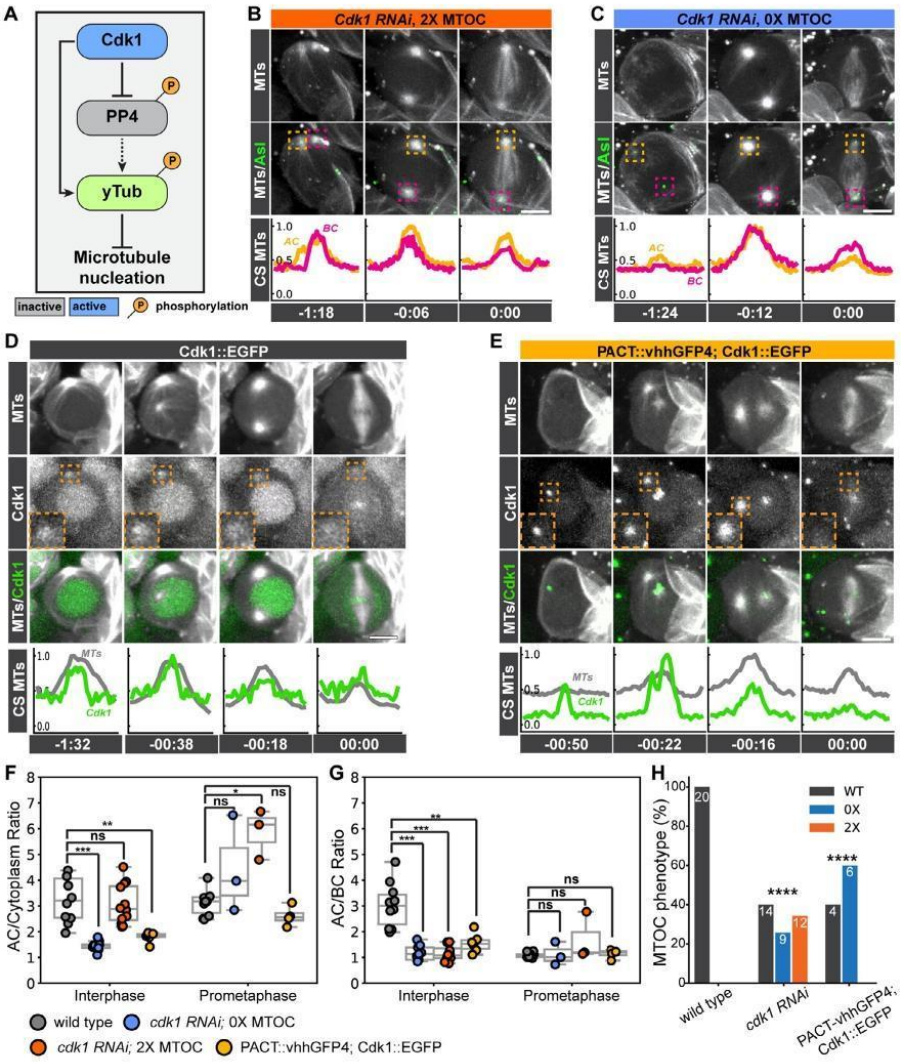

FIGURE 4: Cdk1 is required for centrosome asymmetry(A) Working model from (Alvarado-Kristensson *et al.*, 2009; Voss *et al.*, 2013): active Cdk1 could inhibit Pp4 via phosphorylation or directly phosphorylate γTub. Phosphorylated γTub is proposed to decrease microtubule nucleation activity. (B, C) Representative image sequences of *cdk1 RNAi, worGal4, UAS-mCherry::Jupiter* (top row: white), and *Asl::EGFP* (middle row: green) expressing neuroblasts showing (B) a 2xMTOC or (C) 0xMTOC phenotype. Orange and magenta dashed boxes highlight apical (AC) and basal (BC) centrosomes, respectively. Bottom row shows normalized line scans of microtubule intensity at the apical (orange line) and basal (magenta line) centrosome. Representative time series of a (D) wild-type neuroblast, expressing *Cdk1::EGFP* (middle row: white; green in merge) and *worGal4 UAS-mCherry::Jupiter* (top row and merge: white). (E) Representative neuroblast expressing, *worGal4 UAS-mCherry::Jupiter* (top row and merge: white), *Cdk1::EGFP* (middle row: white; green in merge) and the nanobody *UAS-PACT::vhhGFP4*. Insets show high magnification images of Cdk1::EGFP signal at the apical centrosome. Quantification of (F) AC/Cytoplasm or (G) AC/BC ratios in wild type (gray), *cdk1* RNAi (blue and orange circles; 0xMTOC and 2xMTOC, respectively) and nanobody expressing (*PACT::vhhGFP4; Cdk1::EGFP;* yellow circles) neuroblasts. (H) Frequency of 1X, 2X, or 0X MTOCs in wild type, *cdk1* RNAi, and Cdk1 trapping experiments. Numbers on bars indicate the number of measured neuroblasts. Asl; Asterless. MTs; microtubules. Scale bar denotes 5 µm. Each point denotes one neuroblast. $p < 0.05$ were considered significant; * $p < 0.05$, ** $p < 0.01$, *** $p < 0.001$, **** $p < 0.0001$. Time in: h:mins. The following statistical tests were used; Kruskal–Wallis with uncorrected Dunn's test for multiple comparisons (F, G); chi-squared goodness of fit (H).

Reducing Polo or loss of Cnb causes loss of apical MTOC activity in interphase neuroblasts, similar to the *Pp4* mutant phenotype described here (Januschke *et al.*, 2013a; Singh *et al.*, 2014b; Ramdas Nair *et al.*, 2016a; Gallaud *et al.*, 2020a). We therefore sought to determine whether Pp4 contributes to the localization of either Polo or Cnb during interphase. We imaged $Pp4^{\Delta}$ mutant larval neuroblasts, expressing the MTOC marker mCherry::Jupiter in conjunction with either Polo::EGFP or Cnb::EGFP (Gallaud *et al.*, 2020a). In wild-type neuroblasts, Polo is localized on the apical centrosome in interphase (Figure 5, A and C; timepoints −01:18 and −00:24). Upon entry into mitosis, a subset of Polo is localized to kinetochores, while another fraction is retained at both the apical and basal centrosomes (Figure 5, A and C; timepoints 00:00). In contrast, *Pp4* mutant neuroblasts showed significantly reduced Polo localization at the apical centrosome in interphase, and a significant increase in Polo localization during centrosome maturation (Figure 5, B and C; timepoints −01:00 and 00:00). Additionally, Polo is retained on centrosomes in mitosis but was not detected on kinetochores in $Pp4^{\Delta}$ mutants (Figure 5B; timepoints 00:00). The lack of kinetochore-localized Polo in $Pp4^{\Delta}$ did not significantly impact mitotic progression, despite Polo's role in spindle assembly checkpoint regulation (Conde *et al.*, 2013). However, $Pp4^{\Delta}$ mutant brains had fewer mitotic neuroblasts, compared with control brains (Supplemental Figure S1, C and D).

To better quantify the distribution of Polo in *Pp4* mutants, we imaged Polo::EGFP together with Asl::mCherry (Conduit *et al.*, 2015) and measured Polo's distribution with line scan measurements (Figure 5, D and E; see *Materials and Methods* for details). In contrast to wild-type centrosomes, which display a sharp peak centered on Asl, Polo is more diffusely localized in $Pp4^{\Delta}$ mutant neuroblasts (Figure 5, F and G).

Centrobin is a substrate of Polo and MTOC activity depends on Polo-mediated phosphorylation of Cnb (Januschke *et al.*, 2013a). In wild-type interphase neuroblasts, Centrobin is localized only to the apical daughter centrosome in interphase and weakly localized on both centrosomes in mitosis (Figure 5H and Gallaud *et al.*, 2020a). Surprisingly, in the majority of $Pp4^{\Delta}$ mutants, Cnb is normally localized in interphase centrosomes but slightly elevated in prometaphase (Figure 5, I and J). While Cnb's intensity in $Pp4^{\Delta}$ mutants is statistically similar to wild-type controls, we observed a subset of cells with extremely low levels of Cnb in interphase (Figure 5J). This phenotype is further investigated below. Taken together, we conclude that Pp4 is required for robust and confined Polo localization at the apical interphase centrosome.

Pp4 is required for Centrobin's enrichment on the daughter centriole during mitosis

Asymmetric MTOC activity, manifested in one active and one inactive interphase MTOC, is regulated 2-fold during the neuroblast cell cycle: 1) in mitosis, Centrobin relocalizes from the mother to the daughter centriole via down-regulation of Centrobin on the mother centriole. This is followed by a transfer of the remaining Centrobin, originating from the mother centriole to the daughter centriole. Subsequently, Centrobin increases on the daughter centriole in late mitosis and early interphase. This dynamic Centrobin localization establishes two molecularly distinct centrosomes, which is necessary for interphase MTOC activity (Gallaud *et al.*, 2020a). 2) As neuroblasts enter interphase after cytokinesis, PCM components are shed from the Cnb^{-} mother centrosome that is destined to segregate into the differentiating GMC. PCM is retained on the Cnb^{+} daughter centrosome, which remains in the neuroblast (Rebollo *et al.*, 2007a; Lerit *et al.*, 2013; Singh *et al.*, 2014b). We therefore hypothesized that in addition to Polo, Pp4 could be required for the localization of Centrobin onto the daughter centriole during mitosis. To test this, we performed three-dimensional structured illumination microscopy (3D-SIM) imaging experiments of control and $Pp4^{\Delta}$ mutant neuroblasts expressing Cnb::EGFP. We used microtubules as a reference marker for cell cycle progression and Asterless to differentiate between the mother and daughter centrioles. As previously shown, Asterless intensity increases with centriolar age, providing a Centrobin-independent marker to distinguish between mother and daughter centrioles (Novak *et al.*, 2014; Fu *et al.*, 2016; Gallaud *et al.*, 2020a). We measured Centrobin levels on the mother and daughter centriole and plotted the corresponding daughter-to-mother intensity ratios to quantify the difference between control and $Pp4^{\Delta}$ mutant neuroblasts. As previously shown, in control neuroblasts, Centrobin is first localized on the mother centriole in prophase and prometaphase before enriching on the daughter centriole during metaphase, anaphase, and telophase (Figure 6, A, D, and E; Supplemental Figure S6, A–E). In all control neuroblasts, only the daughter centriole contained Cnb in telophase (Figure 6, A and D–G). In $Pp4^{\Delta}$ mutants, we observed mother centrioles with Centrobin in prophase and prometaphase, comparable to wild-type neuroblasts (Figure 6, B and E–G). However, from metaphase through telophase, we observed three distinct phenotypes, differing from wild-type neuroblasts: 1) Cnb was either completely absent, 2) incorrectly enriched on the mother centriole, or 3) present on both the mother and daughter centriole. Overall, Cnb distribution in $Pp4^{\Delta}$ mutants was only statistically significant in telophase compared with controls (Figure 6, B and E–G).

Polo-mediated Cnb phosphorylation is important for Cnb's timely mother to daughter centriole relocalization in mitosis (Gallaud *et al.*, 2020a). In human cells, Pp4 interacts with Centrobin (Réthi-Nagy *et al.*, 2023) leading us to hypothesize that Pp4-mediated dephosphorylation of Centrobin could be required for mitotic Cnb relocalization. To test this model, we employed a phosphomimetic fluorescent construct of Centrobin, where three of its Polo phosphorylation sites are mutated to glutamic acid, mimicking a phosphorylated state (*YFP::Cnb(T4E,T9E,S82E)*, (Januschke *et al.*, 2013a)). Neuroblasts expressing this phosphomimetic Centrobin mutant showed centriolar transfer defects similar to what we observed in $Pp4^{\Delta}$ mutants (Figure 6, C and E–G). Cnb was mostly localized to mother centrioles in prometaphase and metaphase but failed to shift efficiently to daughter centrioles in anaphase and telophase (Figure 6C). We found several instances with Cnb localized to both the mother and daughter centriole in metaphase and anaphase neuroblasts (Figure 6, C–G; Supplemental Figure S6, B–E). In telophase, neuroblasts expressing phosphomimetic Centrobin displayed a similar variation of Cnb enrichment compared with *Pp4* mutants. 50% of Cnb phosphomimetic-expressing neuroblasts displayed $Cnb^{T4E,T9E,S82E}$ enrichment on daughter centrioles, 40% displayed inverted $Cnb^{T4E,T9E,S82E}$ enrichment on the mother centriole, and 10% showed symmetric $Cnb^{T4E,T9E,S82E}$ enrichment (Figure 6, E–G).

To confirm these results, we live-cell imaged $Pp4^{\Delta}$ mutants expressing Cnb::EGFP and mCherry::Jupiter in late telophase and early anaphase. Because we found $Pp4^{\Delta}$ mutant neuroblasts in telophase either devoid of Cnb or with Cnb on both centrioles with 3D-SIM imaging, we reasoned that these Cnb localization defects in mitosis should give rise to some self-renewed early interphase neuroblasts containing either two Centrobin-positive centrioles or two Centrobin-negative centrioles. In line with this hypothesis and consistent with the measurements described above, we found 16% of *Pp4* mutant neuroblasts where Centrobin appeared

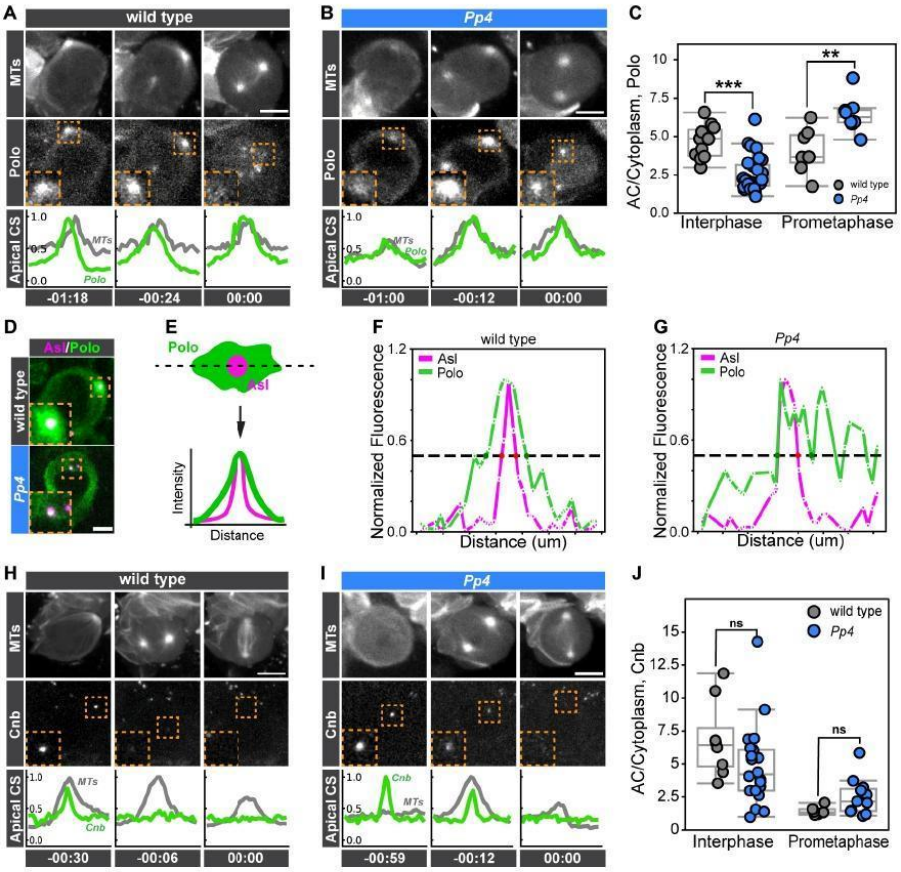

FIGURE 5: Pp4 is required for robust Polo localization on the apical interphase centrosomeRepresentative image sequences of a (A) wild-type or (B) *Pp4*$^{\Delta}$ mutant neuroblast-expressing *worGal4*, *UAS-mCherry::Jupiter* (top row: white), *Polo::GFP* (middle row: white). Orange dashed boxes highlight apical centrosomes. High magnification images are shown in the bottom left corner. Normalized microtubule (gray line) and Polo::GFP (green line) intensity line scans for the apical centrosome are shown below. (C) Quantification of AC/Cytoplasm ratio for Polo::GFP intensity in wild type (gray), and *Pp4*$^{\Delta}$ mutants (blue) at interphase and prometaphase. (D) Representative Images of a wild type (top row) or *Pp4*$^{\Delta}$ mutant (bottom row) neuroblast, expressing endogenous Polo::EGFP (green) and Asterless::mCherry (magenta). (E) Schematic and representative intensity line scans to quantify Polo distribution at the centrosome are shown for (F) wild-type and (G) *Pp4*$^{\Delta}$ mutants. The line scans correspond to the cells shown in D. Green and magenta lines represent Polo and Asl intensity profiles, respectively. The black dashed line indicates the width at half height for each distribution. Representative image sequence of a (H) wild-type or (I) *Pp4* mutant neuroblast-expressing *worGal4*, *UAS-mCherry::Jupiter* (top row: white) and *Cnb::EGFP* (middle row: white). Corresponding intensity line scans are shown below. (J) Quantification of AC/Cytoplasm ratio of Cnb::EGFP fluorescence intensity in wild-type (gray), and *Pp4*$^{\Delta}$ mutants (blue) at interphase and prometaphase. Asl; Asterless. MTs; microtubules. Scale bar denotes 5 µm. Each point denotes one neuroblast. $p < 0.05$ were considered significant; * $p < 0.05$, ** $p < 0.01$, *** $p < 0.001$, **** $p < 0.0001$. Time in: h:mins. The following statistical tests were used: Mann–Whitney U (interphase in C, J); Unpaired Student's *t* test (prometaphase in C).

on both centrosomes and 7% (~ 6% in Figure 5J) where Centrobin was undetectable on either centrosome. The remaining *Pp4*$^{\Delta}$ mutant neuroblasts contained a normal single Cnb^{+} centriole (Figure 7, A–F). Collectively, we conclude that Pp4 is required for efficient and timely transfer of Cnb from the mother to the daughter centriole in mitosis. Furthermore, in agreement with our earlier findings (Gallaud *et al.*, 2020a), the data suggest that Cnb's timely relocalization from the mother to the daughter centriole in mitosis depends on Cnb's phosphorylation status.

DISCUSSION

Biased segregation of molecularly distinct centrosomes has been proposed to be important for asymmetric cell division and cell fate decisions (Sunchu and Cabernard, 2020b). However, the mecha-

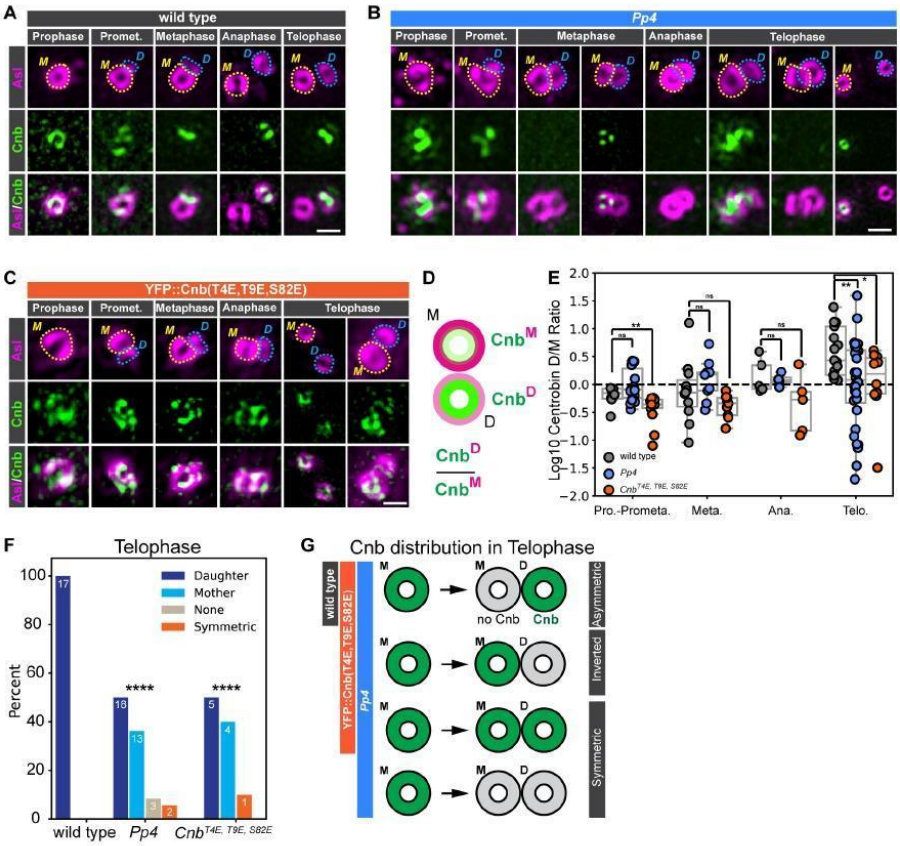

FIGURE 6: Pp4 is required for Centrobin localization in mitosisRepresentative 3D-SIM images for (A) *Cnb::EGFP* expressing wild-type, (B) *Pp4*$^{\Delta}$ or (C) *YFP::Cnb*^{T4E,T9E,S82E} expressing neuroblasts. All samples were costained with anti-Asterless (Asl; top row; magenta). Middle row shows Cnb::EGFP (A, B) or YFP::Cnb^{T4E,T9E,S82E} (C). Merged images are shown in the bottom row. Mother and daughter centrioles are outlined with yellow and blue dashed circles, respectively. (D) Mother centrioles have higher Asl intensity. Centrobin localization at distinct mitotic stages was determined by calculating the ratio of daughter-to-mother centriole Cnb. (E) Centrobin D/M Log_{10}-normalized ratios for prophase—prometaphase, metaphase, anaphase, and telophase for wild type (gray circles), *Pp4*$^{\Delta}$ (blue circles), and YFP::Cnb^{T4E,T9E,S82E} expressing neuroblasts (orange circles). (F) Centrobin D/M Log_{10}-normalized telophase enrichment ratios and (G) corresponding bar graphs for wild type (gray circles), *Pp4*$^{\Delta}$ (blue circles), and YFP::Cnb^{T4E,T9E,S82E} (orange circles), separated by enrichment. Numbers on bars denote number of measured neuroblasts. (H) Schematic summary of telophase Cnb localization in the wild-type, *Pp4*$^{\Delta}$ and YFP::Cnb^{T4E,T9E,S82E} expressing neuroblasts. Asl; Asterless. Cnb; Centrobin. Scale bar denotes 0.5 µm. Each point denotes one neuroblast. $p < 0.05$ were considered significant; * $p < 0.05$, ** $p < 0.01$, *** $p < 0.001$, **** $p < 0.0001$. The following statistical tests were used: Kruskal–Wallis test with uncorrected Dunn's test for multiple comparisons (E); Chi-squared goodness of fit (F).

nisms underlying centrosome asymmetry remain unclear. Here, we show that in fly neural stem cells, the protein phosphatase 4 complex plays a dual role in centrosome asymmetry: in interphase, Pp4 is necessary to maintain MTOC activity on the centrosome destined to be inherited by the self-renewing neural stem cell. In mitosis, Pp4 is required for the timely localization of Cnb from the mother to the daughter centriole.

Previous work revealed that fly neural stem cells contain two molecularly asymmetric interphase centrosomes: a younger, Cnb^{+} centriole and an older, Cnb^{-} centriole. The Cnb^{+} centriole retains the ability to nucleate microtubules, thereby tethering this centrosome to the apical neuroblast cortex. The Cnb^{-} centriole-containing centrosome down-regulates PCM components such as centrosomin (Cnn) or γTubulin in interphase. The Cnb^{-} centrosome migrates through the cytoplasm in interphase and is destined to be inherited by the differentiating GMC in the next division. Thus, biased MTOC activity relies on the establishment of two molecularly distinct centrioles and is necessary for the asymmetric centrosome segregation (Rebollo *et al.*, 2007b; Rusan and Peifer, 2007b; Januschke *et al.*, 2011, 2013b; Gallaud *et al.*, 2020b; Hannaford *et al.*, 2022b).

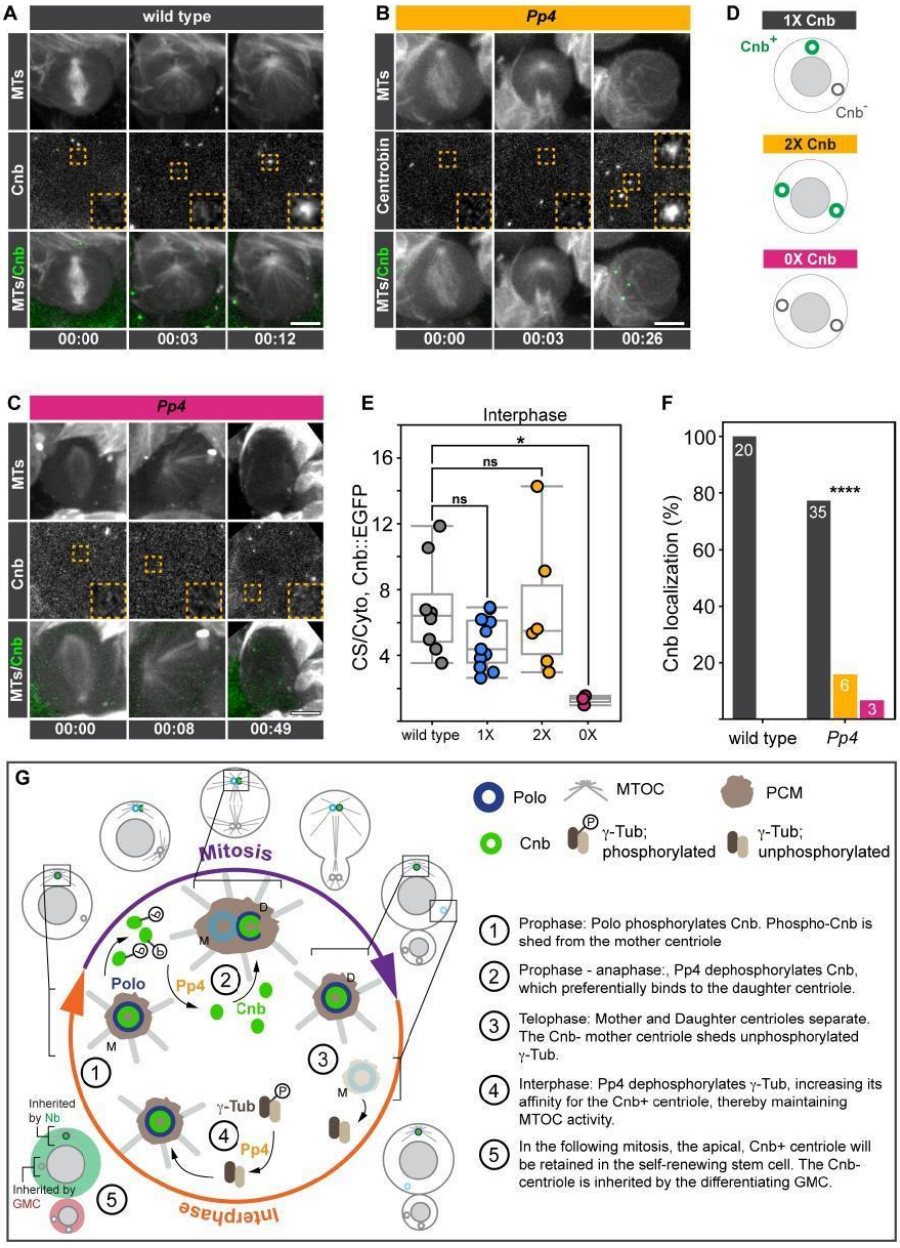

FIGURE 7: Pp4 is required for proper transfer of CentrobinRepresentative image sequence of a (A) wild type or (B, C) two representative $Pp4^{\Delta}$ mutant neuroblasts, expressing *worGal4, UAS-mCherry::Jupiter* (top row: white) and *Cnb::EGFP* (middle row: white; bottom row: green). Orange dashed boxes indicate apical centrosomes. High magnification images are shown in inserts on the bottom left in the middle row. (B) $Pp4^{\Delta}$ mutant neuroblasts either contain Cnb on both centrosomes in early interphase or (C) is not detectable. (D) Schematic representation of the 0x, 1x, and 2x Cnb phenotype. (E) Centrosome/Cytoplasm ratio of Centrobin intensity in wild-type (gray), $Pp4^{\Delta}$ with 1X Cnb (blue), $Pp4^{\Delta}$ with 2X Cnb (yellow), and $Pp4^{\Delta}$ with 0X Cnb (magenta). (F) Cnb localization frequencies are calculated based on (E) for wild-type and $Pp4^{\Delta}$ mutant neuroblasts. (G) Proposed Model. Pp4 is needed to establish centriolar asymmetry in mitosis and to maintain MTOC activity on the Cnb^{+} centriole in interphase. In mitosis, Polo-mediated phosphorylation of Cnb removes it from the mother centriole but needs to be dephosphorylated by Pp4 for its deposition on the daughter centriole. In interphase, Pp4 dephosphorylates γTubulin, which incorporates into the Cnb^{+} centriole-containing centrosome. The Cnb^{-} centriole will shed PCM shortly after separating from the daughter centriole and loses MTOC activity. As a consequence of this centrosome asymmetry cycle, the Cnb^{+} centriole will be retained by the self-renewed neuroblast and the Cnb^{-} centriole will segregate into the differentiating GMC. Numbers

We recently showed that Cnb asymmetry is established in mitosis, when neural stem cell centrioles duplicate. In prophase, Cnb starts to change its localization from the older mother centriole to the newly forming daughter centriole. The mechanisms are not entirely clear but include a down-regulation of Cnb from the mother in prophase, a relocalization of the remaining Cnb from the mother to the daughter centriole between prometaphase and anaphase, and finally recruitment of new Cnb to the maturing daughter centriole in telophase and early interphase. The establishment of asymmetric Cnb localization in mitosis depends on the mitotic kinase Polo and Cnb's phosphorylation status (Gallaud *et al.*, 2020a). Here we show that in addition to Polo, Pp4 is also required for the timely relocalization of Cnb from the mother to the daughter centriole in mitosis. In mitotic *Pp4*$^{\Delta}$ mutants, we found neuroblasts showing either Cnb enrichment on the mother centriole, symmetrical distribution or no Cnb enrichment on either centriole. Pp4 and Centrobin have been shown to interact in vitro (Lipinszki *et al.*, 2015a), suggesting that Cnb's phosphorylation status is important for the timely relocalization in mitosis. Indeed, *polo* mutants, or unphosphorylatable Cnb show defects in Cnb relocalization to the daughter centriole in mitosis (Gallaud *et al.*, 2020a). In support of this finding, we demonstrate that phosphomimetic Centrobin displayed transfer defects like those observed in *Pp4*$^{\Delta}$ mutants. Accurate relocalization of Centrobin in mitosis ensures the formation of a Cnb^{+} centriole and one Cnb^{-} centriole, separating from each other in early interphase. Therefore, Cnb relocalization defects could either give rise to 1) two Cnb^{-}, 2) two Cnb^{+} or 3) one Cnb^{-} and one Cnb^{+} centriole, with Cnb remaining on the older mother centriole. In support of our OMX data, and consistent with this model, our live-cell imaging data showed *Pp4*$^{\Delta}$ mutant neuroblasts with either two Cnb^{+} centrosomes or two Cnb^{-} centrosomes in interphase. The majority of live imaged *Pp4*$^{\Delta}$ mutant neuroblasts showed asymmetric Cnb distribution, but we cannot resolve whether Cnb remained on the mother centriole or correctly localized to the daughter centriole. Based on these data, we propose that in mitosis, Polo is responsible for the removal of Centrobin from the mother centriole in prophase and prometaphase when Polo is strongly enriched on the mother centriole. We further propose that Pp4 is then required to deposit Centrobin onto the nascent daughter centriole, which may have higher affinity for unphosphorylated Cnb. Additionally, we show that Polo enrichment on the apical centrosome in interphase is reduced in *Pp4*$^{\Delta}$ mutants. This finding is consistent with previous work, showing that Polo is not required to maintain Cnb on the interphase daughter centriole (Januschke *et al.*, 2013b).

Pp4 is composed of a catalytic subunit Pp4c, as well as the two regulatory subunits Pp4r2, and Pp4r3, which provide substrate and localization specificity (Park and Lee, 2020). Loss of Pp4c, Pp4r2, or Pp4r3 all cause loss of MTOC activity in interphase, a phenotype resembling the loss of Cnb. Building a robust MTOC requires correctly organized PCM proteins, including γTubulin. *Drosophila* contains two γTubulin genes (γTubulin23C and γTubulin37C), encoding for proteins which physically interact with each other (Wiese, 2008). We found that Pp4 is required for γTubulin23C and γTubulin37C localization at the apical centrosome and both isoforms are necessary for correct MTOC asymmetry. Previous studies revealed that γTubulin23C is required for all centrosomal function whereas γTubulin37C is required for meiotic spindle regulation and early oogenesis (Vázquez *et al.*, 2008; Wiese, 2008). Our results suggest that the two genes are partially redundant with each other, since γTubulin single, but not double mutants still localize γTubulin to centrosomes. Surprisingly, all tested γTub alleles contain two active MTOCs (2xMTOC) in interphase with varied frequencies. This result is difficult to reconcile in light of γTub's molecular function. A possible explanation could be that an imbalance between γTub23C and γTub37C might cause a gain-of-function phenotype. Alternatively, the various point mutations could give rise to misfolded γTub proteins that mask important regulatory sites such as Ser131. For instance, in vitro data suggest that γTubulin is dephosphorylated by Pp4 and that constitutively phosphorylated γTubulin at Ser131 lowers microtubule-nucleating activity (Alvarado-Kristensson *et al.*, 2009; Voss *et al.*, 2013). Ser131 is conserved in both Tubulin23C and γTubulin37C but mutating Serine 131 to non-phosphorylatable Alanine in γTubulin37C is sufficient to maintain two active interphase MTOCs, suggesting that the dephosphorylated state is necessary for MTOC activity in fly neural stem cells. Cdk1 has also been implicated in γTubulin regulation, either via inhibiting Pp4 or by phosphorylating γTubulin. In both cases, preventing γTubulin dephosphorylation diminishes its microtubule-nucleating activity (Alvarado-Kristensson *et al.*, 2009). Consistent with this model, we found that loss of Cdk1, or Cdk1 mislocalization compromises interphase MTOC activity. Despite these results, we have no evidence to suggest that Pp4 dephosphorylates, or Cdk1 phosphorylates γTubulin's Ser131 residue. Surprisingly, lowering Cdk1 levels can also cause a precocious activation of MTOC activity. As hypothesized above, it could be related to creating an imbalance in γTubulin regulation. Alternatively, Cdk1 could regulate other proteins involved in MTOC activity that either enhance or reduce microtubule nucleation.

In conclusion, we propose that Pp4 dephosphorylates Cnb in early mitosis to aid its timely and correct relocalization from the mother to the nascent daughter centriole. Although we have not mapped the potential target sites, previously studied Polo-phosphorylation sites are necessary for the correct relocalization of Cnb. This could mean that Polo and Pp4 both regulate the same site in a sequential manner to first remove—via Polo mediated phosphorylation—and then add back Cnb—via Pp4 dephosphorylation (Figure 7G). Consistent with this model is the finding that in vertebrate cells, Polo mediates the removal of Centrobin from the mother centriole at the prometaphase—metaphase transition (Roux-Bourdieu *et al.*, 2022). We further propose that Cdk1 and Pp4 regulate γTubulin in interphase to maintain robust MTOC activity on only the Cnb^{+} centriole. Although we have not directly implicated specific residues, the conserved Serine 131 residue seems to be important as its unphosphorylated state gives rise to two active MTOCs in interphase. It is tempting to speculate that Pp4's role in mitosis and interphase could be regulated via Pp4r2 and Pp4r3, respectively. Alternatively, Pp4 could be regulated via Cdk1 in mitosis and/or interphase. While protein phosphorylation has been mostly implicated in centrosome maturation during mitosis (Conduit *et al.*, 2014), we know much less about the role of centrosomal protein dephosphorylation during MTOC down-regulation. In the early *Caenorhabditis elegans* embryo, PP2A phosphatases are required for PCM dissolution (Magescas *et al.*, 2019) and the role of Pp4 described here provides additional support for the role of phosphatases in MTOC regulation. Here we provide evidence that Cnb's and γTubulin's posttranslational modifications are tightly regulated to ensure precise MTOC activity and asymmetry in fly neural stem cells. The identification of the target residues and the spatiotemporal activity of Polo, Cdk1, and Pp4 will remain future challenges to provide mechanistic insight into centrosome asymmetry.

MATERIALS AND METHODS

Request a protocol through *Bio-protocol*

Fly strains

Mutant alleles, transgenes, and fluorescent markers:

Pp4$^{\Delta}$/FM7C ActGFP (this work), Pp4 RNAi line (VDCR line Nr. 25317), worGal4, UAS-Cherry::Jupiter (Cabernard and Doe, 2009b), Asl::GFP/CyO (Blachon *et al.*, 2008b), w^{-}; 5X-UAS-Pp4::GFP/CyO, w^{-}; 10X-UAS-Pp4[D85N, H115N]::GFP/CyO (Lipinszki *et al.*, 2015b), y^{1},v^{1}; P{y[+t7.7] v[+t1.8] = TRiP.JF02065}attP2 (Pp4r2 RNAi; BDSC26296), w^{-}; P{ry[+t7.2] = neoFRT}82B flfl[795]/TM6B, Tb[+] (Sousa-Nunes *et al.*, 2009), w^{-}; P{w[+mC] = XP-U}Exel6170/TM6B, Tb[1] (Deficiency, removing Falafel; BDSC7649), ncd-γTubulin37C::GFP/TM6B,Tb (Hallen *et al.*, 2008b, 2008a), γTubulin23C::GFP/TM6B,Tb (Mukherjee *et al.*, 2020), w^{-}; P{w[+mC] = XP-U}Exel6043/CyO (Deficiency, removing γTubulin37C; BDSC7525), w^{-}; Df(2L)JS31, dpp[d-ho]/CyO (Deficiency, removing γTubulin23C; BDSC64238), γTubulin23C[A6-2]/CyO, γTubulin23C[A14-9]/CyO, γTubulin23C[A15-2]/CyO (Vazquez *et al.*, 2008), γTubulin37C[3]/CyO (Wilson and Borisy, 1998b) , PBac{w[+mC] = RB}gammaTub37C[e00793]/CyO (Thibault *et al.*, 2004) , γTubulin37C[S131A]/CyO Actin-GFP; MKRS/TM6B,Tb (this work), γTubulin23C[A15-2], γTubulin37C[3]/CyO Actin-GFP (this work), P{y[+t7.7] v[+t1.8] = TRiP.JF03004}attP2 (RNAi against Cdk1; BDSC28368), w^{-}; lf/CyO-Actin-GFP; Cdk1::EGFP/TM6B, Tb (this work), Sas4::GFP/TM6B,Tb (Peel *et al.*, 2007), w^{-}; UAS-vhh4::GFP/TM6B,Tb (Caussinus *et al.*, 2012), Cnb::GFP/TM6B,Tb (Gallaud *et al.*, 2020a), Polo::GFP/TM6B,Tb (Gallaud *et al.*, 2020a), w^{-}; Asterless::Cherry/CyO (Conduit and Raff, 2010) , w;;pUb-YFP::Cnb[T4E,T9E,S82E] (Januschke *et al.*, 2013a), w^{-}; lf/CyO; cnb e00267/TM6B, Tb (Deficiency removing Cnb; (Januschke *et al.*, 2013b)).

Experimental crosses were performed as outlined in Supplemental Table S1. All strains were raised on standard medium at 25°C, under a 12L:12D light cycle.

Immunohistochemistry

The following antibodies were used for this study: Mouse anti-alpha-tubulin (Sigma, 1:2000, catalogue no. T6199), Guinea Pig anti-Asterless (Gifted from J. Raff, 1:20,000), mouse anti-gamma-tubulin (Millipore Sigma, 1:2000, catalogue no. SAB4701044). Secondary antibodies were from Molecular Probes and all done at 1:1000.

A total of 72 to 96 h after egg laying, larval brains were dissected in Schneider's insect medium (Sigma, catalogue no. S0146-100ML) for no more than 20 min. Briefly, dissection was done by removing the posterior end of the larvae and inverting the entire larvae. After inversion, the fat bodies and gastrointestinal tract were removed, and the axonal connections between the brain lobes and cuticle were severed. This resulted in an inverted cuticle devoid of all other organs save for the brain, which is connected to the cuticle via axonal connections with the ventral nerve cord. After dissection, samples were fixed in 4% paraformaldehyde in Schneider's medium for 20 min on a rotator at room temperature. After fixing, the samples were washed at least three times with PBSBT (1X PBS, 0.1% vol/vol of Triton-X-100, and 1% wt/vol BSA) for 1 h. Primary antibody dilution was prepared in 1X PBSBT, and samples were incubated in primary antibody solution for at least 2 d at 4°C with agitation. After primary labeling, samples were washed with PBSBT at least three times for 20 min each. Secondary antibody solution was prepared in 1X PBSBT, and samples were covered and again incubated for 2 d at 4°C with agitation. After incubation, the [AQ3] samples were washed three times with PBST (1X PBS, 0.1% vol/vol of Triton-X-100). During this final wash, mounting slides were prepared by affixing two glass coverslips onto a glass slide with nail polish to form a thin channel to hold the sample. Final dissections to remove the brains from the cuticles were done in PBSBT, and the brains were then transferred via pipette to equilibrate in Vectashield H-1000 mounting media (Vector laboratories). After equilibration, samples were transferred to the previously prepared slides and sealed with a glass coverslip and VALP (1:1:1 by weight mixture of Vaseline, Lanolin, and Parafin). Samples that were not imaged were stored in Vectashield at 4°C for up to several weeks.

Live-cell imaging

A total of 72 to 96 h after egg laying, larval brains were dissected using microdissection scissors (Fine Science Tools, catalogue no. 15003-08) (Segura and Cabernard, 2023) and forceps (Dumont #5, Electron Microscopy Sciences, item number 0103-5-PO) in Schneider's medium supplemented with 10% bovine growth serum (HyClone, item number SH30541.03) and transferred to chambered slides (Ibidi, catalogue no. 80826) for imaging. Live samples were imaged either with an Intelligent Imaging Innovations (3i) spinning disk confocal system, consisting of a Yokogawa CSU-W1 spinning disk unit and two Prime 95B Scientific CMOS cameras, on an Andor BC43 benchtop confocal microscope. A 60x/1.4NA oil immersion objective mounted on a both microscopes was used for imaging. Live imaging voxels are 0.22 × 0.22 × 1 µm (60x/1.4NA spinning disk). Temporal resolution varied between 30 s and 3 min per frame.

3D-SIM

3D-SIM was performed on fixed brain samples using a DeltaVision OMX-Blaze system (version 4; GE Healthcare), equipped with 405-, 445-, 488-, 514-, 568-, and 642-nm solid-state lasers. Images were acquired using a Plan Apo N 60x, 1.42 NA oil immersion objective lens (Olympus) and 4 liquid-cooled sCMOs cameras (pco.edge 5.5, full frame 2560 × 2160; PCO). Exciting light was directed through a movable optical grating to generate a fine-striped interference pattern on the sample plane. The pattern was shifted laterally through five phases and three angular rotations of 60° for each z section. Optical z sections were separated by 0.125 µm. The laser lines 405, 488, 568, and 642 nm were used for 3D-SIM acquisition. Exposure times were typically between 10 and 120 ms, and the power of each laser was adjusted to achieve optimal intensities of between 5000 and 8000 counts in a raw image of 15-bit dynamic range at the lowest laser power possible to minimize photobleaching. Multichannel imaging was achieved through sequential acquisition of wavelengths by separate cameras.

3D-SIM image reconstruction

Raw 3D-SIM images were processed and reconstructed using the DeltaVision OMX SoftWoRx software package (version 6.1.3, GE Healthcare; Gustafsson, M. G. L. 2000). The resulting size of the reconstructed images was of 512 × 512 pixels from an initial set of 256 × 256 raw images. The channels were aligned in the image plane and around the optical axis using predetermined shifts as measured using a target lens and the SoftWoRx alignment tool. The channels were then carefully aligned using alignment parameter from control measurements with 0.5-µm-diameter multispectral fluorescent beads (Invitrogen, Thermo Fisher Scientific).

Analysis

All analyses were done in Imaris 10.1 and ImageJ 1.54. Imaris was used to determine the mean and integrated fluorescent density present at centrosomes. ImageJ was used to generate line scans of centrosomal intensity. The Imaris spot tool was used to measure the mean and integrated fluorescent density present at centrosomes in interphase and mitosis. Interphase was defined as at least 30 min before nuclear envelope breakdown (NEB), and mitosis was defined as 5 to 7 min before NEB, which was defined as the first frame where microtubule penetration into the nucleus was observed. A 1.83×1.83×1.83 µm (xyz) spot was centered on the centrosome using the location of centriolar signal from either Asterless-GFP or Centrobin-GFP, and then used to measure either the total sum or average fluorescence intensity of either the GFP (Asterless, Centrobin, or Polo) or RFP (Cherry::Jupiter, microtubules) channels. For γTubulin analysis, spot sizes were adjusted to either 1×1×2 µm (xyz) for the BC43 andor microscope or 1.5×1.5×2 µm for the 3i Nikon microscope. To normalize against cytoplasmic intensity, one spot of the same size was placed in the cytoplasm. The average fluorescence intensity of both centrosomal and cytoplasmic measurements were then used to normalize centrosomal signal to cytoplasmic signal, such that:

$$\begin{aligned} &\textit{normalized centrosome intensity} \\ &= \frac{\textit{Centrosome Signal} - \textit{background}}{\textit{Cytoplasmic signal} - \textit{background}} \end{aligned} \quad (1)$$

Where "background" is defined as the minimum value assigned to pixels by the microscope camera. Similarly, asymmetry indices were generated by normalizing the apical centrosome to the basal centrosome for markers of interest, such that:

$$\begin{aligned} &\textit{Asymmetry Index} \\ &= AC/BC = \frac{\textit{Apical Centrosome Signal} - \textit{background}}{\textit{Basal Centrosome Signal} - \textit{background}} \end{aligned} \quad (2)$$

Where AC and BC refer to the apical and basal centrosomes, respectively. These imaris spots were also used to infer centrosome-to-centrosome positioning based on their X, Y, and Z coordinates. The distance between centrosomes was calculated based on the equation for the distance between two points in 3D space, such that if centrosome 1 is defined as (x_1, y_1, z_1) and centrosome 2 is defined as (x_2, y_2, z_2):

$$\begin{aligned} &\textit{Inter} - \textit{Centrosomal Distance} \\ &= \sqrt{(x_2 - x_1)^2 + (y_2 - y_1)^2 + (z_2 - z_1)^2} \end{aligned} \quad (3)$$

This calculation was also applied if the distance between two points was measured, such as the distance between the apical centrosome and the apical cortex.

Imaris measurement points were used to determine the angle of movement between the position of a centrosome in interphase and its ultimate location at metaphase. This was done by placing point A on the centrosome in interphase, point B on the center of the cell, and point C on the centrosome in metaphase, and the measurement of the angle formed by ∠ABC was recorded and plotted.

ImageJ was used to generate intensity plots of centrosomal signal. Using the same cell cycle timepoints as above, the center-most slice of the centrosome was identified. Following this, a summed projection of the center-most slice plus the slices directly above and below the center was generated. Using this summed projection, a line of at least 5 µm was drawn through the center point of the centrosome (again, based on centriolar markers such as Asterless and Centrobin). This line was then used to generate a line plot of intensity, which was recorded and saved as a csv file for analysis.

Centriolar age measurement

To determine centriolar age, Asl intensity was used as a reference. The contours of nonoverlapping centrioles were drawn in ImageJ based on Asl signal and saved as a region of interest (ROI) in imageJ. Total Asl intensity was then used to determine centriolar age because daughter centrioles have lower intensity than mother centrioles (Gallaud *et al.*, 2020a). The same ROIs were then used to measure total pixel intensity for markers of interest (e.g., γTubulin37C::GFP, Cnb::EGFP). Asymmetry ratios for markers of interest were then determined by dividing total daughter centriole intensity with total mother centriole intensity.

Definition of daughter versus mother enrichment of Centrobin

To determine the enrichment of Centrobin on centrioles, we used the raw integrated density of Centrobin signal observed in the cytoplasm (B_{signal}), on the daughter centriole (D_{signal}), and on the mother centriole (M_{signal}). To determine the variation of signal in the background, we measured 60 ROIs in the cytoplasm of one wild-type cell and used the resulting values to determine the percent SD observed. The following logic gates were then used in Python to determine enrichment:

$$\textit{if } M_{signal} > \%St.Dev. * B_{signal} \textit{ AND } M_{signal} > D_{signal} \rightarrow \textit{Mother enrichment} \quad (4a)$$

$$\textit{if } D_{signal} > \%St.Dev. * B_{signal} \textit{ AND } D_{signal} > M_{signal} \rightarrow \textit{Daughter enrichment} \quad (4b)$$

$$\textit{if } M_{signal} < \%St.Dev. * B_{signal} \textit{ AND } D_{signal} < \%St.Dev. * B_{signal} \rightarrow \textit{No enrichment} \quad (4c)$$

The resulting determinations of enrichment were then used to bin the data for visualization.

Determination of daughter:mother centriole ratios

To determine the ratio of daughter to mother centriole signal of either Centrobin or Asterless, the integrated density of signal was used in the following equation:

$$D/M = \frac{\textit{Daughter Centriole Signal} - \textit{background}}{\textit{Mother Centriole Signal} - \textit{background}} \quad (5)$$

In instances where the background signal exceeded that of either the mother or daughter centriole (Supplemental Figure S6, A–E), the following was used instead:

$$D/M = \frac{Observable\ Centriole\ Signal}{background} \quad 6$$

Where *Observable Centriole Signal* is the signal of either the daughter or the mother.

Generation of the PP4 19C null allele

CRISPR target sequences for the PP4-19c locus were identified using the FlyCRISPR Target Finder tool (https://flycrispr.org/target-finder/). Two guide RNAs were identified that flank the PP4-19c gene to generate a precise deletion without affecting neighboring genes: 5′ TTCGCTTCGCTTTTGCAGGC ′3 and 5′ ACTTGTTGAGATAGTCCATG ′3. gRNAs were cloned into the pBbsI-U6-gRNA expression vector (p-U6-BbsI-chiRNA; catalogue no. 45946, Addgene) using BbsI mediated cloning following a standard protocol (https://flycrispr.org/protocols/).

Primer: 5′CTTCGTTCGCTTCGCTTTTGCAGGC′3, 5′CTTCGACTTGTTGAGATAGTCCATG′3

A donor plasmid (pHD-DsRed-attP, catalogue no. 51019, Addgene) was used for homology-directed repair (HDR) to replace the PP4-19c locus with a marker cassette. Approximately 1 kb homology sequences upstream of the 5′ CRISPR site and downstream of the 3′ site were amplified by PCR from genomic DNA and cloned into the donor vector carrying a 3xP3>dsRed cassette to enable identification of successful replacement events via fluorescent screening. The donor vector was assembled using standard molecular cloning techniques and verified by sequencing.

Primer 5′Homology arm (AarI): 5′tgcaCACCTGCgatcctacATGAGGCTATTTCGCAATG′3, 5′attcCACCTGCtgaatcgcCCTTGTCTCTGTGATCTC′3

Primer 3′Homology arm (SapI): 5′ cgagGCTCTTCagacTGCAGAGAAGGAAGACGC′3, 5′ tagtGCTCTTCatatTGCAAAAGCGAAGCGAAC′3

gRNA vectors and the donor plasmid were coinjected into vasa-Cas9 embryos (BL#51324).

Injected embryos were raised to adulthood and crossed to a balancer stock. F1 progenies were screened for dsRed fluorescence in the eye using a fluorescence stereomicroscope. Fluorescent-positive individuals were selected as potential PP4-19c deletion mutants.

Molecular verification of PP4 19C null

Genomic DNA was extracted from fluorescent-positive heterozygous F1 individuals. PCR was performed using primers flanking the PP4 19C locus to confirm successful replacement of the target region with the 3xP3>dsRed cassette (expected size 1.9 kb for control and 1.7 and 1.9 kb for heterozygous mutants). PCR products were validated by Sanger sequencing.

Primers: 5′CAGGCGAACTCAAAAACCG′3, 5′GGTAGAGGTAAACAGATGG′3

Generation of PP4 19C transgenic flies

The full-length PP4-19c ORF was amplified from the PP4-19c cDNA clone) RE58406 obtained from the Drosophila Genomic Research Center (Indiana, USA) using the following primers: 5′CACCATGTCCGACTACAGCGAC′3 and 5′TTAGAGAAAGTAGTCCGCCTG′3

[AQ4]

The ORF was cloned into pENTR using TOPO cloning (Invitrogen) and exchanged into the pUASattB-10xUAS and 5xUAS destination vectors with either no tag, a C-terminal EGFP or an N-terminal EGFP tag. Phosphatase dead versions of PP4 19C were generated using entry vectors carrying PP4 19C^{D85N,H115N} and PP4 19C^{D85N}, kindly provided by Dr. Marcin R. Przewloka (Lipinszki *et al.*, 2015a). All constructs were verified by sequencing and injected into the attP40 genomic landing site (BestGene Inc, California, USA).

Generation of γTubulin phosphomutants

The γγTubulin37C coding sequence region was amplified using the following primers:

5′CTACATTCCTCGTGGG3′

5′GCCGTGCTTTAGCGTA3′

Serine 131 of gamma tubulin37C was mutated to Alanine via CRISPR-mediated HDR. We introduced a double-stranded break via the CRISPR target CGGCTTTAGCCAGGGTGAGAAGG, 50 base pairs (bp) away from Serine131. We then designed rescue templates that introduced a mutated Serine131 (changing TCG to GCG). Rescue templates carrying the specific site mutation could not be generated via PCR and were instead synthesized by GeneWiz. Lowercase bold bases denote homology with the dsRed backbone:

5′**taaagatctccatgcataaggcgcgcc**TCCCCTTTGCAGTTGTACAACCAGGAGAATGTGTTCCTCTCCAAGCACGGCGGTGGAGCAGGAAACAACTGGGCGTCCGGCTTTAGCCAGGGTGAGAAGaTGCAGGAGGAGGTGTTCGACATTCTGGACCGCGAGGCCGATGGCAGCGATg CGCTGGAGGGATTCGTGCTCTG 3′ (homology with AscI, underline bold denotes mutated PAM site, bold underlined italic denotes mutated Serine 131)

The resulting rescue homology templates were then inserted into a EcoRI/NdeI/XhoI/AscI digested dsRed reporter plasmid via an infusion reaction kit. The following primers were used to generate homology arms for insertion into the dsRed vector:

5′**tcgctgaagcaggtggaatt**CTTCTCTGCGATTTTTACG3′ (upstream homology, EcoRI)

5′**tgatcgcaggtgtgcatatg**AGTTTTTTAAATGAAATACATAAAA 3′ (upstream homology, Nde1)

5′CTGGAGGGATTCGTGCTCTGCCACTCGATAGCCGGCGGAA3′ (downstream homology, homology with GeneWiz synthesized fragment)

5′ attgacggaagagcctcgagGCCAAGGCCCTCTTGAAGAG 3′ (downstream homology, XhoI)

Homology rescue templates were designed such that the dsRed reporter would be inserted into an intron upstream of Serine131 as to not interfere with viability. The plasmid and Cas9 delivery system were then injected into flies by BestGene, and dsRed was used to select for positive transformants. Once isolated and balanced over balancer chromosomes CyO-Actin::GFP, the dsRed cassette was floxed out of the newly generated line by crossing against a Cre-expressing line. Final transformants were verified with PCR and sequencing with primer 5′ AGCACCACCACACTGT3′ to confirm the presence of the desired mutation in the final line.

Generation of Cdk1::EGFP Crispr line

Target specific sequences with high efficiency were chosen using the CRISPR Optimal Target Finder (http://tools.flycrispr.molbio.wisc.edu/targetFinder/), the DRSC CRISPR finder (http://www.flyrnai.org/crispr/), and the Efficiency Predictor (http://www.flyrnai.org/evaluateCrispr/) web tools. The gRNA was cloned into the pBbsI-U6-gRNA expression vector (p-U6-BbsI-chiRNA; catalogue no. 45946, Addgene) using BbsI-mediated cloning following a standard protocol (https://flycrispr.org/protocols/). The following primers were used:

Cdk1_C_sgRNA_sense: CTTCGATGCTCCAAAATGTCCTTGG; Cdk1_C_sgRNA_antisense: AAACCCAAGGACATTTTGGAGCATC. 1 kb homology arms flanking the insertion site were cloned into the previously described pHD-DsRed-attP-EGFP::SspB vector using the following primers: Cdk1_C_LHA_203_FWD: CTGGGCCTTTCGCCCGGGCTGAAGATTTTGCAATATTGTTTTT; Cdk1_C_LHA_203_REV: CTCCAAAATGTCCTTGGCtGAAATGCGATGAACTGGATCGT.

Definition of statistical tests and replicates

Data were collected from at least two independent experiments. Statistical analyses and visualization were done in Python. Statistical significance between normal distributions of data was determined via Student's unpaired *t* test to compare the differences in the distribution of collected data. Significance between nonparametric distributions of data was determined with a two-sided Mann–Whitney U statistical test. For multiple comparisons, the Kruskal–Wallis test was used. If significant differences were detected, an uncorrected Dunn's test for multiple comparisons was used. The chi-squared goodness-of-fit statistical test was done to test for differences between frequencies of observed phenotypes. $p < 0.05$ were considered significant; * $p < 0.05$, ** $p < 0.01$, *** $p < 0.001$, **** $p < 0.0001$.

Data visualization

Data were visualized in Python 3.5 Jupyter notebooks. Visualizations were generated using Matplotlib and Seaborn. Statistical tests were done using Scipy. Code, raw data and data used for plotting can be found here: https://github.com/Roberto-Carlos-Segura/PP4_paper_2024.

ACKNOWLEDGMENTS

We thank Cayetano Gonzalez, Tomer Avidor-Reiss and Jordan Raff for fly stocks and antibodies, Jeff Rasmussen and members of the Cabernard laboratory for helpful discussions and comments. This work was supported by the National Institutes of Health (R35GM148160 to C.C.) and the Ford Foundation (to R.C.S.). Stocks were obtained from the Bloomington Drosophila Stock Center (BDSC), which is supported by grant P40OD018537 from the NIH Office of Research Infrastructure Programs (ORIP) in collaboration with the National Institute of General Medical Sciences (NIGMS), National Institute of Neurological Disorders and Stroke (NINDA) and National Institute of Child Health and Human Development (NICHD).

REFERENCES

Albertson R, Chabu C, Sheehan A, Doe CQ (2004). Scribble protein domain mapping reveals a multistep localization mechanism and domains necessary for establishing cortical polarity. J Cell Sci 117, 6061–6070.

Alvarado-Kristensson M, Rodríguez MJ, Silió V, Valpuesta JM, Carrera AC (2009). SADB phosphorylation of γ-tubulin regulates centrosome duplication. Nat Cell Biol 11, 1081–1092.

Blachon S, Gopalakrishnan J, Omori Y, Polyanovsky A, Church A, Nicastro D, Malicki J, Avidor-Reiss T (2008a). Drosophila asterless and vertebrate Cep152 are orthologs essential for centriole duplication. Genetics 180, 2081–2094.

Blachon S, Gopalakrishnan J, Omori Y, Polyanovsky A, Church A, Nicastro D, Malicki J, Avidor-Reiss T (2008b). Drosophila asterless and vertebrate Cep152 are orthologs essential for centriole duplication. Genetics 180, 2081–2094.

Blanco-Ameijeiras J, Lozano-Fernández P, Martí E (2022). Centrosome maturation – in tune with the cell cycle. J Cell Sci 135, jcs259395.

Böhler A, Vermeulen BJA, Würtz M, Zupa E, Pfeffer S, Schiebel E (2021). The gamma-tubulin ring complex: Deciphering the molecular organization and assembly mechanism of a major vertebrate microtubule nucleator. Bioessays 43, e2100114.

Cabernard C, Doe CQ (2009a). Apical/basal spindle orientation is required for neuroblast homeostasis and neuronal differentiation in Drosophila. Dev Cell 17, 134–141.

Cabernard C, Doe CQ (2009b). Apical/basal spindle orientation is required for neuroblast homeostasis and neuronal differentiation in Drosophila. Dev Cell 17, 134–141.

Caussinus E, Kanca O, Affolter M (2012). Fluorescent fusion protein knockout mediated by anti-GFP nanobody. Nat Struct Mol Biol 19, 117–121.

Chen C, Yamashita YM (2021). Centrosome-centric view of asymmetric stem cell division. Open Biol 11, 200314.

Collins A, Ross J, Lang SH (2017). A systematic review of the asymmetric inheritance of cellular organelles in eukaryotes: A critique of basic science validity and imprecision. PLoS One 12, e0178645.

Conde C, Osswald M, Barbosa J, Santos TM, Pinheiro D, Guimarães S, Matos I, Maiato H, Sunkel CE (2013). Drosophila Polo regulates the spindle assembly checkpoint through Mps1-dependent BubR1 phosphorylation. EMBO J 32, 1761–1777.

Conduit PT, Feng Z, Richens JH, Baumbach J, Wainman A, Bakshi SD, Dobbelaere J, Johnson S, Lea SM, Raff JW (2014). The centrosome-specific phosphorylation of Cnn by Polo/Plk1 drives Cnn scaffold assembly and centrosome maturation. Dev Cell 28, 659–669.

Conduit PT, Raff JW (2010). Cnn dynamics drive centrosome size asymmetry to ensure daughter centriole retention in Drosophila neuroblasts. Curr Biol 20, 2187–2192.

Conduit PT, Wainman A, Raff JW (2015). Centrosome function and assembly in animal cells. Nat Rev Mol Cell Bio 16, 611–624.

Connell M, Xie Y, Chen R, Zhu S (2021). Kin17 drives dissociation of Mira from the centrosome in neuroblasts by regulating splicing of Flfl. bioRxiv, 2021.11.03.467193.

Delgado MK, Cabernard C (2020). Mechanical regulation of cell size, fate, and behavior during asymmetric cell division. Curr Opin Cell Biol 67, 9–16.

Fu J, Lipinszki Z, Rangone H, Min M, Mykura C, Chao-Chu J, Schneider S, Dzhindzhev NS, Gottardo M, Riparbelli MG, *et al.* (2016). Conserved molecular interactions in centriole-to-centrosome conversion. Nat Cell Biol 18, 87–99.

Gallaud E, Nair AR, Horsley N, Monnard A, Singh P, Pham TT, Garcia DS, Ferrand A, Cabernard C (2020a). Dynamic centriolar localization of Polo and Centrobin in early mitosis primes centrosome asymmetry. PLoS Biol 18, e3000762.

Gallaud E, Nair AR, Horsley N, Monnard A, Singh P, Pham TT, Garcia DS, Ferrand A, Cabernard C (2020b). Dynamic centriolar localization of Polo and Centrobin in early mitosis primes centrosome asymmetry. PLoS Biol 18, e3000762.

Gambarotto D, Pennetier C, Ryniawec JM, Buster DW, Gogendeau D, Goupil A, Nano M, Simon A, Blanc D, Racine V, *et al.* (2019). Plk4 regulates centriole asymmetry and spindle orientation in neural stem cells. Dev Cell 50, 11–24.e10.

Gillingham AK, Munro S (2000). The PACT domain, a conserved centrosomal targeting motif in the coiled-coil proteins AKAP450 and pericentrin. EMBO Rep 1, 524–529.

Gilmore EC, Walsh CA (2013). Genetic causes of microcephaly and lessons for neuronal development. Wiley Interdiscip Rev Dev Biol 2, 461–478.

Gonzalez C (2021). Centrosomes in asymmetric cell division. Curr Opin Struc Biol 66, 178–182.

Hallen MA, Ho J, Yankel CD, Endow SA (2008a). Fluorescence recovery kinetic analysis of γ-Tubulin binding to the mitotic spindle. Biophys J 95, 3048–3058.

Hallen MA, Liang Z-Y, Endow SA (2008b). Ncd motor binding and transport in the spindle. J Cell Sci 121, 3834–3841.

Hannaford MR, Liu R, Billington N, Swider ZT, Galletta BJ, Fagerstrom CJ, Combs C, Sellers JR, Rusan NM (2022a). Pericentrin interacts with Kinesin-1 to drive centriole motility. J Cell Biol 221, e202112097.

Hannaford MR, Liu R, Billington N, Swider ZT, Galletta BJ, Fagerstrom CJ, Combs C, Sellers JR, Rusan NM (2022b). Pericentrin interacts with Kinesin-1 to drive centriole motility. J Cell Biol 221, e202112097.

Hannaford MR, Rusan NM (2024). Positioning centrioles and centrosomes. J Cell Biol 223, e202311140.

Helps NR, Brewis ND, Lineruth K, Davis T, Kaiser K, Cohen PT (1998). Protein phosphatase 4 is an essential enzyme required for organisation of microtubules at centrosomes in Drosophila embryos. J Cell Sci 111 (Pt 10), 1331–1340.

Homem CCF, Knoblich JA (2012). Drosophila neuroblasts: A model for stem

cell biology. Development 139, 4297–4310.
Hughes SE, Beeler JS, Seat A, Slaughter BD, Unruh JR, Bauerly E, Matthies HJG, Hawley RS (2011). Gamma-tubulin is required for bipolar spindle assembly and for proper kinetochore microtubule attachments during prometaphase I in Drosophila oocytes. PLoS Genet 7, e1002209.
Jaiswal S, Singh P (2021). Centrosome dysfunction in human diseases. Semin Cell Dev Biol 110, 113–122.
Januschke J, Llamazares S, Reina J, Gonzalez C (2011). Drosophila neuroblasts retain the daughter centrosome. Nat Commun 2, 243.
Januschke J, Reina J, Llamazares S, Bertran T, Rossi F, Roig J, Gonzalez C (2013a). Centrobin controls mother–daughter centriole asymmetry in Drosophila neuroblasts. Nat Cell Biol 15, 241–248.
Januschke J, Reina J, Llamazares S, Bertran T, Rossi F, Roig J, Gonzalez C (2013b). Centrobin controls mother–daughter centriole asymmetry in Drosophila neuroblasts. Nat Cell Biol 15, 241–248.
Karman Z, Rethi-Nagy Z, Abraham E, Fabri-Ordogh L, Csonka A, Vilmos P, Debski J, Dadlez M, Glover DM, Lipinszki Z (2020a). Novel perspectives of target-binding by the evolutionarily conserved PP4 phosphatase. Open Biol 10, 200343.
Karman Z, Rethi-Nagy Z, Abraham E, Fabri-Ordogh L, Csonka A, Vilmos P, Debski J, Dadlez M, Glover DM, Lipinszki Z (2020b). Novel perspectives of target-binding by the evolutionarily conserved PP4 phosphatase. Open Biol 10, 200343.
Karpova N, Bobinnec Y, Fouix S, Huitorel P, Debec A (2006). Jupiter, a new Drosophila protein associated with microtubules. Cell Motil Cytoskelet 63, 301–312.
Kloeker S, Wadzinski BE (1999). Purification and identification of a novel subunit of protein serine/threonine phosphatase 4. J Biol Chem 274, 5339–5347.
Lambert JD, Nagy LM (2002). Asymmetric inheritance of centrosomally localized mRNAs during embryonic cleavages. Nature 420, 682–686.
Lerit DA, Jordan HA, Poulton JS, Fagerstrom CJ, Galletta BJ, Peifer M, Rusan NM (2015). Interphase centrosome organization by the PLP-Cnn scaffold is required for centrosome function. J Cell Biol 210, 79–97.
Lerit DA, Smyth JT, Rusan NM (2013). Organelle asymmetry for proper fitness, function, and fate. Chromosome Res 21, 271–286.
Link N, Chung H, Jolly A, Withers M, Tepe B, Arenkiel BR, Shah PS, Krogan NJ, Aydin H, Geckinli BB, *et al.* (2019). Mutations in ANKLE2, a ZIKA virus target, disrupt an asymmetric cell division pathway in Drosophila neuroblasts to cause microcephaly. Dev Cell 51, 713–729.e6.
Lipinszki Z, Lefevre S, Savoian MS, Singleton MR, Glover DM, Przewloka MR (2015a). Centromeric binding and activity of protein phosphatase 4. Nat Commun 6, 5894.
Lipinszki Z, Lefevre S, Savoian MS, Singleton MR, Glover DM, Przewloka MR (2015b). Centromeric binding and activity of protein phosphatase 4. Nat Commun 6, 5894.
Lyu J, Kim H-R, Yamamoto V, Choi SH, Wei Z, Joo C-K, Lu W (2013). Protein phosphatase 4 and Smek complex negatively regulate Par3 and promote neuronal differentiation of neural stem/progenitor cells. Cell Rep 5, 593–600.
Magescas J, Zonka JC, Feldman JL (2019). A two-step mechanism for the inactivation of microtubule organizing center function at the centrosome. Elife 8, e47867.
Marthiens V, Basto R (2020). Centrosomes: The good and the bad for brain development. Biol Cell 112, 153–172.
Martin-Granados C, Philp A, Oxenham SK, Prescott AR, Cohen PTW (2008). Depletion of protein phosphatase 4 in human cells reveals essential roles in centrosome maturation, cell migration and the regulation of Rho GTPases. Int J Biochem Cell Biol 40, 2315–2332.
Mukherjee A, Brooks PS, Bernard F, Guichet A, Conduit PT (2020). Microtubules originate asymmetrically at the somatic golgi and are guided via Kinesin2 to maintain polarity within neurons. Elife 9, e58943.
Nigg EA, Raff JW (2009). Centrioles, centrosomes, and cilia in health and disease. Cell 139, 663–678.
Nigg EA, Stearns T (2011). The centrosome cycle: Centriole biogenesis, duplication and inherent asymmetries. Nat Cell Biol 13, 1154–1160.
Novak ZA, Conduit PT, Wainman A, Raff JW (2014). Asterless licenses daughter centrioles to duplicate for the first time in Drosophila embryos. Curr Biol 24, 1276–1282.
Park J, Lee D-H (2020). Functional roles of protein phosphatase 4 in multiple aspects of cellular physiology: A friend and a foe. BMB Rep 53, 181–190.
Peel N, Stevens NR, Basto R, Raff JW (2007). Overexpressing centriole-replication proteins in vivo induces centriole overduplication and de novo formation. Curr Biol 17, 834–843.
Ramdas Nair A, Singh P, Salvador Garcia D, Rodriguez-Crespo D, Egger B, Cabernard C (2016a). The microcephaly-associated protein Wdr62/CG7337 is required to maintain centrosome asymmetry in Drosophila neuroblasts. Cell Rep 14, 1100–1113.
Ramdas Nair A, Singh P, Salvador Garcia D, Rodriguez-Crespo D, Egger B, Cabernard C (2016b). The microcephaly-associated protein Wdr62/CG7337 is required to maintain centrosome asymmetry in Drosophila neuroblasts. Cell Rep 14, 1100–1113.
Rebollo E, Sampaio P, Januschke J, Llamazares S, Varmark H, González C (2007a). Functionally unequal centrosomes drive spindle orientation in asymmetrically dividing Drosophila neural stem cells. Dev Cell 12, 467–474.
Rebollo E, Sampaio P, Januschke J, Llamazares S, Varmark H, Gonzalez C (2007b). Functionally unequal centrosomes drive spindle orientation in asymmetrically dividing Drosophila neural stem cells. Dev Cell 12, 467–474.
Réthi-Nagy Z, Ábrahám E, Sinka R, Juhász S, Lipinszki Z (2023). Protein phosphatase 4 is required for centrobin function in DNA damage repair. Cells 12, 2219.
Robinson BV, Faundez V, Lerit DA (2020). Understanding microcephaly through the study of centrosome regulation in Drosophila neural stem cells. Biochem Soc Trans 48, 2101–2115.
Roux-Bourdieu ML, Dwivedi D, Harry D, Meraldi P (2022). PLK1 controls centriole distal appendage formation and centrobin removal via independent pathways. J Cell Sci 135, jcs259120.
Royall LN, Jessberger S (2021). How stem cells remember their past. Curr Opin Cell Biol 69, 17–22.
Royall LN, Machado D, Jessberger S, Denoth-Lippuner A (2023). Asymmetric inheritance of centrosomes maintains stem cell properties in human neural progenitor cells. Elife 12, e83157.
Rusan NM, Peifer M (2007a). A role for a novel centrosome cycle in asymmetric cell division. J Cell Biol 177, 13–20.
Rusan NM, Peifer M (2007b). A role for a novel centrosome cycle in asymmetric cell division. J Cell Biol 177, 13–20.
Saerens D, Pellis M, Loris R, Pardon E, Dumoulin M, Matagne A, Wyns L, Muyldermans S, Conrath K (2005). Identification of a universal VHH framework to graft non-canonical antigen-binding loops of camel single-domain antibodies. J Mol Biol 352, 597–607.
Sandal P, Jong CJ, Merrill RA, Song J, Strack S (2021). Protein phosphatase 2A – structure, function and role in neurodevelopmental disorders. J Cell Sci 134, jcs248187.
Segura RC, Cabernard C (2023). Live-cell imaging of Drosophila melanogaster third instar larval brains. J Vis Exp.
Shlyakhtina Y, Moran KL, Portal MM (2019). Asymmetric inheritance of cell fate determinants: Focus on RNA. Noncoding RNA 5, 38.
Singh P, Nair AR, Cabernard C (2014a). The centriolar protein Bld10/Cep135 is required to establish centrosome asymmetry in Drosophila neuroblasts. Curr Biol 24, 1548–1555.
Singh P, Ramdas Nair A, Cabernard C (2014b). The Centriolar protein Bld10/Cep135 is required to establish centrosome asymmetry in Drosophila neuroblasts. Curr Biol 24, 1548–1555.
Sousa-Nunes R, Chia W, Somers WG (2009). Protein phosphatase 4 mediates localization of the Miranda complex during Drosophila neuroblast asymmetric divisions. Gene Dev 23, 359–372.
Sumiyoshi E, Sugimoto A, Yamamoto M (2002). Protein phosphatase 4 is required for centrosome maturation in mitosis and sperm meiosis in C. elegans. J Cell Sci 115, 1403–1410.
Sunchu B, Cabernard C (2020a). Principles and mechanisms of asymmetric cell division. Development 147, dev167650.
Sunchu B, Cabernard C (2020b). Principles and mechanisms of asymmetric cell division. Development 147, dev167650.
Sunkel CE, Gomes R, Sampaio P, Perdigão J, González C (1995). Gamma-tubulin is required for the structure and function of the microtubule organizing centre in Drosophila neuroblasts. EMBO J 14, 28–36.
Tariq A, Green L, Jeynes JCG, Soeller C, Wakefield JG (2020). In vitro reconstitution of branching microtubule nucleation. ELife 9, e49769.
Tavosanis G, Llamazares S, Goulielmos G, Gonzalez C (1997). Essential role for γ-tubulin in the acentriolar female meiotic spindle of Drosophila. EMBO J 16, 1809–1819.
Thibault ST, Singer MA, Miyazaki WY, Milash B, Dompe NA, Singh CM, Buchholz R, Demsky M, Fawcett R, Francis-Lang HL, *et al.* (2004). A complementary transposon tool kit for Drosophila melanogaster using P and piggyBac. Nat Genet 36, 283–287.
Toyo-oka K, Mori D, Yano Y, Shiota M, Iwao H, Goto H, Inagaki M, Hiraiwa N, Muramatsu M, Wynshaw-Boris A, *et al.* (2008). Protein phosphatase 4 catalytic subunit regulates Cdk1 activity and microtubule organization

via NDEL1 dephosphorylation. J Cell Biol 180, 1133–1147.
Umezawa T, Nakashima K, Miyakawa T, Kuromori T, Tanokura M, Shinozaki K, Yamaguchi-Shinozaki K (2010). Molecular basis of the core regulatory network in ABA responses: Sensing, signaling and transport. Plant Cell Physiol 51, 1821–1839.
Varadarajan R, Rusan NM (2018). Bridging centrioles and PCM in proper space and time. Essays Biochem 62, 793–801.
Vaźquez M, Cooper MT, Zurita M, Kennison JA (2008). γTub23C interacts genetically with brahma chromatin-remodeling complexes in Drosophila melanogaster. Genetics 180, 835–843.
Voss M, Campbell K, Saranzewa N, Campbell DG, Hastie CJ, Peggie MW, Martin-Granados C, Prescott AR, Cohen PT (2013). Protein phosphatase 4 is phosphorylated and inactivated by Cdk in response to spindle toxins and interacts with γ-tubulin. Cell Cycle 12, 2876–2887.
Wang X, Tsai J-W, Imai JH, Lian W-N, Vallee RB, Shi S-H (2009). Asymmetric centrosome inheritance maintains neural progenitors in the neocortex. Nature 461, 947–955.
Wiese C (2008). Distinct Dgrip84 isoforms correlate with distinct γ-tubulins in Drosophila. Mol Biol Cell 19, 368–377.
Wilson PG, Borisy GG (1998a). Maternally expressed γTub37CD in Drosophila is differentially required for female meiosis and embryonic mitosis. Dev Biol 199, 273–290.
Wilson PG, Borisy GG (1998b). Maternally expressed γTub37CD in Drosophila is differentially required for female meiosis and embryonic mitosis. Dev Biol 199, 273–290.
Xie Y, Jüschke C, Esk C, Hirotsune S, Knoblich JA (2013). The phosphatase PP4c controls spindle orientation to maintain proliferative symmetric divisions in the developing neocortex. Neuron 79, 254–265.
Yamashita YM, Mahowald AP, Perlin JR, Fuller MT (2007). Asymmetric inheritance of mother versus daughter centrosome in stem cell division. Science 315, 518–521.

3.1 SUPPLEMENTAL FIGURES FROM SEGURA ET AL 2025

3.1.1 *Supplemental Figure 1: Pp4$^{\Delta}$ mutants exhibit mitotic deficiencies*

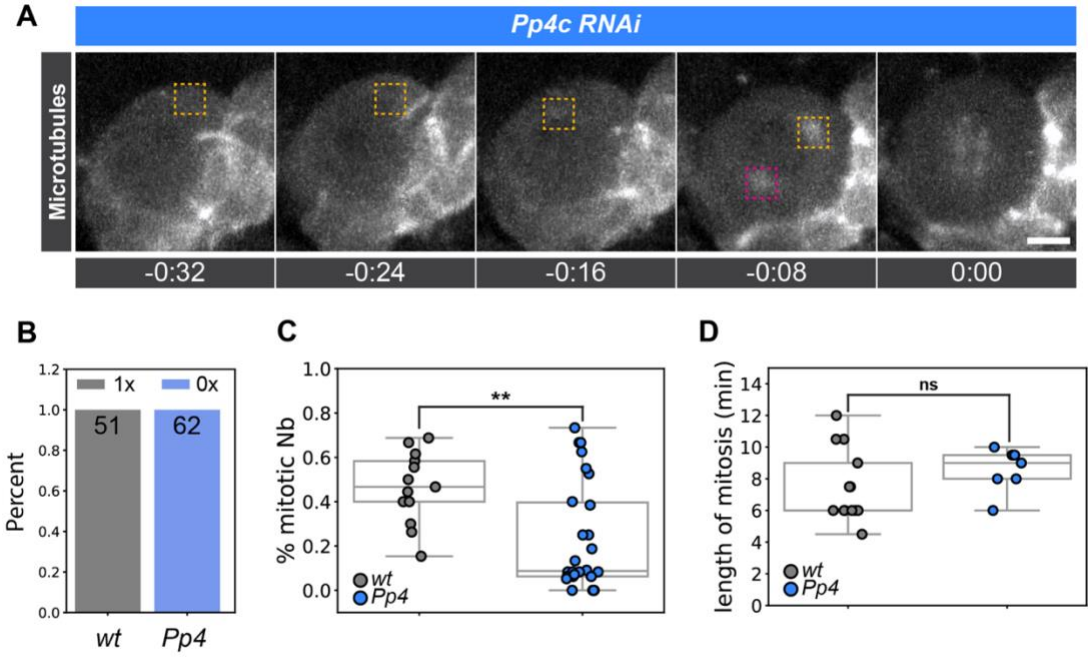

Supplemental Figure 1

(A) Representative image of a Pp4c RNAi mutant neuroblast. **(B)** Bar plot of frequency of 1X MTOC (gray) and 0X MTOC (blue) in wild type (left) and *Pp4$^{\Delta}$* mutants (right). **(C)** length of mitosis in minutes in wild type and *Pp4$^{\Delta}$* mutant brains. **(D)** Percent of mitotic neuroblasts in wild type and *Pp4$^{\Delta}$* mutant brains. Scale bar denotes 5 µm. Each point denotes one neuroblast. $p < 0.05$ were considered significant; * $p < 0.05$, ** $p < 0.01$, *** $p < 0.001$, **** $p < 0.0001$. The following statistical tests were used; Mann-Whitney U test (B, C).

3.1.2 *Supplemental Figure 2: Pp4r2 and Falafel are required for MTOC asymmetry in interphase*

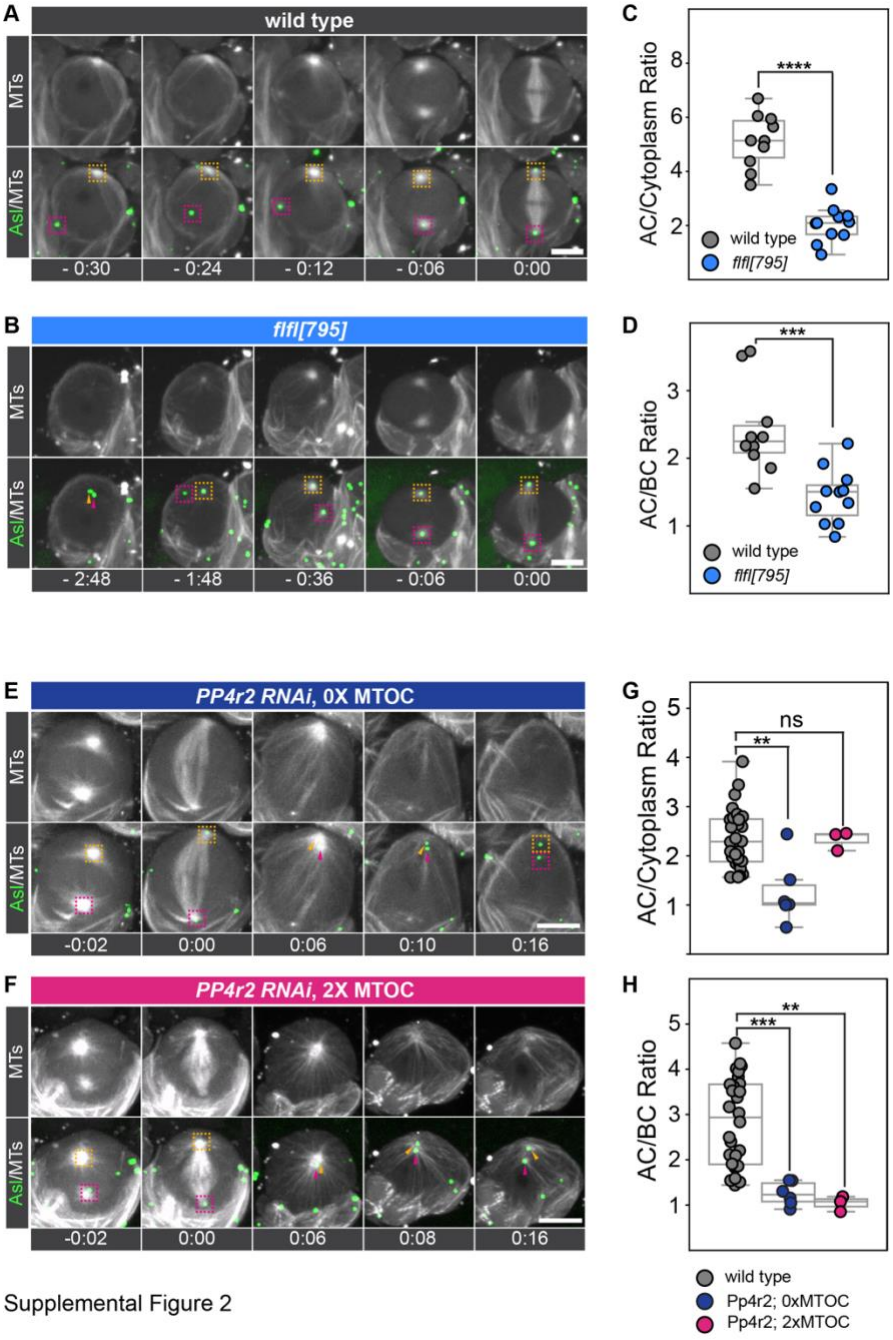

Supplemental Figure 2

Representative image sequences of **(A)** wild type, **(B)** *flfl[795]*, **(E, F)** *Pp4r2 RNAi* expressing neuroblasts. All neuroblasts also express *worGal4, UAS-mCherry::Jupiter* (top row and middle row: white) and *Asterless::GFP* (bottom row: green). Microtubule intensity at the **(C)** apical centrosome normalized to cytoplasmic signal or **(D)** apical to basal centrosome intensity ratios in wild type (gray) and *flfl[795]* mutants (blue).Microtubule intensity at the **(G)** apical centrosome normalized to cytoplasmic signal or **(H)** apical to basal centrosome intensity for wild type (gray) and *Pp4r2 RNAi* expressing neuroblasts (blue). Asl; Asterless. MTs; microtubules. Scale bar denotes 5 μm. Each point denotes one neuroblast. $p < 0.05$ were considered significant; * $p < 0.05$, ** $p < 0.01$, *** $p < 0.001$, **** $p < 0.0001$. Time in: h:mins. The following statistical tests were used: Unpaired Student's T-test (C,D); Kruskal-Wallis test with uncorrected Dunn's test for multiple comparisons (G,H).

3.1.3 *Supplemental Figure 3: γTubulin mutants show a loss of MTOC asymmetry*

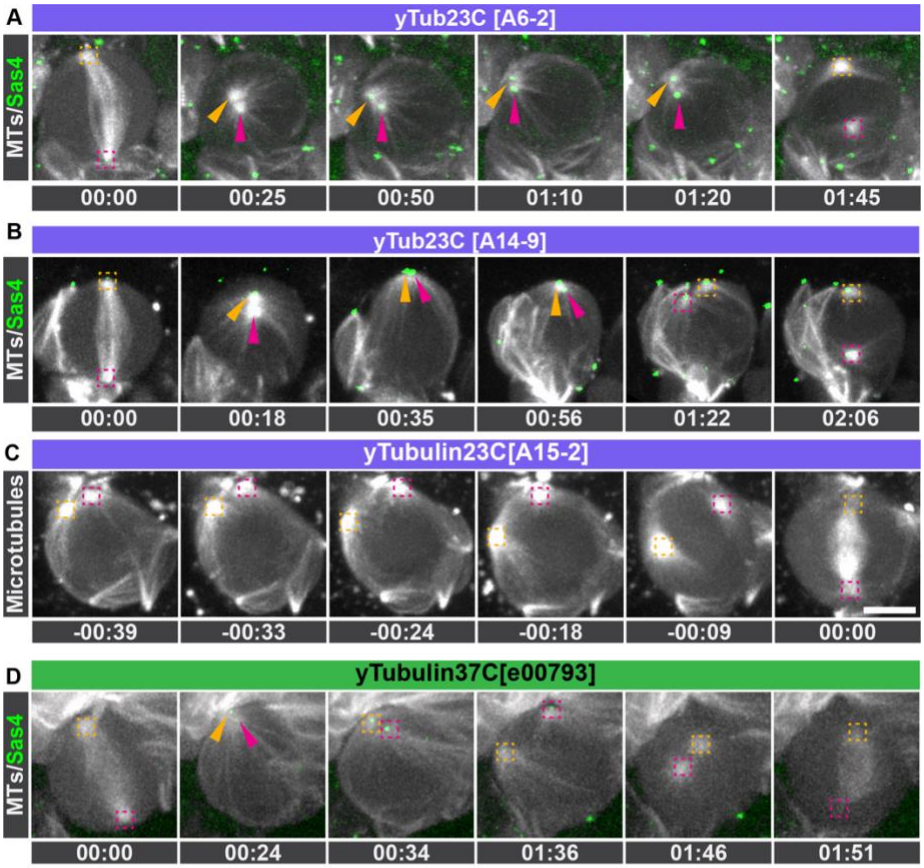

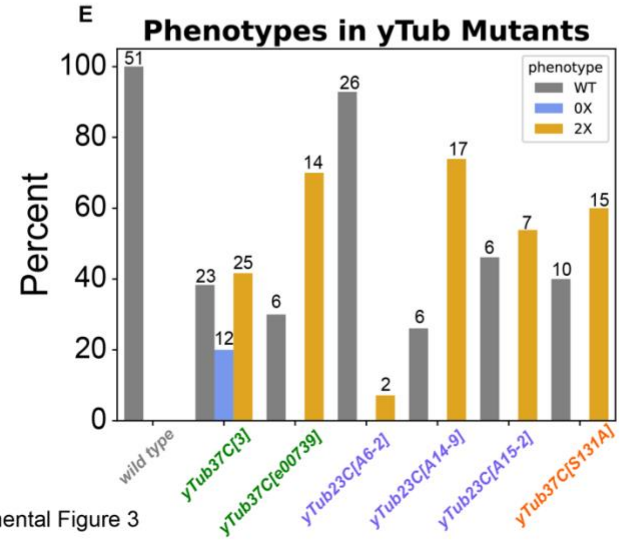

Supplemental Figure 3

Representative images of **(A)** *γTub23C*$^{[A6\text{-}2]}$, **(B)** *γTub23C*$^{[A14\text{-}9]}$, **(C)**, *γTub23C*$^{[A15\text{-}2]}$, and **(D)** *γTub37C*$^{[e00793]}$ mutants expressing *worGal4, UAS-mCherry::Jupiter* and *Sas4::GFP*. Orange and magenta arrrowheads and dashed boxes denote the apical (AC) and basal centrosome (BC), respectively. **(E)** Phenotypic penetrance in percent. wild type (WT); one active MTOC; 0x: no active MTOC; 2x: 2 active MTOCs. MTs; microtubules. Scale bar denotes 5 μm. Time in: h:mins.

3.1.4 *Supplemental Figure 4: gTub23C and gTub37C are redundant for MTOC formation in Drosophila neuroblasts*

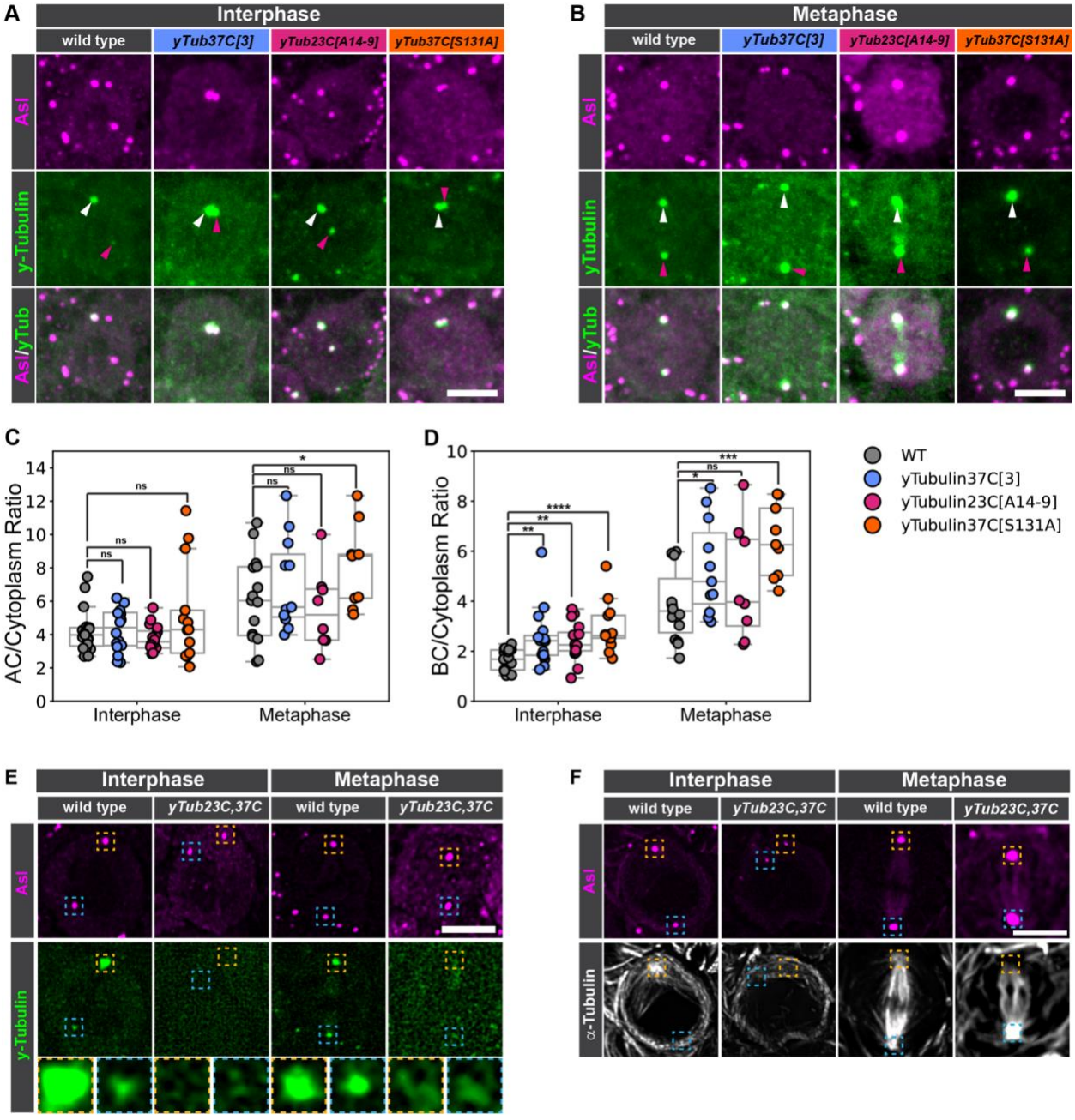

Supplemental Figure 4

Representative **(A)** interphase and **(B)** metaphase images of wild type, γTubulin37C[3], γTubulin23C[A14-9], and γTubulin37C[S131A] mutants stained with anti-Asterless (Asl; magenta, top

and bottom row) and γTubulin (green, middle and bottom row). **(C)** AC/Cytoplasm or **(D)** BC/Cytoplasm ratios for wild type (grey), γTubulin37C$^{[3]}$ (blue), γTubulin23C$^{[A14\text{-}9]}$ (magenta), and γTubulin37C$^{[S131A]}$ (orange) mutants in interphase and metaphase. **(E)** Representative images of wild type and γTubulin23C$^{[A15\text{-}2]}$, γTubulin37C$^{[3]}$ double mutant stained with anti-Asl (magenta, top row) and γTubulin (green, middle and bottom row). High magnification images of γTubulin at the apical (yellow dashed box) and basal (blue dashed box) centrosome are shown in the bottom row. Left column shows representative images in interphase, and the right column shows representative images at metaphase. **(F)** Representative images of wild type and γTubulin23C$^{[A15\text{-}2]}$, γTubulin37C$^{[3]}$ recombinants with anti-αTubulin (gray, top row) and anti-Asl (magenta, second row). Left column shows representative images in interphase, and the right column shows representative images at metaphase. Asl; Asterless. MTs; microtubules. Scale bar denotes 5 μm. Each point denotes one neuroblast. $p < 0.05$ were considered significant; * $p < 0.05$, ** $p < 0.01$, *** $p < 0.001$, **** $p < 0.0001$. The following statistical tests were used: Kruskal-Wallis test with uncorrected Dunn's test for multiple comparisons (C,D).

3.1.5 *Supplemental Figure 5: gTub23C[A15-3], gTub37C[3] homozygous mutants exhibit MTOC deficiencies*

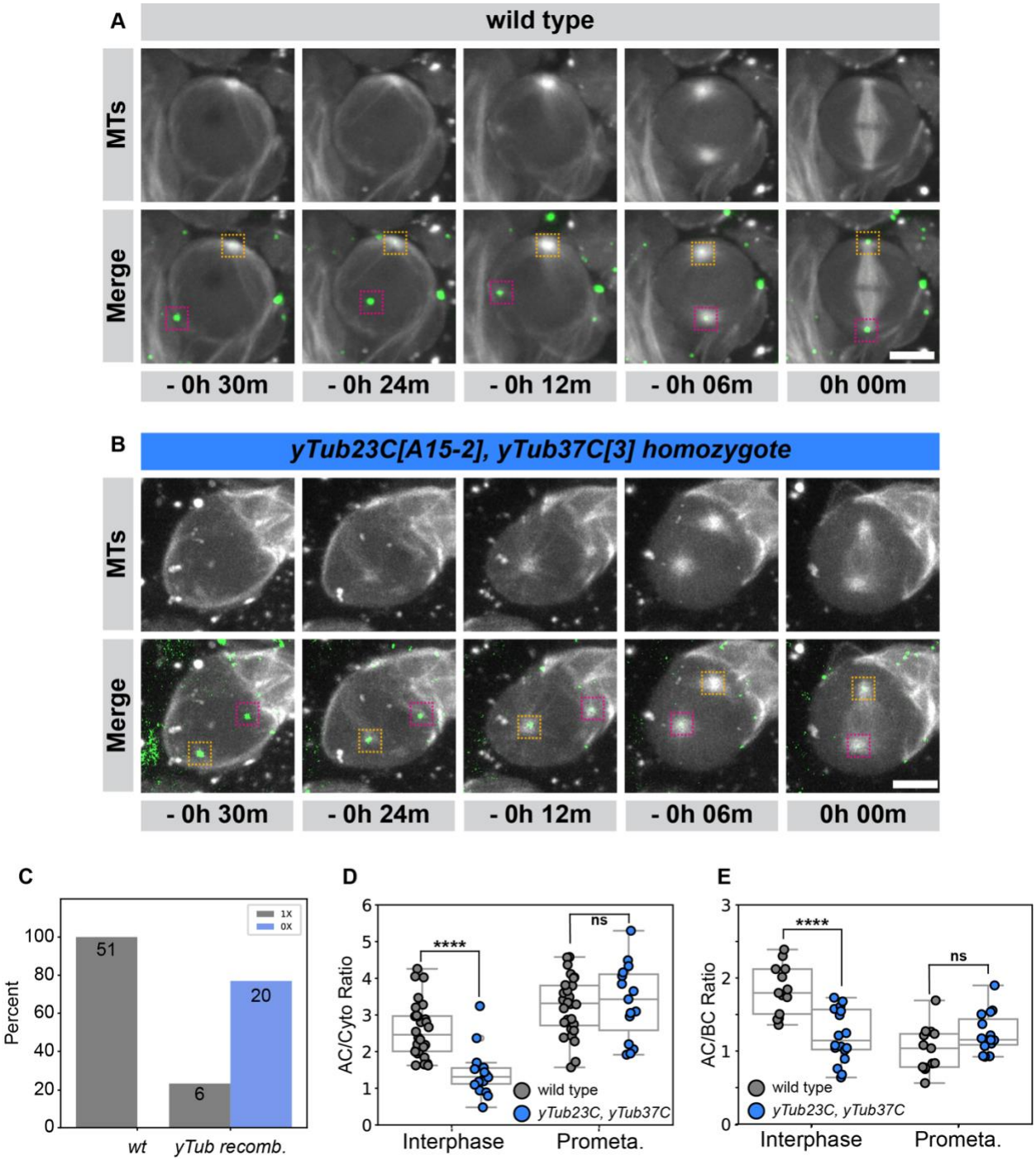

Representative image series of a **(A)** wild type and **(B)** g*Tub23C[A15-3], g*Tub37C[3]* homozygous mutant. Neuroblasts expressing Cherry::Jupiter and Sas4::GFP. **(C)** Bar plot of

frequency of 1X MTOC (gray) and 0X MTOC (blue) in wild type (left) and g*Tub23C[A15-3],* g*Tub37C[3]* homozygous mutants (right). **(D)** Normalized AC/Cytoplasm ratio of microtubule intensity in wild type (gray) and and g*Tub23C[A15-3],* g*Tub37C[3]* mutant (blue) neuroblasts for interphase and prometaphase. **(E)** Normalized AC/BC ratio of microtubule intensity in wild type (gray) and and g*Tub23C[A15-3],* g*Tub37C[3]* mutant (blue) neuroblasts for interphase and prometaphase. Each point denotes one neuroblast. $p < 0.05$ were considered significant; * $p < 0.05$, ** $p < 0.01$, *** $p < 0.001$, **** $p < 0.0001$. The following statistical tests were used; Mann-Whitney U test (D, interphase, E, interphase); Unpaired Student's T-test (D, prometaphase, E, prometaphase).

3.1.6 *Supplemental Figure 6: 3D-SIM image analysis*

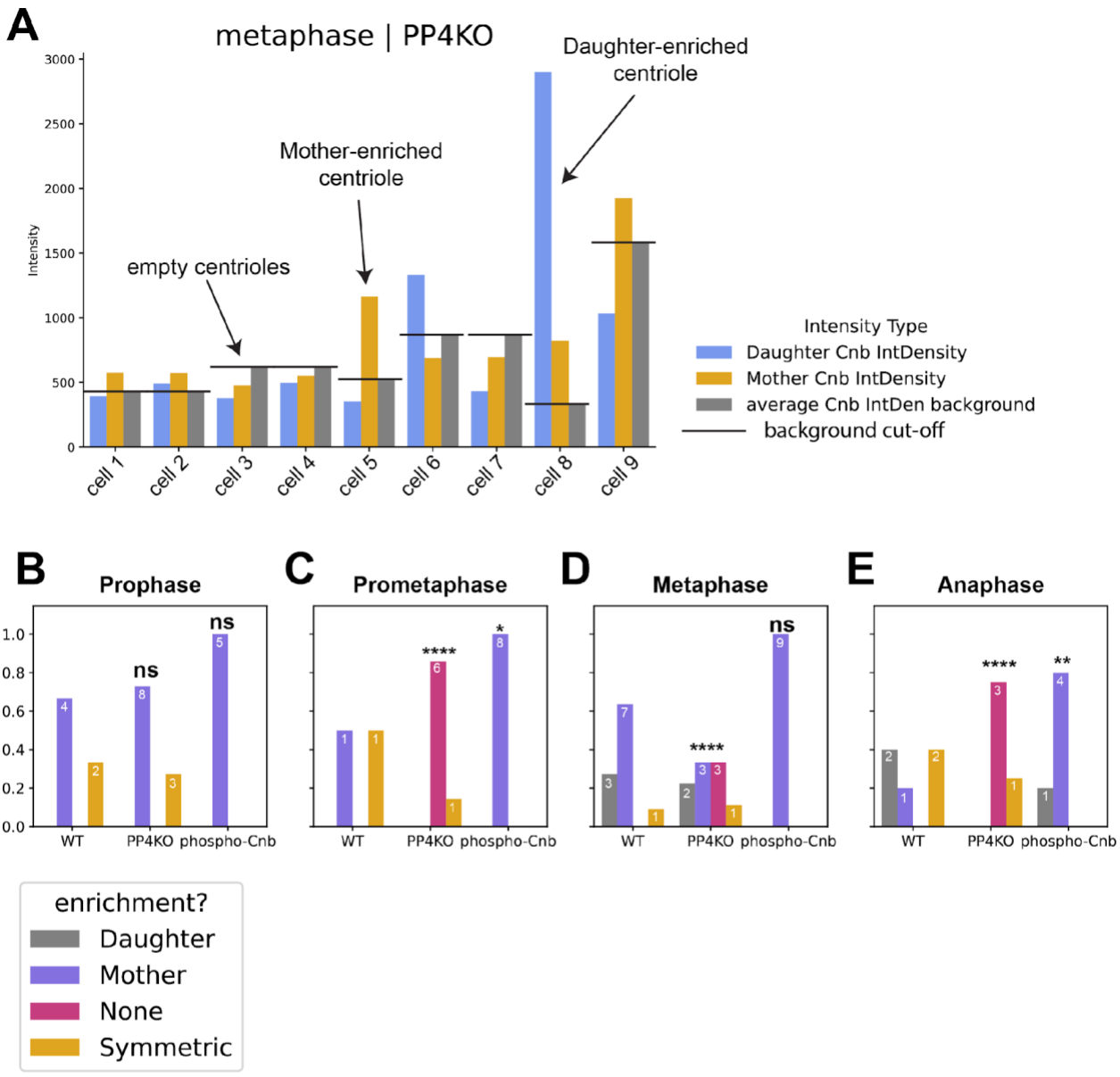

Supplemental Figure 6

(A) plots of individual values of Centrobin intensity at the daughter centriole (blue), mother centriole (yellow) and background (grey) for *Pp4*$^{\Delta}$ mutant interphase neuroblasts. Background values (black lines) were used to evaluate Cnb intensity levels. If background intensity exceeded detectable Cnb on the mother or daughter centriole, the ratio was arbitrarily set to '1' and were also counted towards the pool of neuroblasts with no Cnb signal on either centrosome. **(B-E)** representative bar plots of frequency of wild type (grey), *Pp4*$^{\Delta}$ mutant (blue), and YFP::Cnb^{T4E,T9E,S82E} expressing (orange) neuroblasts in prophase **(A)**, prometaphase **(B)**, metaphase **(C)**, anaphase **(D)**, and telophase **(E)**.Each point denotes one neuroblast. $p < 0.05$ were considered significant; * $p < 0.05$, ** $p < 0.01$, *** $p < 0.001$, **** $p < 0.0001$. The following statistical tests were used: Chi-squared goodness of fit (B-E).

CHAPTER 4. DISCUSSION

4.1 PP4 PLAYS TWO ROLES IN THE CELL CYCLE TO REGULATE CENTROSOME ASYMMETRY.

My findings revealed that Protein Phosphatase 4, a conserved serine/threonine phosphatase, is required for centrosome asymmetry in *Drosophila* neural stem cells. I show that all three members of the PP4 complex (the catalytic unit PP4-19C, and the regulatory subunits PP4r2 and PP4r3 (Falafel)) are required for proper centrosome MTOC asymmetry in interphase ((Segura *et al.*, 2025) Figure 1, Supplemental Figure 1). I further show that *pp4* mutants, despite lacking MTOC activity in interphase, can mature into functional MTOCs during mitosis and form a proper bipolar spindle, resulting in normal asymmetric cell division resulting in one neuroblast and one GMC ((Segura *et al.*, 2025) Figure 1). I additionally show that the PP4 complex is required for proper γTubulin localization at the apical centrosome ((Segura *et al.*, 2025), Figure 2), and that constitutively dephosphorylated γTubulin results in an increase of MTOC activity in interphase ((Segura *et al.*, 2025) Figure 3). Additionally, I show that both isoforms of γTubulin are required for proper MTOC formation in *Drosophila* neuroblasts ((Segura *et al.*, 2025) Supplemental Figure 2). Further, I identified Cdk1 as a putative kinase that acts upon γTubulin in opposition to PP4's dephosphorylation activity and show that trapping Cdk1 on centrosomes resulted in a decrease in MTOC activity in interphase ((Segura *et al.*, 2025) Figure 4). These data are consistent with our proposed model where dephosphorylation of γTubulin at Serine 131 results in an increase of microtubule nucleation, and phosphorylation of Serine 131 results in a decrease of microtubule nucleation.

Because of these changes to MTOC activity in interphase, we next examined if the PP4 complex is required for the proper localization and function of Polo and Centrobin, which are dependent on one other and on microtubule nucleation (Januschke *et al.*, 2013; Ramdas Nair *et al.*, 2016; Gallaud *et al.*, 2020). I observed that *pp4* mutants exhibited reduced Polo localization at the apical centrosome, but paradoxically, Centrobin was properly localized to the apical centrosome ((Segura *et al.*, 2025) Figure 5 and Supplemental Figure 5). This led me to hypothesize that Centrobin may have a mitotic phenotype instead of an interphase one. To address this, I next focused on mitosis, where Centrobin is shed from the mother centriole and deposited onto the daughter centriole, which fundamentally establishes centrosome asymmetry for the following cell cycle (Gallaud *et al.*, 2020). This transfer is mediated by the phosphorylation of Centrobin by Polo, implicating phospho-status as a potential regulator of Centrobin transfer.

Due to a putative interaction between a regulatory subunit of PP4 (Falafel, PP4r3) and Centrobin via a conserved recognition motif (Lipinszki *et al.*, 2015), I hypothesized that PP4 may also be required for the transfer of Centrobin during mitosis. Indeed, I observed that *pp4* mutants exhibited a delay in transfer of Centrobin, with some cells showing either enrichment on the mother centriole or no enrichment on either centriole (Chapter 3, Segura *et al.*, 2025, Figure 6). This was further supported when phospho-mimetic Centrobin displayed transfer delays similar to those observed in *pp4* mutants, showing that phospho-state of Centrobin is critical to its transfer from mother to daughter centriole, and that PP4 may promote enrichment of Centrobin on the daughter centriole by de-phosphorylating the residues phosphorylated by Polo. These data are therefore consistent with a model wherein Polo is responsible for the removal of Centrobin from the mother centriole, and PP4 is required for the deposit of Centrobin onto the daughter centriole. Finally, these data provide additional evidence for the difference in centrosomal regulation in interphase

versus in mitosis, where (1) PP4 may regulate interphase MTOC formation via interactions with γTubulin, and (2) establishes centriole identity during mitosis via interactions with Centrobin (Chapter 3, Segura *et al.*, 2025, Figure 7).

4.2 Phosphorylation state of γTubulin Regulates Microtubule Organization Center Formation.

High levels of phosphorylated Serine 131 on γTubulin has been shown to reduce astral microtubule nucleation at centrioles, and Ser131Asp γTubulin mutants showed reduced capacity to regrow microtubules after depolymerization, implying that phosphorylation of Serine 131 carries functional consequences for MTOC formation (Alvarado-Kristensson *et al.*, 2009). Additional *in vitro* data have suggested that the PP4 complex acts upon γTubulin, but prior to this study, these findings have not been confirmed *in vivo* (Voss *et al.*, 2013). Here, I show *in vivo* data consistent with these prior findings, where we show that the phosphorylation state of γTubulin regulates MTOC formation in *Drosophila* neural stem cells (Chapter 3, Segura *et al.*, 2025, Figure 3 and Supplemental Figure 3). Specifically, I show that the removal of de-phosphorylation activity in *pp4* mutants results in γTubulin that I presume to be phosphorylated, resulting in a loss of MTOC activity. I additionally show that mutation of Serine 131 on γTubulin to an Alanine, thereby rendering it un-phosphorylatable, results in a gain of MTOC activity, and finally show that forced phosphorylation of γTubulin via nanobody-trapped Cdk1 led to a decrease in MTOC activity (Chapter 3, Segura *et al.*, 2025, Figure 3, Figure 4). These data are consistent with our model wherein phosphorylation of γTubulin contributes to regulation of MTOC formation, and PP4/Cdk1 may oppose one another as antagonistic regulators.

4.3 Both isoforms of γTubulin are Required for MTOC Formation in Drosophila Neuroblasts.

Previous to this study, the understanding of the two γTubulin isoforms in *Drosophila* was that γTubulin23C is required for all centrosomal function, and γTubulin37C is required for meiotic spindle regulation and early oogenesis (Wilson and Borisy, 1998; Vázquez *et al.*, 2008). Despite this, both γTubulin23C and γTubulin37C physically interact with each other, implying a shared complex between the two proteins (Wiese, 2008). Here I show that both isoforms of γTubulin are required for MTOC formation in interphase (Chapter 3, Segura *et al.*, 2025, Supplemental Figure 3). The null allele of γTubulin23C (γTubulin23C$^{[A15-2]}$) shows a gain-of-function phenotype where two active MTOCs are present in interphase, while γTubulin37C null allele (γTubulin37C$^{[3]}$) showed cells that had two active MTOCs in interphase, or cells with no MTOCs in interphase (Chapter 3, Segura *et al.*, 2025, Figure 3, Supplemental Figure 3). Importantly, both null alleles show the capacity to form MTOCs, implying that γTubulin is still properly incorporated into the centrosome under these mutations. However, homozygous *γTubulin23C$^{[A15-2]}$, γTubulin37C$^{[3]}$* mutants showed a complete loss of γTubulin at centrosomes, and thereby lacked any meaningful nucleation of microtubules in interphase (Chapter 3, Segura *et al.*, 2025, Supplemental Figure 4, Supplemental Figure 5). Furthermore, single mutations to γTubulin37C alone were sufficient to cause a change in MTOC activity, implying that γTubulin37C is involved in centrosomal regulation outside of meiotic spindle regulation and early development (Chapter 3, Segura *et al.*, 2025, Figure 3 and Supplemental Figure 3). Therefore, I propose a new model wherein both isoforms of γTubulin are functionally required for proper MTOC formation in interphase neuroblasts.

4.4 Polo is Dependent on proper MTOC Activity, While Centrobin is Not.

Polo and Centrobin are co-dependent on one another, and work together to promote the formation of an active apical MTOC in interphase neuroblasts (Januschke *et al.*, 2013; Ramdas Nair *et al.*, 2016; Gallaud *et al.*, 2020). Further, Polo promotes the retention of Centrobin on the apical centrosome via phosphorylation activity. Because *pp4* mutants lacked interphase MTOC activity, I hypothesized that *pp4* mutants would show reduced levels of Polo and Centrobin. Indeed, my findings show that Polo is drastically reduced at the apical centrosome, likely due to the lack of microtubule activity needed to recruit it to the apical centrosome (Chapter 3, Segura *et al.*, 2025, Figure 5). This was verified by looking at Polo signal with reference to a centriole marker, verifying that Polo is still present on centrioles, but is vastly reduced compared to wild type (Chapter 3, Segura *et al.*, 2025, Figure 5). These findings could suggest that *pp4* mutants would show a similar reduction in Centrobin localization at the apical centrosome; however, the apical centrosome in *pp4* mutants can recruit Centrobin at levels comparable to those seen in wild type controls (Chapter 3, Segura *et al.*, 2025, Figure 5). One possible explanation for this could be that the reduced level of Polo in *pp4* mutants is permissive to phosphorylate and thereby retain Centrobin, but Centrobin alone cannot form an active MTOC. Importantly, this marks the first observation that Centrobin can persist at the apical centrosome with reduced MTOC activity and Polo localization, decoupling the feedback loop that these three components participate in. These new data instead suggest that Centrobins presence on the apical centrosome is equally contributed to by the mitotic transfer of Centrobin from mother to daughter centriole, followed by a secondary incorporation of Centrobin at the apical centrosome after mitosis in the following interphase.

4.5 Dephosphorylation of Centrobin is Required for Mother to Daughter Transfer in Mitosis.

Centrosome asymmetry is characterized by the biased retention of Centrobin, where the younger daughter centrosome (which contains the younger daughter centriole) retains Centrobin, while the older mother centrosome (which contains the older mother centriole) does not (Januschke *et al.*, 2013; Gallaud *et al.*, 2020). Polo is responsible for phosphorylating and thereby transferring Centrobin from the mother centriole to the daughter centriole during mitosis. Falafel, the regulatory subunit of PP4, interacts with Centrobin *in vitro* (Lipinszki *et al.*, 2015), which lead me to hypothesize that PP4-mediated dephosphorylation may contribute to Centrobin transfer. Indeed, in *pp4* and phospho-mimetic Centrobin mutants, Centrobin fails to faithfully enrich on the daughter centrosome. My 3D-SIM data suggests that *pp4* mutants have centrioles with either no Centrobin on either centriole or improper localization of Centrobin on the mother centriole, while in live cells we observe proper localization of Centrobin in *pp4* mutants. To verify this, I imaged *pp4* mutant neuroblasts as they exited mitosis, and observed a subset of cells where neuroblasts either displayed (1) one Cnb+ centrosome, (2) two Cnb+ centrosomes, or (3) two Cnb- centrosomes (Chapter 3, Segura *et al.*, 2025, Figure 7). The frequency of these occurrences in my live cell dataset closely correlated with the frequency observed in my 3D-SIM dataset, suggesting that there does indeed exist a small sub-population of cells where Centrobin is miss-localized from the apical centrosome (Chapter 3, Segura *et al.*, 2025, Figure 7). Importantly, these data suggest that this miss-localization is a consequence of impaired centriolar transfer during mitosis preceding interphase, and not a consequence of deficient MTOC activity at the apical interphase centrosome.

4.6 Limitations of the Study.

While we show that the three independent components of the PP4 complex are required for centrosome asymmetry, we do not empirically show that the three components form a heterotrimer in *Drosophila* neuroblasts. While it is possible that there may be other combinations of regulatory subunits, PP4 most abundantly forms a heterotrimer of PP4r2-PP4r3-PP4c, and the CRISPR-Cas9 knockout of PP4c, knock-down of PP4r2, and *falafel* mutant data presented here strongly suggest that PP4 is forming a heterotrimer in *Drosophila* neuroblasts. Similarly, we verified the catalytic activity of PP4 by generating mutants of PP4 with inactive catalytic domains, composed of a pair of amino acid substitutions ([D85N, H115N]). One residue may be more critical than the other – however, due to the conservation of active sites between members of the phospho-protein phosphatase superfamily (Park and Lee, 2020), we deemed the double mutant suitable for our experiments.

A similar issue arises in the expression of our rescue constructs: our catalytically dead construct is driven by a 10X UAS-driver, while our wild type construct is driven by a 5X UAS-driver. This resulted in a subset of *pp4* mutants rescued with the 10X PP4-dead construct displaying a gain-of-function phenotype, where both centrosomes maintained active MTOCs (data not shown). We addressed this discrepancy by taking advantage of the temperature sensitivity of the Worgal4 UAS system. Indeed, when reared at a lower temperature, *pp4* mutants rescued with the 10X PP4-dead construct failed to form active MTOCs (Chapter 3, Segura *et al.*, 2025, Supplemental Figure 1).

Additionally, our mislocalization of γTubulin37C may be described as ectopic, as it is being driven by a embryo-specific driver instead of a neuroblast-specific one. In addition to this, γTubulin23C is seen as the *de facto* γTubulin gene responsible for microtubule nucleation at

neuroblast centrosomes, leading one to propose the alternative explanation wherein γTubulin23C is the upstream-most effector of regulation, consistent with γTubulin23C's established role in centrosome regulation, and any phenotypes seen in γTubulin mutants is chiefly ascribed to miss-regulation of γTubulin23C. However, both previously described mutant alleles and our endogenous phospho-mimetic γTubulin37C$^{[S131A]}$ mutant showed robust MTOC phenotypes in interphase (Chapter 3, Segura *et al.*, 2025, Figure 3), implying that γTubulin37C and γTubulin23C are equally important to centrosome regulation. Were γTubulin37C to be a downstream effector of γTubulin dynamics, a single edit to the coding sequence of γTubulin37C would have minimal consequences. However, single edits to γTubulin37C were sufficient to cause a phenotypic increase in MTOC activity at centrosomes in interphase, further implying the importance of γTubulin37C (Chapter 3, Segura *et al.*, 2025, Figure 3).

Additionally, there are multiple residues on γTubulin that can act as regulatory domains for centrosome regulation (Kristensson, 2021), and it is likely that other residues are equally important. Because Serine 131 is the most well-characterized residue, we focused on it for this work. While the possibility of performing multiple single-base edits on all relevant residues on both γTubulin23C and γTubulin37C and all the different combinations therein is an exciting proposal, it is beyond the scope of this work.

Lastly, another discrepancy is in our Cdk1 RNAi experiments (Chapter 3, Segura *et al.*, 2025, Figure 4), where a subset of cells show a loss of function. If Cdk1 is responsible for phosphorylating γTubulin, and this phosphorylation results in a loss of MTOC formation, then the removal of Cdk1 should lead to an increase in MTOC activity. Why then do we observe a subset of cells that lack MTOC activity? This may be ascribed to the ubiquity of Cdk1, which has multiple targets, and due in part to penetrance issues of our selected RNAi. To address this, we performed

trapping experiments where GFP-tagged Cdk1 was sequestered to the centrosome. Under those conditions, we observed a decrease in MTOC formation, which we ascribed to the phosphorylation activity of Cdk1 on γTubulin, which is consistent with our model.

CHAPTER 5. FUTURE DIRECTIONS AND CONCLUSION

5.1 WHAT ARE OTHER PHOSPHO-REGULATORY SITES OF γTUBULIN?

As discussed above, a major limitation of my study is that I only tested one edit (Serine □ Alanine) on only one gene (yTubulin37C). It is equally likely that other residues carry functional consequences on microtubule nucleation; indeed, several phosphorylation sites have been mapped to yTubulin and have been tested in *S. cerevisiae* and in human cell culture (Sulimenko *et al.*, 2022). Therefore, one could envision a set of experiments wherein all of these putative phosphorylation sites are assayed for their importance in microtubule nucleation. To achieve this, one would need to generate single-base edits to each of the identified phospho-sites on both yTubulin23C and yTubulin37C, and mutate them to either be un-phosphorylatable by mutating to an alanine or make them phosphor-mimetic by mutating them to either a glutamic acid or aspartic acid. I have already generated a recombinant null chromosome removing both gamma tubulin genes (Chapter 3, Segura *et al.*, 2025, Supplemental Figure 4 and 5); one would have to pair this with a recombinant chromosome containing a gamma tubulin edit and a gamma tubulin null allele. For example, I will outline this experimental cross for Serine 32 on yTubulin23C, asumming a yTub23C[S32A] allele has been generated and recombined with yTubulin37C[3], which is the null allele of yTubulin37C:

Parental Cross:

$$\frac{\gamma Tub23C[S32A], \gamma Tubulin37C[3]}{CyO, Actin :: GFP} \times \frac{\gamma Tub23C[A15-2], \gamma Tubulin37C[3]}{CyO, Actin :: GFP}$$

Larval Progeny to Image/Test:

$$\frac{\gamma Tub23C[S32A], \gamma Tubulin37C[3]}{\gamma Tub23C[A15-2], \gamma Tubulin37C[3]}$$

This would result in larvae expressing only phospho-mutant gamma tubulin, allowing for the study of each residue and its impact on cellular function, assuming that larvae tolerate these mutations. In an ideal scenario, the above experimental flowthrough would be performed for each residue (17 total between both genes, totaling 34 edits and recombinant lines).

Should this be constricted to a smaller number of targets, the *Drosophila* equivalents of human Y443 and S385 and yeast Y445 prove interesting candidates due to their direct impact on microtubule nucleation (Sulimenko *et al.*, 2022). yTubulin23C only has equivalent residues for human y443 and yeast Y445 on the same residue, Y443. yTubulin37C has an equivalent residue for human Y445 and yeast Y443 at the same reside, Y444, and the same residue as human S385. By focusing just on these residues, the experimental load could be reduced from looking at all possible residues to only three in each gene. This could be paired with any number of residues from the predicted phospho-sites (shown in blue in Figure 1), as these un-tested residues would represent novel and new data on the importance of nascent untested phosphorylation stites, which would expand our understanding of gamma tubulin regulation.

5.2 How does phospho-regulation of γTubulin impact γTuRC/MTOC formation?

By performing the above experiments, one would also have the ability to determine if any of these phospho-sites are critical for the incorporation of gamma tubulin into gamma tubulin ring

complexes (yTuRCs). From my work, I infer that mutations to Serine 131 on yTubulin37C interfere with yTubulin's ability to incorporate into yTuRCs, manifesting as a defect in MTOC activity. However, I did not generate evidence to prove this point. Expanding this study to include other residues grants the potential to perform experiments testing for yTuRC assembly in mutant lines. To achieve this, one could perform co-immunoprecipitation paired with mass spectrometry on mutant lines to determine if mutations to phosphor-sites are permissive to yTuRC formation. At minimum, this could be performed on the Serine131Alanine line I already generated for my work, and would serve as a test-of-concept before moving on to perform similar experiments on other residues.

5.3 How do PP4 and Polo differentiate between mother and daughter centrioles?

In my work, I propose that the centriolar transfer of Centrobin is a two-step procedure, where in early mitosis, Cnb is phosphorylated by Polo to remove it from the mother centriole, and in late mitosis, PP4 dephosphorylates Cnb to enrich Cnb on the daughter centriole. This proposed model generates an interesting question: How do Polo and PP4 differentiate between mother and daughter centrioles? Or in other words, what prevents Polo from removing Cnb from the daughter centriole, and what prevents PP4 from enriching Cnb on the mother centriole? To answer this question, more work is needed to identify structural and molecular differences between centrioles in *Drosophila* neuroblasts. To date, molecular factors that associate with the mother centriole include Ninein (Nin), Outer Dense Fiber protein 2 (ODF2), and Cep164, while Centrobin is the only known marker for daughter centrioles. Nin has been observed at both centrosomes in fly embryos (Kowanda 2016), but it has not yet been determined if an asymmetry in Nin can be

observed in centrioles undergoing duplication during neuroblast mitosis, and if Cep164 localizes to centrosomes at all in neuroblasts. Should either protein show an asymmetry favoring the mother centriole, it would provide us with a system to test if these components are required for Polo and PP4 to differentiate between mother and daughter centrioles in a Cnb-independent manner. Should this be the case, partial knock-down , interference, or knock-out of Cep164 or Nin (or any other mother-exclusive protein) could be used to determine impact on Cnb transfer, which would support this hypothesis. Following this, one could determine functional domains of Nin/Cep164 to molecularly determine the mechanism of action between centriolar components, Polo, and PP4. An alternative to this is the centriolar protein Asterless (Asl), which is used to differentiate between mother and daughter centrioles in a Cnb-independent fashion. Mother centrioles, due to being older and more mature than their daughters, have more Asl incorporated into them. Therefore, an alternative hypothesis could be that in fly neuroblasts, PP4 and Polo differentiate between mother and daughter centrioles based on Asterless levels. Testing this would require a new marker to differentiate mother and daughter centrioles, which would then allow for the removal of Asl from mitotic neuroblasts to study the impact of *asl* mutants on Cnb transfer.

5.4 What is the impact of MTOC asymmetry miss-regulation on cell fate?

In neuroblasts, the functional difference between centrosomes in part determines their segregation pattern. The apical daughter centrosome, which maintains MTOC activity, is thought to remain anchored in the apical region of the cell due to microtubule-dependent interactions with the apical cortex. This then facilitates the biased positioning of the daughter centrosome such that it segregates into the renewing stem cell. Could there be functional consequences to this biased

segregation? In the mollusk embryo, centrosomes act as a vehicle of biased mRNA delivery to daughter cells with different fates, implicating centrosomes as delivery mediators of cell fate determinants (Lambert and Nagy, 2002). Indeed, several mRNA transcripts have been observed at centrosomes in *Drosophila* larvae – it remains to be seen if these same transcripts or other, yet unidentified transcripts localize to centrosomes in larval neuroblasts (Lécuyer *et al.*, 2007). To date, the only mRNA observed at centrosomes in neuroblasts is a minor population of Miranda and Orb2 RNA at the apical centrosome (Ramat *et al.*, 2017; Robinson *et al.*, 2021). Therefore, an exciting proposal would be to perform a two-part experiment, where one would (1) assay for centrosomal localization of candidate RNA species at centrosomes, and (2) assay for unidentified RNA species at centrosomes. To test candidate, one would employ single-molecule RNA fluorescent *in situ* hybridization (smRNA-FISH) as done previously (Lécuyer *et al.*, 2007). Identifying novel RNA species however would be a more involved process. Initially, I had proposed using the Biotinylation via antibody recognition (BAR) approach, wherein biotinylation is induced at a limited locus to tag proteins and nucleic acids for extraction with magnetic anti-biotin beads. In this approach, I proposed using our endogenous Centrobin::GFP construct, as this would allow us to restrict Biotinylation to the region around the apical centrosome, which would in turn allow us to identify RNA species that uniquely localize to the apical centrosome, and thus presumably segregate into the neuroblast. Similarly, using Asterless::GFP would identify all RNA species at centrosomes, and would potentially identify species that segregate into the GMC. However, I struggled to get specific Biotinylation at Cnb::GFP and Asl::GFP centrosomes, presumably due to an inefficient affinity between our GFP constructs and our selected anti-GFP antibodies. The antibodies selected did not recognize Asl::GFP or Cnb::GFP, but could recognize

Pins::GFP (Figure 2). Therefore, should a suitable antibody be identified, this experiment would be able to proceed after further troubleshooting.

Should candidate RNA species be found at either the apical or basal centrosome, it would be enlightening to observe their localization patterns *in vivo*. This has been achieved with the MS2 RNA-tagging system, where candidate RNA transcripts are edited to introduce MS2-loops to their terminal non-coding regions. When paired with a fluorescently-tagged coat protein that recognizes and binds to these MS2 loops, one can effectively monitor RNA localization via fluorescent microscopy *in vivo*. Indeed, this approach has been used in neuroblasts to track Miranda RNA localization, though the signal to noise ratio was best when done in neuroblast culture instead of *ex vivo* brains (Ramat *et al.*, 2017). Indeed, I struggled to replicate the ex vivo findings reported in Ramat *et al.*, 2017, and could not detect any noticeable localization patterns of Prospero RNA using the same MS2 system (Figure 3). Therefore, it is likely that outside of neuroblast culture, resolving RNA localization in *ex vivo* brains would prove challenging. However, smRNA-FISH should provide sufficient information about localization patterns throughout interphase and mitosis with sufficient N's.

5.5 Do centrosomal defects in PP4 mutants lead to developmental defects?

Centrosomes and centrosomal regulation have been implicated numerous times in developmental defects such as microcephaly. However, it remains unexplored if these defects are ascribed to MTOC asymmetry miss-regulation. For this reason, the *pp4* mutant characterized here provides an excellent candidate to probe for the impact of MTOC asymmetry on the developing larval brain. Unlike other mutants that remove MTOC asymmetry in interphase, *pp4* mutants retain

Cnb on the apical centrosome, and retain a small (albeit reduced) population of Polo on the apical centrosome. While mitosis is largely unaffected, a small population of cells undergo miss-regulated transfer of Cnb during mitosis, while a larger subset of cells yield a neuroblast with Cnb enriched on the daughter centriole (Chapter 3, Segura *et al.*, 2025). This provides us with an excellent model to test for developmental impact of MTOC asymmetry, as *pp4* mutants lose functional MTOC asymmetry in interphase, and retain the centrosome-specific localization of Centrobin (Chapter 3, Segura *et al.*, 2025).

The only current barrier to probing this question further is the lethality of the *pp4* null mutant, which affects all cells in the organism (leading to other *pp4*-specific phenotypes) and is homozygous lethal, eliminating all mutants sometime during pupation. To get around this barrier, one would have to identify other means to selectively knock-down PP4 activity in neuroblasts at different stages of development. The regulatory subunits PP4r2 and PP4r3 (Falafel) show similar MTOC phenotypes to *pp4* mutants, making these proteins prime targets for knock-down for developmental experiments (Chapter 3, Segura *et al.*, 2025). In addition, RNAi against the catalytic subunit PP4-19C may also be used, providing yet another avenue to remove MTOC asymmetry. When paired with the temperature sensitivity of the WorniuGal4-UAS system, it may be possible to inhibit total MTOC asymmetry loss until later developmental stages, allowing one to observe developmental defects at different developmental timepoints. Should this be unfeasible, there are several putative PP4-inhibiting proteins (DHX38, TIPRL, PP4IP) that could be expressed in neuroblasts via optogenetics to give temporal control over knock-down of PP4 (Park and Lee, 2020). Finally, one could also generate PP4c::GFP, PP4r2::GFP, or PP4r3::GFP constructs and selectively trap them to nanobody domains to miss-localize them at different developmental timepoints. Utilizing these tools, one would assay for (1) brain morphology, (2) brain composition

(stem vs non-stem cell counts), (3) single cell RNA sequencing, and (4) behavioral assays (larva: rolling, adults: climbing) at the larval and adult timepoints to determine the impact of MTOC asymmetry on development. In particular, should larvae with MTOC defects survive to adulthood, it would be interesting to observe the differences between control brains and MTOC-deficient brains.

5.6 SPATIAL-TEMPORAL ACTIVITY OF PP4

Finally, it remains to be seen if and how PP4 performs dual regulatory roles in neuroblasts. One explanation could be differential regulation via PP4's regulatory subunits, which may impact the localization of the catalytic subunit (Park and Lee, 2020). To investigate this further, I attempted to generate an endogenous PP4::GFP construct. While I was able to generate transformants, the signal of PP4::GFP was extremely diffuse in the cytoplasm, and required excessive exposure settings (Figure 4, ~50% laser power and at least 500 ms of exposure time) to generate detectable signal. As an alternative approach, I tried to use antibodies against PP4c, PP4r2, and PP4r3. The PP4c antibody, which was an alternative antibody used to observe PP4 at centrosomes in embryos (Helps *et al.*, 1998) , proved to be non-specific, as *pp4* mutants presented anti-PP4 signal. PP4r2, and PP4r3 presented prominent nuclear signal, though this was not verified with appropriate stainings in PP4r2, and PP4r3 mutant controls. Therefore, a possible continuation of this work should include (1) a re-assessment of PP4r2 and PP4r3 antibodies and potential generation of PP4c, PP4r2, and PP4r3 endogenous GFP CRISPR tags. This would allow for the identification of localization and thus regulatory dynamics of the PP4 complex and would allow for several of the other experiments outlined above (nanobody trapping, RNA identification via pull-down).

5.7 CONCLUSION

Here I show that Protein Phosphatase 4 is required for centrosome asymmetry in neural stem cells. I show that *pp4* mutants fail to form MTOCs in interphase, and that *pp4* mutants show reduced levels of γTubulin. I show that phospho-mimetically inactive γTubulin increases MTOC formation in interphase and that Cdk1-phosphorylated γTubulin decreases MTOC formation, implying that PP4 regulates interphase MTOC activity by dephosphorylating γTubulin, likely at Serine 131. Lastly, I show that PP4 reduces interphase Polo localization, and that PP4 regulates the centriolar transfer of Centrobin during mitosis, where *pp4* mutants fail to enrich Centrobin on the daughter centriole. Future work will explore the mechanism by which PP4 and Polo differentiate between mother and daughter centrioles and will test other Serine/Threonine residues on γTubulin for possible regulatory sites of microtubule nucleation.

5.8 FIGURES

5.8.1 *Figure 1: Conserved phospho-sites of gamma tubulin in Drosophila*

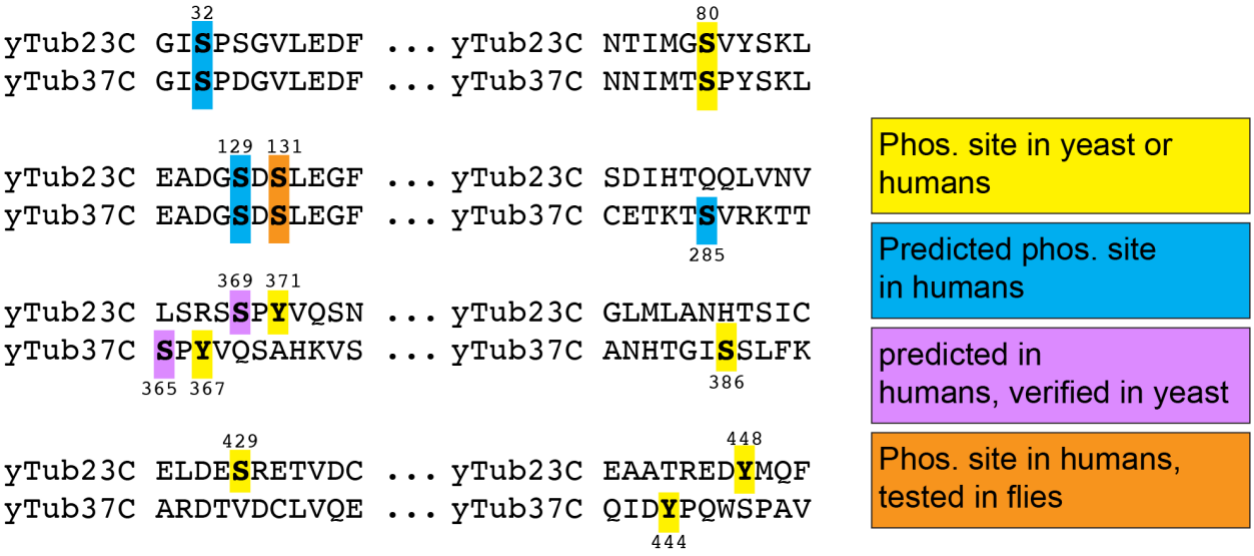

Shown are the conserved phosphorylation sites of gamma tubulin 23C and 37C in *Drosophila*. Conserved sites were identified by aligning each gamma tubulin gene using either *S. cerevisiae* Tub4 or *H. sapiens* TUBG1. The top row contains the yTubulin23C sequence, while the bottom row contains the yTubulin37C sequence. Residues highlighted in yellow denote phosphorylation sites identified and verified in yeast and humans; blue denotes predicted phosphorylation sites of human TUBG1; purple denotes sites that are predicted in human TUBG1, and have been verified in yeast Tub4; orange denotes residues identified in human TUBG1 and tested in *Drosophila* neuroblasts.

5.8.2 *Figure 2: Anti-GFP candidate antibodies.*

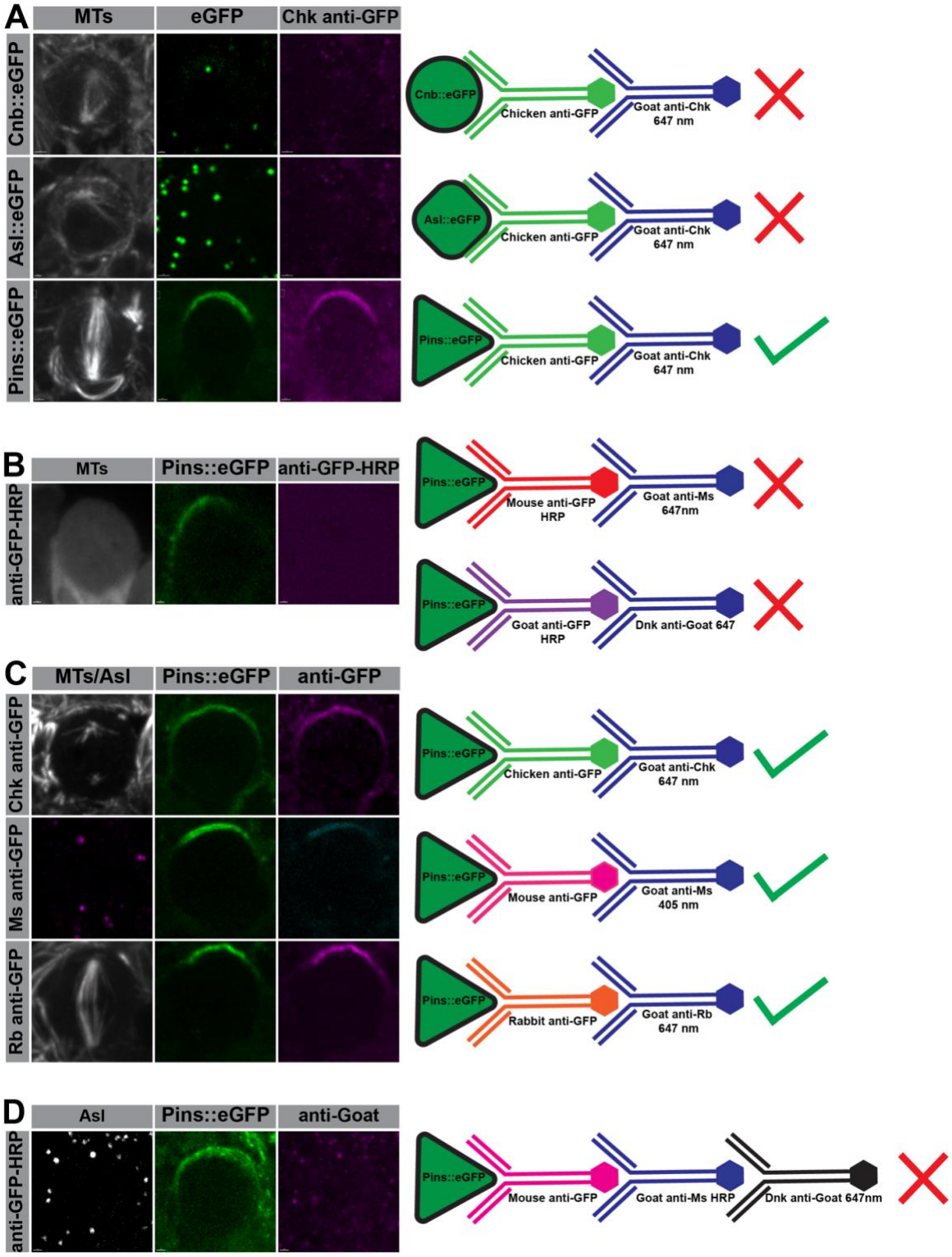

Figure 2: Anti-GFP antibody testing. (A) Chicken anti-GFP used in parallel on Cnb::GFP, Asl::GFP, and Pins::GFP. (B) mouse anti-GFP-HRP used on Pins::GFP. (C) Chicken, mouse, and rabbit anti-GFP used on Pins::GFP. (D) Goat anti-GFP-HRP used on Pins::GFP.

5.8.3 *Figure 3: Miranda RNA in the MS2 RNA-tagging system.*

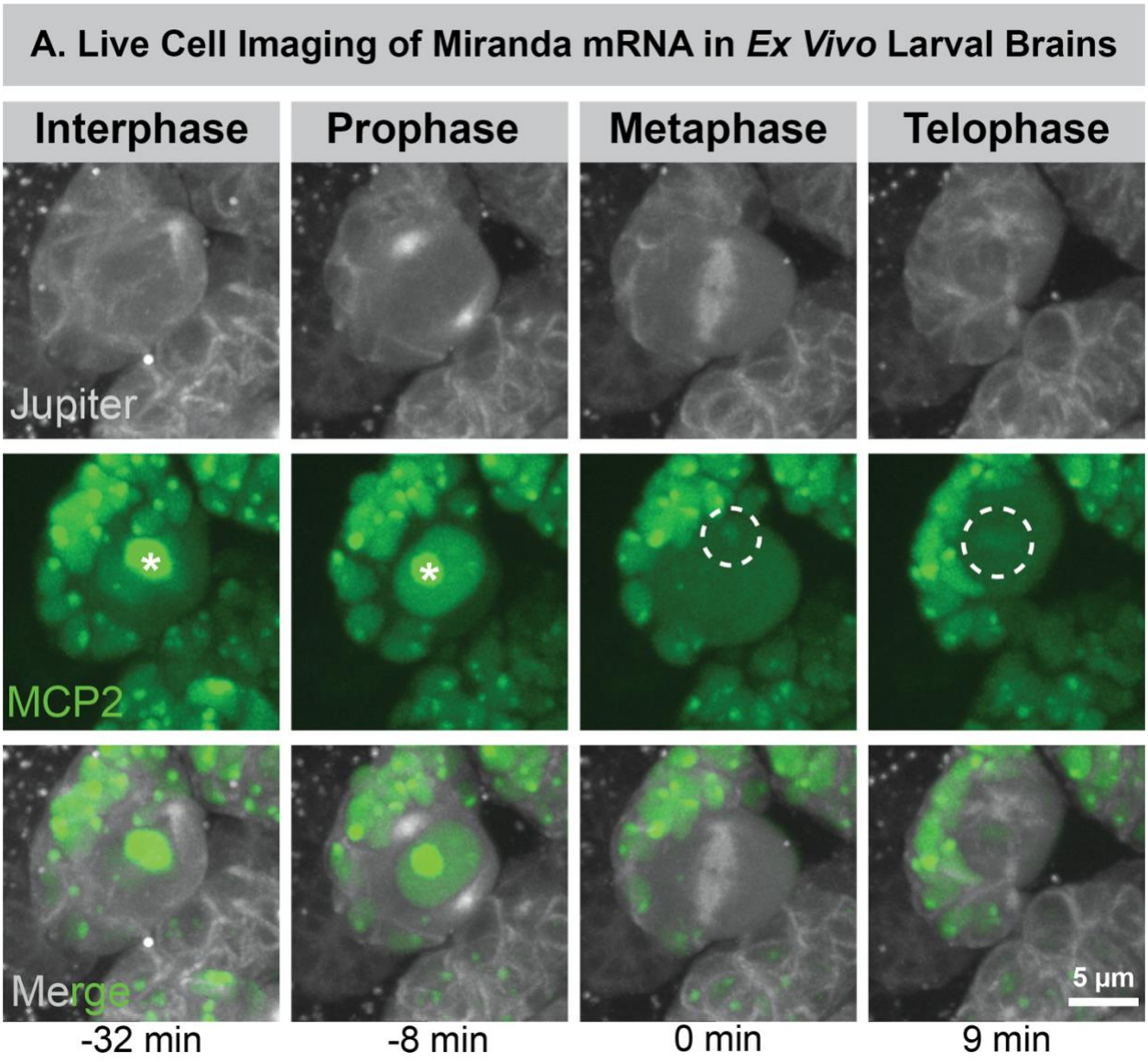

Figure 3: Miranda RNA in the MS2 RNA-tagging system. Asterix denotes nucleolus. Dashed line denotes Miranda RNA signal at the apical centrosome (metaphase) and basal cortex (telophase).

5.8.4 *Figure 4: Endogenous CRISPR-mediated PP4c::GFP*

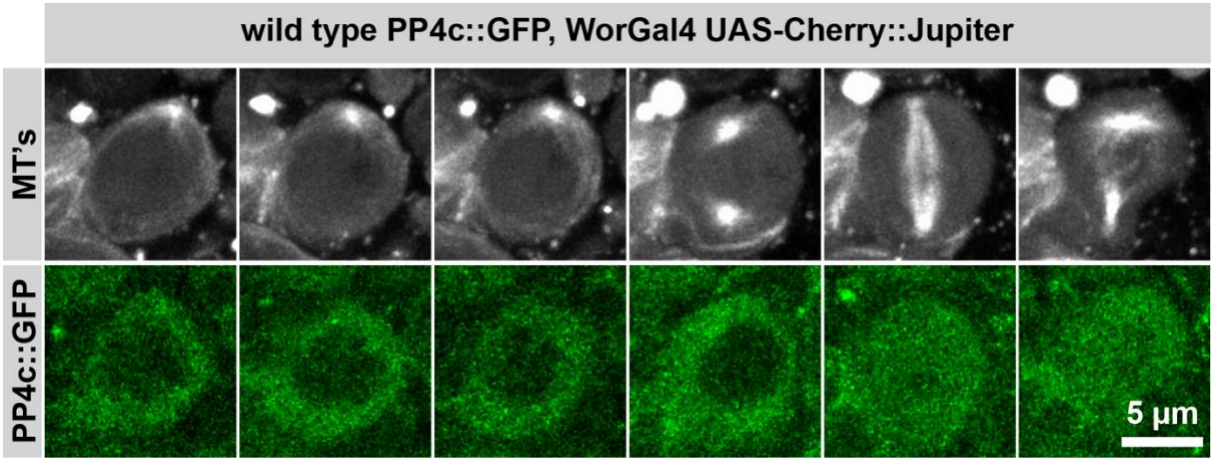

Figure 4: Representative PP4c::GFP image.

WORKS CITED

Alvarado-Kristensson, M, Rodríguez, MJ, Silió, V, Valpuesta, JM, and Carrera, AC (2009). SADB phosphorylation of γ-tubulin regulates centrosome duplication. Nat Cell Biol 11, 1081–1092.

Basto, R, Lau, J, Vinogradova, T, Gardiol, A, Woods, CG, Khodjakov, A, and Raff, JW (2006). Flies without Centrioles. Cell 125, 1375–1386.

Bohl, B, Jabali, A, Ladewig, J, and Koch, P (2022). Asymmetric Notch activity by differential inheritance of lysosomes in human neural stem cells. Sci Adv 8, eabl5792.

Breugel, M van, Hirono, M, Andreeva, A, Yanagisawa, H, Yamaguchi, S, Nakazawa, Y, Morgner, N, Petrovich, M, Ebong, I-O, Robinson, CV, *et al.* (2011). Structures of SAS-6 Suggest Its Organization in Centrioles. Science 331, 1196–1199.

Broadus, J, Fuerstenberg, S, and Doe, CQ (1998). Staufen-dependent localization of prospero mRNA contributes to neuroblast daughter-cell fate. Nature 391, 792–795.

Brown, A, and Zhang, R (2020). Primary Cilia: A Closer Look at the Antenna of Cells. Curr Biol 30, R1494–R1496.

Brunet, M, Thomas, J, Lapart, J-A, Krüttli, L, Laporte, MH, Riparbelli, MG, Callaini, G, Durand, B, and Morel, V (2025). Author Correction: Drosophila Alms1 proteins regulate centriolar cartwheel assembly by enabling Plk4-Ana2 amplification loop. EMBO J, 1–1.

Burkhalter, MD, Stiff, T, Maerz, LD, Tena, TC, Wiese, H, Gerhards, J, Sailer, SA, Vu, LAT, Phu, MD, Donow, C, *et al.* (2024). Cilia defects upon loss of WDR4 are linked to proteasomal hyperactivity and ubiquitin shortage. Cell Death Dis 15, 660.

Cabernard, C, and Doe, CQ (2009). Apical/Basal Spindle Orientation Is Required for Neuroblast Homeostasis and Neuronal Differentiation in Drosophila. Dev Cell 17, 134–141.

Cabernard, C, Prehoda, KE, and Doe, CQ (2010). A spindle-independent cleavage furrow positioning pathway. Nature 467, 91–94.

Candelas, A, Vianay, B, Gelin, M, Faivre, L, Larghero, J, Blanchoin, L, Théry, M, and Brunet, S (2024). Heterotypic interaction promotes asymmetric division of human hematopoietic progenitors. Development 151.

Chan, Y-HM, and Marshall, WF (2014). Organelle Size Scaling of the Budding Yeast Vacuole Is Tuned by Membrane Trafficking Rates. Biophys J 106, 1986–1996.

Chan, Y-HM, Reyes, L, Sohail, SM, Tran, NK, and Marshall, WF (2016). Organelle Size Scaling of the Budding Yeast Vacuole by Relative Growth and Inheritance. Curr Biol 26, 1221–1228.

Chelius, X, Bartosch, V, Rausch, N, Haubner, M, Schramm, J, Braun, RJ, Klecker, T, and Westermann, B (2023). Selective retention of dysfunctional mitochondria during asymmetric cell division in yeast. PLOS Biol 21, e3002310.

Chelius, X, Rausch, N, Bartosch, V, Klecker, M, Klecker, T, and Westermann, B (2025). A protein interaction map of the myosin Myo2 reveals a role for Alo1 in mitochondrial inheritance in yeast. J Cell Sci 138.

Chen, C, and Yamashita, YM (2021). Centrosome-centric view of asymmetric stem cell division. Open Biol 11, 200314.

Chodisetty, S, Arora, A, Malik, KK, Goel, H, and Tyagi, S (2024). MLL/WDR5 complex recruits centriolar satellite protein Cep72 to regulate microtubule nucleation and spindle formation. Sci Adv 10, eadn0086.

Clark, I, Giniger, E, Ruohola-Baker, H, Jan, LY, and Jan, YN (1994). Transient posterior localization of a kinesin fusion protein reflects anteroposterior polarity of the Drosophila oocyte. Curr Biol 4, 289–300.
Clay, L, Caudron, F, Denoth-Lippuner, A, Boettcher, B, Frei, SB, Snapp, EL, and Barral, Y (2014). A sphingolipid-dependent diffusion barrier confines ER stress to the yeast mother cell. ELife 3, e01883.
Conduit, PT, and Raff, JW (2010). Cnn Dynamics Drive Centrosome Size Asymmetry to Ensure Daughter Centriole Retention in Drosophila Neuroblasts. Curr Biol 20, 2187–2192.
Conduit, PT, Wainman, A, and Raff, JW (2015). Centrosome function and assembly in animal cells. Nat Rev Mol Cell Bio 16, 611–624.
Connell, M, Xie, Y, Deng, X, Chen, R, and Zhu, S (2024). Kin17 regulates proper cortical localization of Miranda in Drosophila neuroblasts by regulating Flfl expression. Cell Rep 43, 113823.
Coumailleau, F, Fürthauer, M, Knoblich, JA, and González-Gaitán, M (2009). Directional Delta and Notch trafficking in Sara endosomes during asymmetric cell division. Nature 458, 1051–1055.
Dahanukar, A, Walker, JA, and Wharton, RP (1999). Smaug, a Novel RNA-Binding Protein that Operates a Translational Switch in Drosophila. Mol Cell 4, 209–218.
Dalton, CM, and Carroll, J (2013). Biased inheritance of mitochondria during asymmetric cell division in the mouse oocyte. J Cell Sci 126, 2955–2964.
Dharmadhikari, AV, Abad, MA, Khan, S, Maroofian, R, Sands, TT, Ullah, F, Samejima, I, Shen, Y, Wear, MA, Moore, KE, *et al.* (2024). RNA methyltransferase SPOUT1/CENP-32 links mitotic spindle organization with the neurodevelopmental disorder SpADMiSS. MedRxiv 16, 2024.01.09.23300329.
Doe, CQ (2008). Neural stem cells: balancing self-renewal with differentiation. Development 135, 1575–1587.
Dzhindzhev, NS, Yu, QD, Weiskopf, K, Tzolovsky, G, Cunha-Ferreira, I, Riparbelli, M, Rodrigues-Martins, A, Bettencourt-Dias, M, Callaini, G, and Glover, DM (2010). Asterless is a scaffold for the onset of centriole assembly. Nature 467, 714–718.
Ekal, L, Alqahtani, AMS, Ayscough, KR, and Hettema, EH (2024). Spatiotemporal regulation of organelle transport by spindle position checkpoint kinase Kin4. J Cell Sci 137, jcs261948.
Forrest, KM, Clark, IE, Jain, RA, and Gavis, ER (2004). Temporal complexity within a translational control element in the nanos mRNA. Development 131, 5849–5857.
Gallaud, E, Caous, R, Pascal, A, Bazile, F, Gagné, J-P, Huet, S, Poirier, GG, Chrétien, D, Richard-Parpaillon, L, and Giet, R (2014). Ensconsin/Map7 promotes microtubule growth and centrosome separation in Drosophila neural stem cells. J Cell Biol 204, 1111–1121.
Gallaud, E, Nair, AR, Horsley, N, Monnard, A, Singh, P, Pham, TT, Garcia, DS, Ferrand, A, and Cabernard, C (2020). Dynamic centriolar localization of Polo and Centrobin in early mitosis primes centrosome asymmetry. Plos Biol 18, e3000762.
Gallaud, E, Nair, AR, Horsley, N, Monnard, A, Singh, P, Pham, TT, Garcia, DS, Ferrand, A, and Cabernard, C (2020). Dynamic centriolar localization of Polo and Centrobin in early mitosis primes centrosome asymmetry. Plos Biol 18, e3000762.
Gallo, CM, Wang, JT, Motegi, F, and Seydoux, G (2010). Cytoplasmic Partitioning of P Granule Components Is Not Required to Specify the Germline in C. elegans. Science 330, 1685–1689.

Gambarotto, D, Pennetier, C, Ryniawec, JM, Buster, DW, Gogendeau, D, Goupil, A, Nano, M, Simon, A, Blanc, D, Racine, V, *et al.* (2019). Plk4 Regulates Centriole Asymmetry and Spindle Orientation in Neural Stem Cells. Dev Cell 50, 11-24.e10.
Gao, Q, Hofer, FW, Filbeck, S, Vermeulen, BJA, Würtz, M, Neuner, A, Kaplan, C, Zezlina, M, Sala, C, Shin, H, *et al.* (2025). Structural mechanisms for centrosomal recruitment and organization of the microtubule nucleator γ-TuRC. Nat Commun 16, 2453.
González-Reyes, A, Elliott, H, and Johnston, DS (1995). Polarization of both major body axes in Drosophila by gurken-torpedo signalling. Nature 375, 654–658.
Graser, S, Stierhof, Y-D, Lavoie, SB, Gassner, OS, Lamla, S, Clech, ML, and Nigg, EA (2007). Cep164, a novel centriole appendage protein required for primary cilium formation. J Cell Biol 179, 321–330.
Habedanck, R, Stierhof, Y-D, Wilkinson, CJ, and Nigg, EA (2005). The Polo kinase Plk4 functions in centriole duplication. Nat Cell Biol 7, 1140–1146.
Habib, SJ, Chen, B-C, Tsai, F-C, Anastassiadis, K, Meyer, T, Betzig, E, and Nusse, R (2013). A Localized Wnt Signal Orients Asymmetric Stem Cell Division in Vitro. Science 339, 1445–1448.
Hannaford, MR, Liu, R, Billington, N, Swider, ZT, Galletta, BJ, Fagerstrom, CJ, Combs, C, Sellers, JR, and Rusan, NM (2022). Pericentrin interacts with Kinesin-1 to drive centriole motility. J Cell Biol 221, e202112097.
Hannaford, MR, and Rusan, NM (2024). Positioning centrioles and centrosomes. J Cell Biol 223, e202311140.
Helps, NR, Brewis, ND, Lineruth, K, Davis, T, Kaiser, K, and Cohen, PT (1998). Protein phosphatase 4 is an essential enzyme required for organisation of microtubules at centrosomes in Drosophila embryos. J Cell Sci 111 (Pt 10), 1331–1340.
Heym, RG, and Niessing, D (2012). Principles of mRNA transport in yeast. Cell Mol Life Sci 69, 1843–1853.
Higuchi-Sanabria, R, Pernice, WMA, Vevea, JD, Wolken, DMA, Boldogh, IR, and Pon, LA (2014). Role of asymmetric cell division in lifespan control in Saccharomyces cerevisiae. FEMS Yeast Res 14, 1133–1146.
Homem, CCF, and Knoblich, JA (2012). Drosophila neuroblasts: a model for stem cell biology. Development 139, 4297–4310.
Homem, CCF, and Knoblich, JA (2012). Drosophila neuroblasts: a model for stem cell biology. Development 139, 4297–4310.
Huttner, WB, and Kosodo, Y (2005). Symmetric versus asymmetric cell division during neurogenesis in the developing vertebrate central nervous system. Curr Opin Cell Biol 17, 648–657.
Imtiaz, MK bin, Royall, LN, Gonzalez-Bohorquez, D, and Jessberger, S (2022). Human neural progenitors establish a diffusion barrier in the endoplasmic reticulum membrane during cell division. Development 149, dev200613.
Jaiswal, S, and Singh, P (2021). Centrosome dysfunction in human diseases. Semin Cell Dev Biol 110, 113–122.
Januschke, J, and Gonzalez, C (2010). The interphase microtubule aster is a determinant of asymmetric division orientation in Drosophila neuroblasts. J Cell Biol 188, 693–706.
Januschke, J, Llamazares, S, Reina, J, and Gonzalez, C (2011). Drosophila neuroblasts retain the daughter centrosome. Nat Commun 2, 243.

Januschke, J, Reina, J, Llamazares, S, Bertran, T, Rossi, F, Roig, J, and Gonzalez, C (2013). Centrobin controls mother–daughter centriole asymmetry in Drosophila neuroblasts. Nat Cell Biol 15, 241–248.
Januschke, J, Reina, J, Llamazares, S, Bertran, T, Rossi, F, Roig, J, and Gonzalez, C (2013). Centrobin controls mother–daughter centriole asymmetry in Drosophila neuroblasts. Nat Cell Biol 15, 241–248.
Jaramillo, AM, Weil, TT, Goodhouse, J, Gavis, ER, and Schupbach, T (2008). The dynamics of fluorescently labeled endogenous gurken mRNA in Drosophila. J Cell Sci 121, 887–894.
Johnston, DS (2005). Moving messages: the intracellular localization of mRNAs. Nat Rev Mol Cell Bio 6, 363–375.
Katajisto, P, Döhla, J, Chaffer, CL, Pentinmikko, N, Marjanovic, N, Iqbal, S, Zoncu, R, Chen, W, Weinberg, RA, and Sabatini, DM (2015). Asymmetric apportioning of aged mitochondria between daughter cells is required for stemness. Science 348, 340–343.
Kiermaier, E, Stötzel, I, Schapfl, MA, and Villunger, A (2024). Amplified centrosomes—more than just a threat. EMBO Rep 25, 4153–4167.
Klebba, JE, Buster, DW, McLamarrah, TA, Rusan, NM, and Rogers, GC (2015). Autoinhibition and relief mechanism for Polo-like kinase 4. Proc Natl Acad Sci 112, E657–E666.
Kressmann, S, Campos, C, Castanon, I, Fürthauer, M, and González-Gaitán, M (2015). Directional Notch trafficking in Sara endosomes during asymmetric cell division in the spinal cord. Nat Cell Biol 17, 333–339.
Kristensson, MA (2021). The Game of Tubulins. Cells 10, 745.
Kukhtevich, IV, Rivero-Romano, M, Rakesh, N, Bheda, P, Chadha, Y, Rosales-Becerra, P, Hamperl, S, Bureik, D, Dornauer, S, Dargemont, C, *et al.* (2022). Quantitative RNA imaging in single live cells reveals age-dependent asymmetric inheritance. Cell Rep 41, 111656.
Kumar, D, and Reiter, J (2021). How the centriole builds its cilium: of mothers, daughters, and the acquisition of appendages. Curr Opin Struct Biol 66, 41–48.
Kusek, G, Campbell, M, Doyle, F, Tenenbaum, SA, Kiebler, M, and Temple, S (2012). Asymmetric Segregation of the Double-Stranded RNA Binding Protein Staufen2 during Mammalian Neural Stem Cell Divisions Promotes Lineage Progression. Cell Stem Cell 11, 505–516.
Lambert, JD, and Nagy, LM (2002). Asymmetric inheritance of centrosomally localized mRNAs during embryonic cleavages. Nature 420, 682–686.
Lange, BM, and Gull, K (1995). A molecular marker for centriole maturation in the mammalian cell cycle. J Cell Biol 130, 919–927.
Lawo, S, Hasegan, M, Gupta, GD, and Pelletier, L (2012). Subdiffraction imaging of centrosomes reveals higher-order organizational features of pericentriolar material. Nat Cell Biol 14, 1148–1158.
Lécuyer, E, Yoshida, H, Parthasarathy, N, Alm, C, Babak, T, Cerovina, T, Hughes, TR, Tomancak, P, and Krause, HM (2007). Global Analysis of mRNA Localization Reveals a Prominent Role in Organizing Cellular Architecture and Function. Cell 131, 174–187.
Lee, CS, Chen, S, Berry, CT, Kelly, AR, Herman, PJ, Oh, S, O'Connor, RS, Payne, AS, and Ellebrecht, CT (2024). Fate induction in CD8 CAR T cells through asymmetric cell division. Nature 633, 670–677.
Lee, K, and Rhee, K (2011). PLK1 phosphorylation of pericentrin initiates centrosome maturation at the onset of mitosis. J Cell Biol 195, 1093–1101.

Lee, ZY, Prouteau, M, Gotta, M, and Barral, Y (2016). Compartmentalization of the endoplasmic reticulum in the early C. elegans embryos. J Cell Biol 214, 665–676.
Legesse-Miller, A, Zhang, S, Santiago-Tirado, FH, Pelt, CKV, and Bretscher, A (2006). Regulated Phosphorylation of Budding Yeast's Essential Myosin V Heavy Chain, Myo2p. Mol Biol Cell 17, 1812–1821.
Lerit, DA, Smyth, JT, and Rusan, NM (2013). Organelle asymmetry for proper fitness, function, and fate. Chromosome Res 21, 271–286.
Lipinszki, Z, Lefevre, S, Savoian, MS, Singleton, MR, Glover, DM, and Przewloka, MR (2015). Centromeric binding and activity of Protein Phosphatase 4. Nat Commun 6, 5894.
Loeffler, D, Wehling, A, Schneiter, F, Zhang, Y, Müller-Bötticher, N, Hoppe, PS, Hilsenbeck, O, Kokkaliaris, KD, Endele, M, and Schroeder, T (2019). Asymmetric lysosome inheritance predicts activation of haematopoietic stem cells. Nature 573, 426–429.
Loyer, N, and Januschke, J (2020). Where does asymmetry come from? Illustrating principles of polarity and asymmetry establishment in Drosophila neuroblasts. Curr Opin Cell Biol 62, 70–77.
Luedeke, C, Frei, SB, Sbalzarini, I, Schwarz, H, Spang, A, and Barral, Y (2005). Septin-dependent compartmentalization of the endoplasmic reticulum during yeast polarized growth. J Cell Biol 169, 897–908.
Manno, GL, Soldatov, R, Zeisel, A, Braun, E, Hochgerner, H, Petukhov, V, Lidschreiber, K, Kastriti, ME, Lönnerberg, P, Furlan, A, *et al.* (2018). RNA velocity of single cells. Nature 560, 494–498.
Marshall, JD, Muller, J, Collin, GB, Milan, G, Kingsmore, SF, Dinwiddie, D, Farrow, EG, Miller, NA, Favaretto, F, Maffei, P, *et al.* (2015). Alström Syndrome: Mutation Spectrum of ALMS1. Hum Mutat 36, 660–668.
McFaline-Figueroa, JR, Vevea, J, Swayne, TC, Zhou, C, Liu, C, Leung, G, Boldogh, IR, and Pon, LA (2011). Mitochondrial quality control during inheritance is associated with lifespan and mother–daughter age asymmetry in budding yeast. Aging Cell 10, 885–895.
Moore, DL, Pilz, GA, Araúzo-Bravo, MJ, Barral, Y, and Jessberger, S (2015). A mechanism for the segregation of age in mammalian neural stem cells. Science 349, 1334–1338.
Munro, E, and Bowerman, B (2009). Cellular Symmetry Breaking during Caenorhabditis elegans Development. Cold Spring Harb Perspect Biol 1, a003400.
Nakagawa, Y, Yamane, Y, Okanoue, T, Tsukita, S, and Tsukita, S (2001). Outer Dense Fiber 2 Is a Widespread Centrosome Scaffold Component Preferentially Associated with Mother Centrioles: Its Identification from Isolated Centrosomes. Mol Biol Cell 12, 1687–1697.
Nelson, MR, Leidal, AM, and Smibert, CA (2004). Drosophila Cup is an eIF4E-binding protein that functions in Smaug-mediated translational repression. EMBO J 23, 150–159.
Noctor, SC, Martínez-Cerdeño, V, Ivic, L, and Kriegstein, AR (2004). Cortical neurons arise in symmetric and asymmetric division zones and migrate through specific phases. Nat Neurosci 7, 136–144.
Ohta, M, Ashikawa, T, Nozaki, Y, Kozuka-Hata, H, Goto, H, Inagaki, M, Oyama, M, and Kitagawa, D (2014). Direct interaction of Plk4 with STIL ensures formation of a single procentriole per parental centriole. Nat Commun 5, 5267.
Park, J, and Lee, D-H (2020). Functional roles of protein phosphatase 4 in multiple aspects of cellular physiology: a friend and a foe. Bmb Rep 53, 181–190.
Pei, S-L, Chen, R-S, and Chen, M-H (2025). The crucial role of centrioles in tooth growth and development. J Formos Méd Assoc 124, 271–277.

Peng, Y, and Weisman, LS (2008). The Cyclin-Dependent Kinase Cdk1 Directly Regulates Vacuole Inheritance. Dev Cell 15, 478–485.
Pereira, G, Tanaka, TU, Nasmyth, K, and Schiebel, E (2001). Modes of spindle pole body inheritance and segregation of the Bfa1p–Bub2p checkpoint protein complex. EMBO J 20, 6359–6370.
Pilaz, L, and Silver, DL (2017). Moving messages in the developing brain—emerging roles for mRNA transport and local translation in neural stem cells. Febs Lett 591, 1526–1539.
Pokrywka, NJ, and Stephenson, EC (1991). Microtubules mediate the localization of bicoid RNA during Drosophila oogenesis. Development 113, 55–66.
Prehoda, KE (2009). Polarization of Drosophila Neuroblasts During Asymmetric Division. Cold Spring Harb Perspect Biol 1, a001388.
Ramat, A, Hannaford, M, and Januschke, J (2017). Maintenance of Miranda Localization in Drosophila Neuroblasts Involves Interaction with the Cognate mRNA. Curr Biol 27, 2101-2111.e5.
Ramat, A, Hannaford, M, and Januschke, J (2017). Maintenance of Miranda Localization in Drosophila Neuroblasts Involves Interaction with the Cognate mRNA. Curr Biol 27, 2101-2111.e5.
Ramdas Nair, A, Singh, P, Salvador Garcia, D, Rodriguez-Crespo, D, Egger, B, and Cabernard, C (2016). The Microcephaly-Associated Protein Wdr62/CG7337 Is Required to Maintain Centrosome Asymmetry in Drosophila Neuroblasts. Cell Reports 14, 1100–1113.
Ramdas Nair, A, Singh, P, Salvador Garcia, D, Rodriguez-Crespo, D, Egger, B, and Cabernard, C (2016). The Microcephaly-Associated Protein Wdr62/CG7337 Is Required to Maintain Centrosome Asymmetry in Drosophila Neuroblasts. Cell Reports 14, 1100–1113.
Rebollo, E, Sampaio, P, Januschke, J, Llamazares, S, Varmark, H, and González, C (2007). Functionally Unequal Centrosomes Drive Spindle Orientation in Asymmetrically Dividing Drosophila Neural Stem Cells. Dev Cell 12, 467–474.
Rebollo, E, Sampaio, P, Januschke, J, Llamazares, S, Varmark, H, and González, C (2007). Functionally Unequal Centrosomes Drive Spindle Orientation in Asymmetrically Dividing Drosophila Neural Stem Cells. Dev Cell 12, 467–474.
Robinson, BV, Fang, J, Mehta, DS, Buehler, J, and Lerit, DA (2021). The RNA-binding protein Orb2 is associated with microcephaly and supports centrosome asymmetry in neural stem cells. Biorxiv, 2021.11.23.469707.
Roubinet, C, Tsankova, A, Pham, TT, Monnard, A, Caussinus, E, Affolter, M, and Cabernard, C (2017). Spatio-temporally separated cortical flows and spindle geometry establish physical asymmetry in fly neural stem cells. Nat Commun 8, 1383.
Royall, LN, Machado, D, Jessberger, S, and Denoth-Lippuner, A (2023). Asymmetric inheritance of centrosomes maintains stem cell properties in human neural progenitor cells. ELife 12, e83157.
Rusan, NM, and Peifer, M (2007). A role for a novel centrosome cycle in asymmetric cell division. J Cell Biol 177, 13–20.
Rushforth, R, Shamseldin, HE, Costantino, N, Michaels, J-R, Sawyer, SL, Osmond, M, Kurdi, W, Abdulwahab, F, DiStasio, A, Consortium, CC, *et al.* (2025). NUBP2 deficiency disrupts the centrosome-check point in the brain and causes primary microcephaly. MedRxiv, 2025.01.16.25320041.

Saima, Khan, A, Ali, S, Jiang, J, Miao, Z, Kamil, A, Khan, SN, and Arold, ST (2024). Clinical genomics expands the link between erroneous cell division, primary microcephaly and intellectual disability. Neurogenetics 25, 179–191.
Sallés, FJ, Lieberfarb, ME, Wreden, C, Gergen, JP, and Strickland, S (1994). Coordinate Initiation of Drosophila Development by Regulated Polyadenylation of Maternal Messenger RNAs. Science 266, 1996–1999.
Salzmann, V, Chen, C, Chiang, C-YA, Tiyaboonchai, A, Mayer, M, and Yamashita, YM (2014). Centrosome-dependent asymmetric inheritance of the midbody ring in Drosophila germline stem cell division. Mol Biol Cell 25, 267–275.
Sankaralingam, P, Wang, S, Liu, Y, Oegema, KF, and O'Connell, KF (2024). The kinase ZYG-1 phosphorylates the cartwheel protein SAS-5 to drive centriole assembly in C. elegans. EMBO Rep 25, 2698–2721.
Schuldt, AJ, Adams, JHJ, Davidson, CM, Micklem, DR, Haseloff, J, Johnston, DS, and Brand, AH (1998). Miranda mediates asymmetric protein and RNA localization in the developing nervous system. Gene Dev 12, 1847–1857.
Sdelci, S, Schütz, M, Pinyol, R, Bertran, MT, Regué, L, Caelles, C, Vernos, I, and Roig, J (2012). Nek9 Phosphorylation of NEDD1/GCP-WD Contributes to Plk1 Control of γ-Tubulin Recruitment to the Mitotic Centrosome. Curr Biol 22, 1516–1523.
Segura, RC, and Cabernard, C (2023). Live-Cell Imaging of Drosophila melanogaster Third Instar Larval Brains. J Vis Exp.
Segura, RC, Gallaud, E, Sythoff, A von B, Aavula, K, Taylor, JA, Vahdat, D, Otte, F, Pielage, J, and Cabernard, C (2025). Asymmetry of centrosomes in Drosophila neural stem cells requires protein phosphatase 4. Mol Biol Cell, mbcE25010021.
Shcheprova, Z, Baldi, S, Frei, SB, Gonnet, G, and Barral, Y (2008). A mechanism for asymmetric segregation of age during yeast budding. Nature 454, 728–734.
Shlyakhtina, Y, Moran, KL, and Portal, MM (2019). Asymmetric Inheritance of Cell Fate Determinants: Focus on RNA. Non-Coding Rna 5, 38.
Singh, P, Ramdas Nair, A, and Cabernard, C (2014). The Centriolar Protein Bld10/Cep135 Is Required to Establish Centrosome Asymmetry in Drosophila Neuroblasts. Curr Biol 24, 1548–1555.
Singh, P, Ramdas Nair, A, and Cabernard, C (2014). The Centriolar Protein Bld10/Cep135 Is Required to Establish Centrosome Asymmetry in Drosophila Neuroblasts. Curr Biol 24, 1548–1555.
Smyth, JT, Schoborg, TA, Bergman, ZJ, Riggs, B, and Rusan, NM (2015). Proper symmetric and asymmetric endoplasmic reticulum partitioning requires astral microtubules. Open Biol 5, 150067.
Sonnen, KF, Gabryjonczyk, A-M, Anselm, E, Stierhof, Y-D, and Nigg, EA (2013). Human Cep192 and Cep152 cooperate in Plk4 recruitment and centriole duplication. J Cell Sci 126, 3223–3233.
Spinelli, JB, and Zaganjor, E (2022). Mitochondrial efficiency directs cell fate. Nat Cell Biol 24, 125–126.
Sulimenko, V, Dráberová, E, and Dráber, P (2022). γ-Tubulin in microtubule nucleation and beyond. Frontiers Cell Dev Biology 10, 880761.

Sun, G, Hwang, C, Jung, T, Liu, J, and Li, R (2023). Biased placement of Mitochondria fission facilitates asymmetric inheritance of protein aggregates during yeast cell division. PLOS Comput Biol 19, e1011588.
Sunchu, B, and Cabernard, C (2020). Principles and mechanisms of asymmetric cell division. Development 147, dev167650.
Sunchu, B, Lee, NM, Taylor, JA, Segura, RC, Roubinet, C, and Cabernard, C (2022). Asymmetric chromatin retention and nuclear envelopes separate chromosomes in fused cells in vivo. Commun Biology 5, 953.
Suter, B (2018). RNA localization and transport. Biochimica Et Biophysica Acta Bba - Gene Regul Mech 1861, 938–951.
Tang, CC, Lin, S, Hsu, W, Lin, Y, Wu, C, Lin, Y, Chang, C, Wu, K, and Tang, TK (2011). The human microcephaly protein STIL interacts with CPAP and is required for procentriole formation. EMBO J 30, 4790–4804.
Thomas, A, Gallaud, E, Pascal, A, Serre, L, Arnal, I, Richard-Parpaillon, L, Savoian, MS, and Giet, R (2021). Peripheral astral microtubules ensure asymmetric furrow positioning in neural stem cells. Cell Rep 37, 109895.
Tsankova, A, Pham, TT, Garcia, DS, Otte, F, and Cabernard, C (2017). Cell Polarity Regulates Biased Myosin Activity and Dynamics during Asymmetric Cell Division via Drosophila Rho Kinase and Protein Kinase N. Dev Cell 42, 143-155.e5.
Vázquez, M, Cooper, MT, Zurita, M, and Kennison, JA (2008). γTub23C Interacts Genetically With Brahma Chromatin-Remodeling Complexes in Drosophila melanogaster. Genetics 180, 835–843.
Voss, M, Campbell, K, Saranzewa, N, Campbell, DG, Hastie, CJ, Peggie, MW, Martin-Granados, C, Prescott, AR, and Cohen, PT (2013). Protein phosphatase 4 is phosphorylated and inactivated by Cdk in response to spindle toxins and interacts with γ-tubulin. Cell Cycle 12, 2876–2887.
Wang, X, Tsai, J-W, Imai, JH, Lian, W-N, Vallee, RB, and Shi, S-H (2009). Asymmetric centrosome inheritance maintains neural progenitors in the neocortex. Nature 461, 947–955.
Wiese, C (2008). Distinct Dgrip84 Isoforms Correlate with Distinct γ-Tubulins in Drosophila. Mol Biol Cell 19, 368–377.
Wilson, PG, and Borisy, GG (1998). Maternally Expressed γTub37CD inDrosophilaIs Differentially Required for Female Meiosis and Embryonic Mitosis. Dev Biol 199, 273–290.
Xu, Y, Chen, J, Wang, X, Huang, M, Wei, X, Luo, X, Wei, Y, and She, Z (2025). KIF11 Inhibition Induces Retinopathy Progression by Affecting Photoreceptor Cell Ciliogenesis and Cell Cycle Regulation in Development. Adv Biol, e2400748.
Yamashita, YM, Mahowald, AP, Perlin, JR, and Fuller, MT (2007). Asymmetric Inheritance of Mother Versus Daughter Centrosome in Stem Cell Division. Science 315, 518–521.
Yang, EJ, Liao, P, and Pon, L (2024). Mitochondrial protein and organelle quality control—Lessons from budding yeast. IUBMB Life 76, 72–87.
Yang, EJ, Pernice, WM, and Pon, LA (2022). A role for cell polarity in lifespan and mitochondrial quality control in the budding yeast Saccharomyces cerevisiae. IScience 25, 103957.
Yu, L, Li, G, Deng, J, Jiang, X, Xue, J, Zhu, Y, Huang, W, Tang, B, and Duan, R (2020). The UFM1 cascade times mitosis entry associated with microcephaly. FASEB J 34, 1319–1330.

Zimyanin, VL, Belaya, K, Pecreaux, J, Gilchrist, MJ, Clark, A, Davis, I, and Johnston, DS (2008). In Vivo Imaging of oskar mRNA Transport Reveals the Mechanism of Posterior Localization. Cell 134, 843–853.
Zou, C, Li, J, Bai, Y, Gunning, WT, Wazer, DE, Band, V, and Gao, Q (2005). Centrobin. J Cell Biol 171, 437–445.
Zou, W, Lv, Y, Zhang, S, Li, L, Sun, L, and Jiao, J (2024). Lysosomal dynamics regulate mammalian cortical neurogenesis. Dev Cell 59, 64-78.e5.

APPENDIX

ascb
an international forum for cell biology

MBoC

MOLECULAR BIOLOGY OF THE CELL

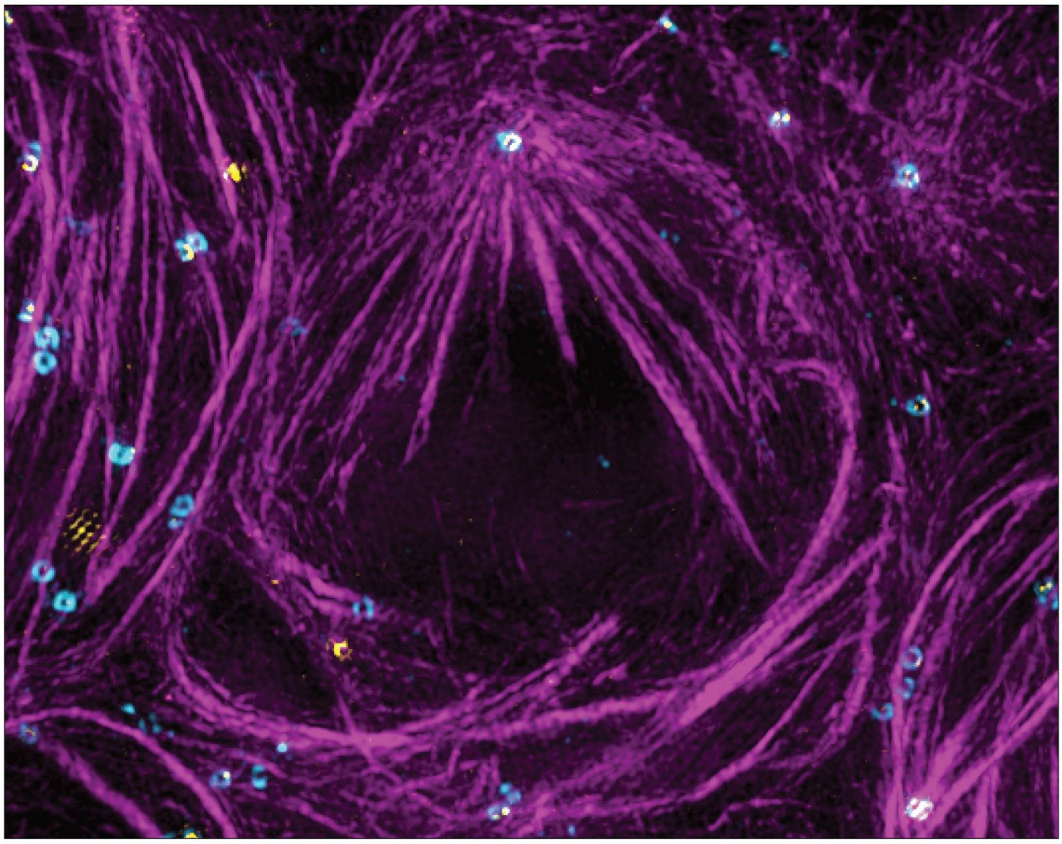

VOLUME 36 • NUMBER 6 • JUNE 1, 2025

MBoC
MOLECULAR BIOLOGY OF THE CELL
Published by the American Society for Cell Biology

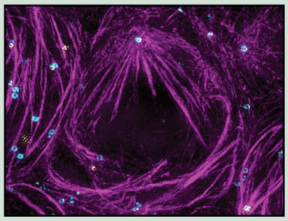

Volume 36 • Number 6 • June 1, 2025

In this issue of *MBoC*, *Segura et al.* (ar58) show a *Drosophila* neural stem cell (neuroblast) fixed and stained with antibodies against alpha-tubulin (magenta), Centrobin (yellow), and the centriolar protein asterless (cyan). Samples were imaged using three-dimensional structured illumination microscopy (3D-SIM), which greatly increases the resolution of microscopy images and allows for the resolution of individual microtubule strands and subcentrosomal components. The selected neuroblast is in interphase, where one centrosome maintains active microtubule activity and is Cnb^{+}, while the other centrosome remains inactive and is Cnb^{-}. 3D-SIM allows researchers to ask questions about protein dynamics at the subcentrosomal level while retaining the ability to label multiple proteins at once (Image: Roberto Carlos Segura, University of Washington).

The Philosophy of *Molecular Biology of the Cell*

Molecular Biology of the Cell (*MBoC*) is published by the nonprofit American Society for Cell Biology (ASCB) and is free from commercial oversight and influence. We believe that the reporting of science is an integral part of research itself and that scientific journals should be instruments in which scientists are at the controls. Hence, *MBoC* serves as an instrument of the ASCB membership and as such advocates the interests of both contributors and readers through fair, prompt, and thorough review coupled with responsible editorial adjudication and thoughtful suggestions for revision and clarification. Our most essential review criterion is that the work significantly advances our knowledge and/or provides new concepts or approaches that extend our understanding. At *MBoC*, active working scientists—true peers of the contributors—render every editorial decision.

The Society and *MBoC* are committed to promoting the concept of open access to the scientific literature. *MBoC* seeks to facilitate communication among scientists by

- publishing original papers that include full documentation of Methods and Results, with Introductions and Discussions that frame questions and interpret findings clearly (even for those outside an immediate circle of experts) and
- exploiting technical advances to enable rapid dissemination of articles prior to print publication and transmission and archiving of videos, large datasets, and other materials that enhance understanding.

Scope of *MBoC*

MBoC publishes research articles that present conceptual advances of broad interest and significance within all areas of cell, molecular, and developmental biology. We welcome manuscripts that describe advances with applications across topics including but not limited to: cell growth and division; nuclear and cytoskeletal processes; membrane trafficking and autophagy; organelle biology; quantitative cell biology; physical cell biology and mechanobiology; cell signaling; stem cell biology and development; cancer biology; cellular immunology and microbial pathogenesis; cellular neurobiology; prokaryotic cell biology; and cell biology of disease.

Submissions that report novel methodologies or large datasets are also encouraged, particularly when the technology or data will be widely useful, when it will significantly accelerate progress within the field, or when it reveals a new result of biological significance.

Authors should include with their manuscript submissions all previously unpublished data and methods essential to support the conclusions drawn.

VITA

Roberto Carlos Segura grew up in South San Francisco, California. His academic career began in 2014 when he began attending Skyline College in San Bruno pursuing an associates degree for transfer in Biology. During this time, he worked as a supplemental instructor for Calculus I and Calculus II while also working part-time jobs in the food service and retail industries. In 2015, he participated in the National Institutes of Health (NIH) Bridges to the Baccalaureate Program, a joint research program with San Francisco State University (SFSU). Starting in 2016, He worked with Dr. Yee-Hung Mark Chan until 2019, where he studied organelle regulation using confocal microscopy and the budding yeast *Saccharomyces cerevisiae*. Carlos eventually transferred to SFSU as a NIH Maximizing Access to Research Careers (MARC) fellow in 2017 to complete his undergraduate degree in Biology with a concentration in Cellular and Molecular Biology. While pursuing his undergraduate degree, Carlos was heavily involved with the Society for the Advancement of Chicanos/Hispanics and Native Americans in Science (SACNAS), eventually becoming a board member and chapter president of the SFSU Chapter. Thanks to the funding from the NIH MARC program, Carlos was able to commit full-time to research in the Chan lab, leading him to develop a deep appreciation for quantitative image analysis techniques.

Carlos began his doctoral training at the University of Washington (UW) in 2019 immediately after the completion of his undergraduate degree, where he worked with Dr. Clemens Cabernard to study centrosome asymmetry in *Drosophila* neural stem cells. During his graduate studies, Carlos became involved with the UW SANCAS Chapter, similar to his work with the SFSU Chapter. Additionally, Carlos was awarded the NIH T32 training grant in Cellular and Molecular Biology from the UW, and the Ford Foundation Pre-Doctoral fellowship from the Ford Foundation. At the completion of his doctoral studies in 2025, Carlos transitioned to working as a Scientist I at Alpenglow Biosciences in Seattle.